12-2013

KOLSKY BAR EXPERIMENT FOR HIGH-RATE LARGE DEFORMATIONS OF POLYCARBONATE

Jason G. Vogeler
University of Nebraska-Lincoln, jason.vogeler@outlook.com

KOLSKY BAR EXPERIMENT FOR HIGH-RATE LARGE DEFORMATIONS OF POLYCARBONATE

By

Jason G. Vogeler

A THESIS

Presented to the Faculty of

The Graduate College at the University of Nebraska

In Partial Fulfillment of Requirements

For the Degree of Master of Science

Major: Mechanical Engineering and Applied Mechanics

Under the Supervision of Professor Ruqiang Feng

Lincoln, Nebraska

December, 2013

KOLSKY BAR EXPERIMENT FOR HIGH-RATE LARGE DEFORMATIONS OF POLYCARBONATE

Jason Gerald Vogeler, M.S.

University of Nebraska, 2013

Advisor: Ruqiang Feng

Polycarbonate (PC) is a tough, transparent engineering thermoplastic. Its impact strength and ability undergo large plastic deformations without shatter make PC an ideal protective material for impact-resilient eyewear, aircraft windows and transparent armor. A good understanding of the response of this material to large deformations at high strain rates is critical for its utilization in these applications. To this end, a striker-less Kolsky bar device is employed in this work for the needed material characterization. The apparatus allow impulsive torsion and/or compression loadings with pulse durations sufficiently long for the plastic flow behavior to develop fully. Three new testing techniques based on the device are developed and applied to measure the response of PC to large plastic deformations of various modes at various strain rates and under various temperatures.

The first new technique is a modified torsional Kolsky bar method that loads the PC sample in high rate of simple shear. In addition to measuring the shear stress as the conventional method, the new technique also measures the axial stress induced by shear deformation. The measurements show that the material expands as it undergoes elastic shear and contracts as the shear becomes increasingly plastic. The results for the elastic response confirm the prediction by a non-linear elastic model for PC.

The second new technique applies a static axial compression to the sample before dynamic shear loading. The experiments with this technique seek to determine if and to what extent the deviatoric yield and flow stresses of PC are affected by the volumetric stress. For the stress states examined, both the deviatoric yield and flow stresses show linear dependence on the compressive volumetric stress.

The final Kolsky bar technique developed uses a friction clamp to store and release a compressive pulse. This new technique allows for loading pulses that are much longer than the achievable pulses in the traditional split Hopkinson bar tests. They are sufficient for the material flow behavior to develop fully in the compressive strain rate range of mid hundreds to lower thousands per second. Tests with the technique are performed on PC over an array of temperatures and strain rates. The temperature and strain rate dependences of the yield and flow stresses under dynamic compression are studied. The volumetric stresses are considerably more intense for the compression tests than for the torsion tests and combined compression-torsion tests. The data from the three types of tests together indicates consistent pressure-dependent increases in the deviatoric yield and flow stresses of PC subjected to high-rate large deformations.

ACKNOWLEDGEMENTS

My deepest thanks to my advisor Dr. Ruqiang Feng for his support and guidance in this research. I would also like to thank my final examination committee members Dr. Feng, Dr. Mehrdad Negahban, and Dr. Joseph Turner for their time and input allowing me to perform my thesis defense during holiday break. Also a deep thanks to Dr. Negahban for his expertise and guidance in especially in material modeling.

I am grateful for the financial support of the Army Research Office. The quality machining of samples and components performed by the talented staff of the UNL Engineer Science Research Support Facility is greatly appreciated. Dr. Ashwani Goel was a great help with the material model prediction of a shear induced axial stress. I am thankful for the administrative support of Kathie Hiatt during my time as both an on campus student and a distance student. I would also like to thank my employer Naval Nuclear Power Training Command for their flexibility as I took distance classes and wrote this thesis.

Most of all I thank my wonderful family. My wife Tram has motivated me, given me excellent advice, and given me the support I needed to finish this thesis. Her support this final busy month of preparing this thesis is especially appreciated. My 5 month old daughter Evangeline has also motivated me. I will never forget the time I spent writing this paper with her on my lap playing or sleeping.

CONTENTS

LIST OF FIGURES

LIST OF TABLES

CHAPTER 1. INTRODUCTION

1.1 Research Motivation and Objectives

This work will develop and apply striker-less Kolsky bar to the study of polycarbonate (PC) and compares results and adds to existing models and study. PC is a transparent polymer with impact resistance that rivals many metals (Wright, Fleck, & Stronge, 1993). This makes polycarbonate ideally suited for applications that require a lightweight transparent material that need to be able to withstand impact such as eyewear, aircraft window, and transparent armor. The impact resistance of polycarbonate comes in its ability to undergo large plastic deformations even at high rates. To better understand and utilize this material and other glassy polymers, it needs to be studied under high rates of deformation. The loading must occur in a long enough pulse so that the plastic flow behavior, crucial for impact resistance, has time to develop. These strains are orders of magnitude larger than strains observed in metal testing for which Kolsky bar techniques were initially developed.

Material models (Goel, Strabala, Negahban, & Turner, 2009) suggest that there should be an axial stress induced a sample experiencing dynamic torsion in the elastic range if the sample is constrained in that direction. A method will be developed to measure that axial response. The axial response during elastic, yielding, and plastic flow deformation will be observed and the elastic region will be compared to the model.

While the temperature and strain rate effects on yielding and plastic flow in polycarbonate have been observed and modeled by many (Fleck, Stronge, & Liu, 1990) (Moy, Weerasooriya, Hsieh, & Chen, 2009) (Mehta & Prakas, 2009) (Rietsch & Bouette,

1990) (Shen, 2007), the effect of pressure has not been studied or modeled. Torsion tests have effectively zero pressure. Compressive tests have high pressures. Intermediate pressures can be obtained by adding a static compression before performing the torsion test. The data from these various types test will be compared to determine if a dependence on pressure for yield and flow stress can be proven to exist and quantized.

Striker-less or friction clamp type Kolsky methods are well suited testing of PC and similar materials because it offers high rates of loading and relatively long loading pulses needed to observe the plastic flow deformation that occurs at large strains. The Kolsky bar methods developed in this thesis also allows for the studying of the distortion-dilation coupling in glassy polymers. Distortion-dilation coupling is typically negligible in harder materials where strains are much smaller, but will be shown to be significant for this class of materials.

1.2 Scope and Organization of Thesis

This thesis is divided into six chapters. Since the three Kolsky bar techniques are based on modifications to standard torsional Kolsky bar (TKB) techniques, Chapter 2 describes the set-up, analysis and typical result for the standard TKB method. The standard TKB method has thin walled tube sample secured between two cylindrical aluminum bars. A friction clamp and pulley are used to store and release a torsional pulse. The torsion pulse travels through the bar and loads the sample. The sample deforms during the pulse with a high (500 s^{-1} to 4000 s^{-1}), nearly constant strain rate. The shear stress and shear strain rate histories are determined from the measured voltage in shear strain gauge bridges on the bars and torsional wave propagation analysis. Chapters 3-5 describe the three modified Kolsky bar methods, as well as the associated analyses and findings.

Chapter 3 describes how the standard TKB method is modified to measure the relatively small axial response to shear in the sample. Axial strain gauges are added to the second bar to obtain an axial stress history of the sample. The second bar is replaced with a hollow bar and the clamped distance is adjusted to obtain a clear axial stress history. The measured axial stress response is compared to material models. These pure torsion test results will also be compared to the following combined loading and compression tests.

Chapter 4 combines the dynamic shear loading of the TKB method with static axial compression. The entire apparatus including the sample before the torsion pulse is stored or released. The axial strain gauges in the second bar are used to obtain a sample axial stress history. The shear and axial stress histories are combined to get a deviatoric invariant stress and mean stress histories.

In Chapter 5 the sample is loaded with a compression pulse rather than a torsion pulse. In this case compression is stored in the clamped section and released with the friction clamp. A compressional pulse travels through the bars and loads the sample at a high strain rate. The sample strain rate and stress history are obtained from axial strain bridges and longitudinal wave propagation analysis. Deviatoric invariant stress history is calculated from the stress history and deviatoric invariant yield and flow stress are compared for the three types of tests. Chapter 6 gives the conclusions.

1.3 Literature Review

The literature review focusses on high rate experimental characterization of polycarbonate and elastic and viscous flow material models.

1.3.1 Experimental Polycarbonate Characterization

High rate test using split-Hopkinson pressure bar and low rate test using servo-hydraulic tests on polycarbonate (PC) and polymethylmethacrylate over a wide range of temperatures (-197 C to 220 C). The strength of PC was found to have a weak dependence on strain rate and moderate temperature dependence (Blumenthal, Cady, Lopez, Gray III, & Idar, 2001). Also PC was found to remain ductile to -197 C. Torsional Kolsky bar(TKB) tests performed on PC in the shear strain rate range of $500s^{-1}$ to $2200s^{-1}$ and temperature range from -100 C to 200 C show that yield behavior follow an Eyring model for viscous flow between the beta transition temperature(~-100 C) and the glass transition temperature (147 C) (Fleck, Stronge, & Liu, 1990). TKB tests were performed over the temperature range of 20 C to 100 C and shear strain rate range of 500 s^{-1} to 2000 s^{-1} and flow stress was fitted to an Eyring model (Shen, 2007).

1.3.2 Material Modeling in Elastic Range

A mathematical model for Cauchy stress tensor (**T**) in the elastic range (Goel, Strabala, Negahban, & Turner, 2009) based on moduli taken from ultrasonic wave speed measurements is as follows:

$$\boldsymbol{T} = \kappa\frac{(J-1)}{J}\boldsymbol{I} + J^{-\frac{5}{3}}\left(\boldsymbol{B} - \frac{tr(\boldsymbol{B})}{3}\boldsymbol{I}\right) \tag{1-1}$$

where J is the volume ratio, which is equal to the determinant of the deformation gradient (**F**), **I** is the identity tensor, and **B** is the left Cauchy stretch tensor defined as $\mathbf{B} = \mathbf{F}\mathbf{F}^T$. The two material parameters κ and G are respectively, the bulk modulus and shear modulus at zero load (Goel, Strabala, Negahban, & Turner, 2009) as

$$\kappa = 4760\ MPa, G = 1072\ MPa.$$

1.3.3 Material Modeling of Yielding and Plastic Flow

Eyring theory (Eyring, 1936) is a thermal activation theory. Under a sufficient shear stress, a kink in the polymer chain will be able to overcome the activation barrier and jump to an available hole. This viscous flow is typically assumed to start at the point of yielding. The strain rate resulting from Eyring theory is given by:

$$\dot{\gamma} = 2\dot{\gamma}_0 \exp\left(-\frac{\Delta H}{kT}\right)\sinh\left(\frac{v\tau}{kT}\right) \tag{1-2}$$

where $\dot{\gamma}$ is the shear strain rate, $\dot{\gamma}_0$ is a reference strain rate, ΔH is the molecular activation energy required for molecular displacement, k is Boltzmann constant, T is the absolute temperature, v is an activation volume and τ is the shear yield stress. Since $\gamma=2\gamma 0\exp -\Delta HkT\sinh vtkT$ (1-2 can be solved for shear yield stress as:

$$\frac{\tau}{T} = A\left[\ln(2C\dot{\gamma}) + \frac{\Delta H}{kT}\right] \tag{1-3}$$

where A and C are material constants. This expression takes into account a single activation process only. Over a large range of strain rates there may be multiple thermal activated deformation processes; this is known as the Ree-Eyring theory (Ree & Eyring, 1955). Starting from that theory, Bauwens (Bauwens-Crowet, Bauwens, & Homes, 1969) deduced a general expression for the determination of the yield stress:

$$\sigma_{yield} = T\left[A_\alpha\left(\ln(2C_\alpha\varepsilon)\dot{+}\frac{Q_\alpha}{RT}\right) + A_\beta sin^{-1}\left(C_\beta\dot{\varepsilon}\exp\left(\frac{Q_\beta}{RT}\right)\right)\right] \tag{1-4}$$

T is the absolute temperature in Kelvin. R is the universal gas constant $1.987\times10^{-3}\ \frac{kcal}{molK}$. A_α, C_α, Q_α, A_β, C_β, and Q_β are experimentally determined.

CHAPTER 2. ANALYSIS OF STANDARD TKB

2.1 Introduction

Polycarbonate has been tested in a standard Torsional Kolsky bar tests by Shen (Shen, 2007) and Fleck (Fleck, Stronge, & Liu, 1990). Since all the methods developed and described in this thesis are variations on this standard TKB method, this chapter will introduce that method.

2.2 Background

Hopkinson pioneered the concept of propagating and measuring stress waves in long cylindrical bars (Hopkinson, 1914). Hopkinson bars, as they were called, allowed for study of the metal bars themselves. The innovation introduced by Kolsky was to use a Hopkinson bar on each side of a testing sample (Kolsky, 1949). The sample is loaded by introducing pressure pulse in first (incident) bar and having that pressure partially transmitted through the sample to the second (output) bar. By analyzing the incident, reflected and transmitted stress pulses, the material response can be measured. The method is known as the split-Hopkinson pressure bar (SHPB) or Kolsky bar technique. Early experiments used explosives to create the incident stress pulse (Hopkinson, 1914), while in current practice a small bar is accelerated by a gas gun to collide with the incident bar. The limitations of this method include that the sample can only be used in compression and that duration of loading pulses can be short. The disadvantage of compression is that the length and cross-sectional area of the sample change as the sample deforms, making measurements of true stress and true strain more difficult. The short duration of these SHPB test results in little time for plastic deformation behavior to develop at strain rates lower than a few thousand s^{-1}. Baker and Yew introduced a

Kolsky bar method for dynamic torsion loading (Baker & Yew, 1966). With torsion loading the sample dimensions don't change significantly as the sample deforms, therefore true stress and true strain can be measured directly. The TKB method has been further developed by a number of researchers e.g. (Lewis, 1972) (Hartley, Duffy, & Hawley, 1985). A torsional pulse is created using a friction clamp to store a torque in a portion of the incident bar and instantly releasing that torque. This method called torsional Kolsky bar (TKB) method allows for larger pulse lengths than are possible than for traditional SHPB tests. The same friction clamp set up can also be used to store and release compression pulses. This method is called the compressional Kolsky bar (CKB) method and will be described later in the paper.

2.3 TKB Set-up

The multi-mode friction clamp type Kolsky apparatus used in all of the methods

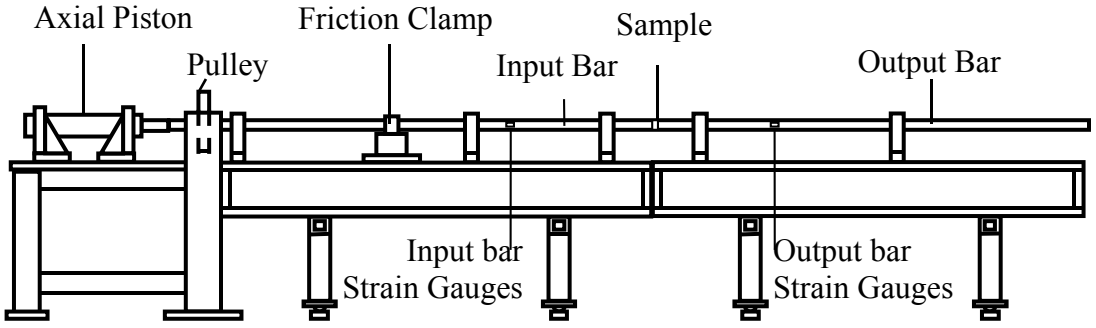

Figure 2-1 Multimode Kolsky Bar Apparattus

described and developed in this paper is shown in Figure 2-1. The friction clamp, shown

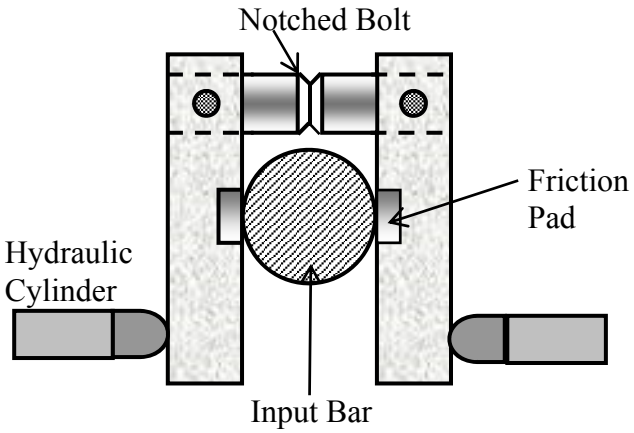

Figure 2-2: Friction Clamp

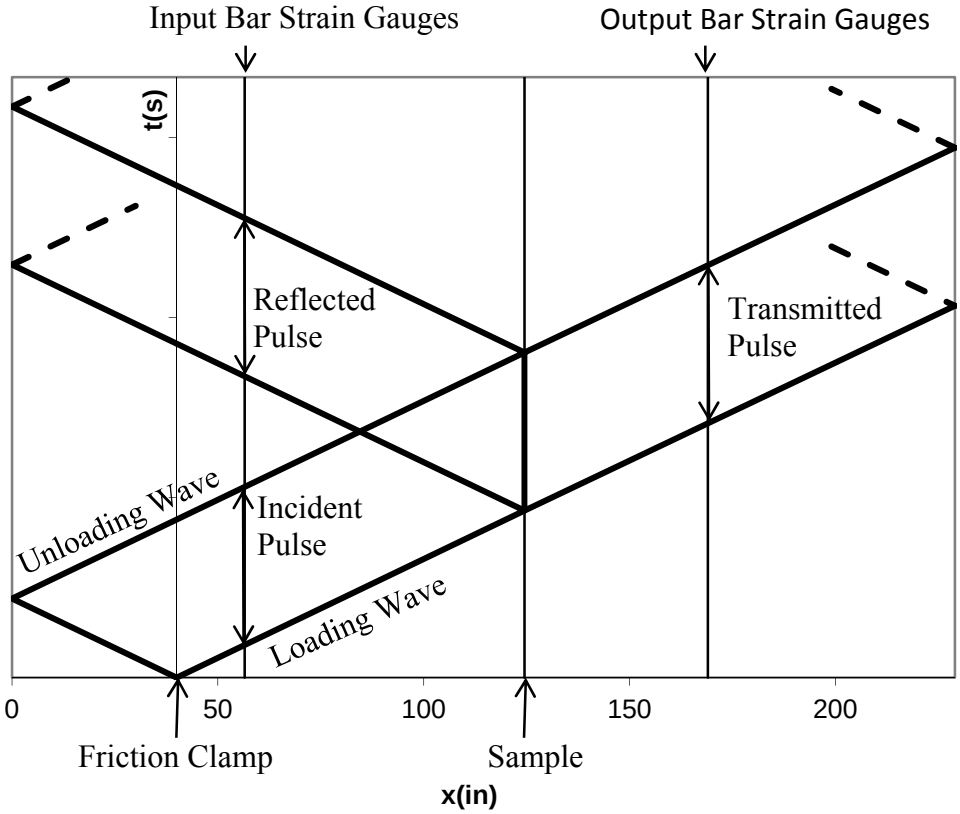

Figure 2-3: X-T Diagram

in Figure 2-2, designed by Duffy (Hartley, Duffy, & Hawley, 1985) is integral for storing and quick release of torsion pulses. A hydraulic cylinder is used to tighten the clamp on the bar. Another hydraulic cylinder attached to the pulley is used to apply the desired torque to the section of the bar between the pulley and the clamp. After applying the torque, pressure is added to the hydraulic cylinder for the clamp until the notched bolt

breaks. At the instant the notched bolt breaks, elastic torsional loading wave front travels from the clamp toward the sample. At the same instant an unloading wave front traveled towards the pulley and is reflected back toward the sample. Together the loading and unloading waves fronts form a torsional pulse called the incident pulse. The incident pulse travels toward the sample and is partially transmitted through the sample and partially reflected. The x-t diagram in Figure 2-4 shows this propagation of the wave through the bars. By measuring and analyzing the transmitted and reflected pulses, the material response of the sample can be determined. The incident, reflected, and transmitted pulses are measured by shear strain gauges on the

Figure 2-5 Shear Strain Gauge

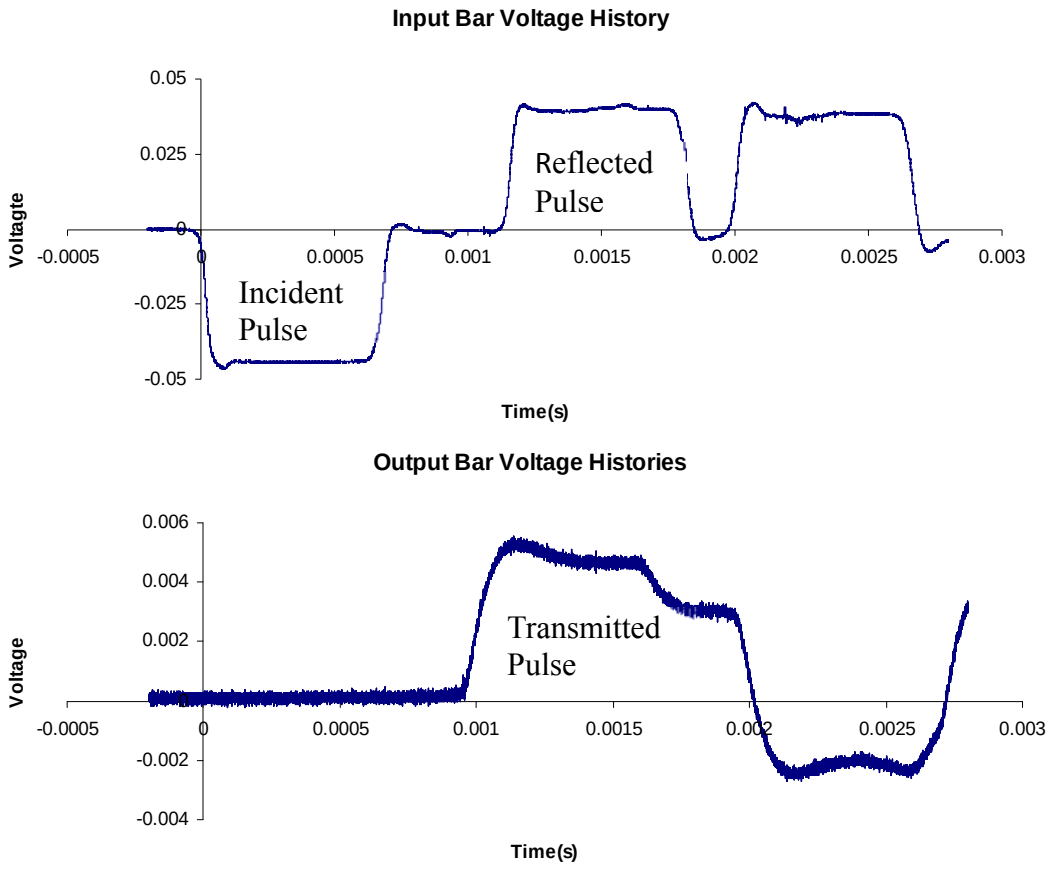

Figure 2-3 Input and Output Voltage Histories

input and output bars. The location of the shear strain gauges and the friction clamp are chosen to prevent reflected pulses from overlapping with each other as can be seen in Figure 2-3. The strain gauges are Micro-Measurements shear strain gauges with a nominal resistance of 1000Ω resistance and are shown in Figure 2-4. The higher resistance allow for higher excitation voltages that are typically 25 V to 35 V which increases the signal to noise ratio. Four shear strain gauges are configured in a Wheatstone bridge circuit (Figure 2-7). The bridge voltage is measured using a Nicolet MultiPro digital oscilloscope with a 10 MHz sampling rate. The measured voltage from the input and output bar strain gauge bridges from a typical test can be seen in Figure 2-5.

The spool shaped sample is shown in in Figure 2-6. The thick outer edges allow the sample to be attached to the bar. The inner section deforms and is studied during the test.

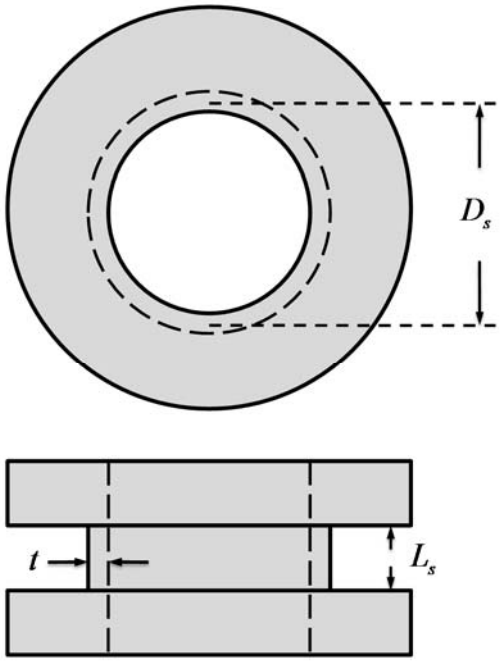

Figure 2-6 PC Torsion Sample

Because it is a thin-walled tube, it can be approximated as having a uniform shear stress.

2.3.1 Strain Gauge Measurement Analysis

The torsion pulses are measured using shear strain gauges in full Wheatstone bridge

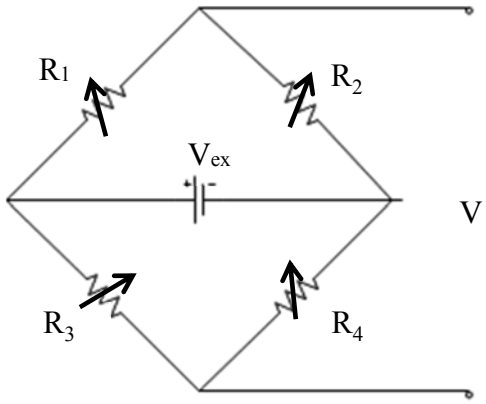

Figure 2-7 Wheatstone bridge where V_{ex}=Excitation Voltage, V= Measured Voltage, and R_{1-4} are the four shear strain gauges

configuration seen in Figure 2-7. Equation 2-1 is the general equation for the measured voltage in a Wheatstone bridge.

$$V = V_{ex}\left[\frac{R_3}{R_3+R_4} - \frac{R_2}{R_1+R_2}\right] \quad (2\text{-}1)$$

All four strain gauges have the same nominal resistance of 1000Ω which is denoted as 'R_n'. The orientation of the gauges ensures that for a given twist in the bar the change in resistance (ΔR) of strain gauges 1 and 3 will be equal in magnitude and opposite in sign of the change in resistance in strain gauges 2 and 4.

$$R_1 = R_3 = R_n + \Delta R \quad (2\text{-}2)$$

$$R_2 = R_4 = R_n - \Delta R \quad (2\text{-}3)$$

Adding the relations in equations 2-2 and 2-3 simplifies equation 2-1 to:

$$V = V_{ex}\frac{\Delta R}{R_n} \tag{2-4}$$

The change in resistance in a strain gauge is proportional to the applied strain (ε). The constant of proportionality is called the gauge factor (f). $f\varepsilon = \frac{\Delta R}{R_n}$ therefore:

$$V = V_{ex} f\varepsilon \; or \; \varepsilon = \frac{V}{V_{ex} f}. \tag{2-5}$$

The measured strain needs to be converted to shear strain for the purpose of these experiments. Figure 2-8 shows a unit square (L=1) where the x direction goes about the

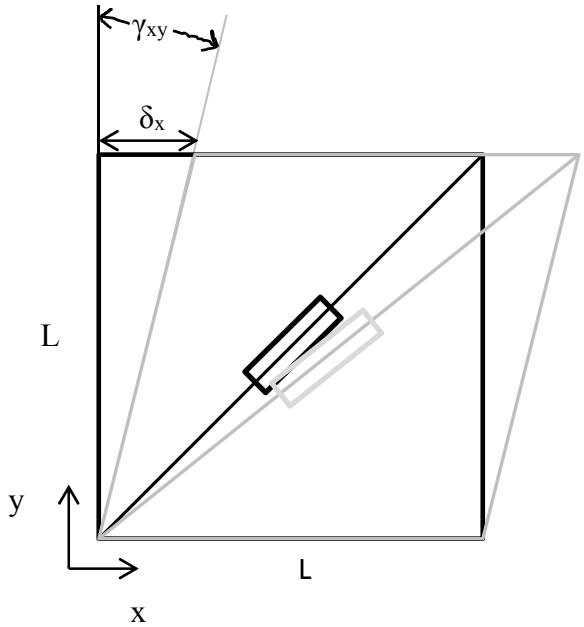

Figure 2-8 Unit square and shear deformed unit square

circumference of the bar and the y direction is parallel to the axis of the bar. ε_{xx} and ε_{yy} are assumed to be zero based on the torsion loading of the bar and the fact that the orientation of the gauges and the full bridge circuitry makes the measured voltage insensitive to those strains. Shear strain (γ_{xy}) is the angle in radians of the deformation.

Since for small angles $\theta \cong \sin\theta$, the displacement (δ_x) of the upper part of square is equal to the shear strain.

$$\gamma_{xy} \cong \sin\gamma_{xy} = \frac{\delta_X}{L} = \delta_X \tag{2-6}$$

The strain measured (ε_{xy}) is at a 45° angle from the x-axis. The original length of the diagonal is $\sqrt{2}$ and its deformed length is $\sqrt{2}(1 + \varepsilon_{xy})$. By the Pythagorean theorem:

$$\left[\sqrt{2}(1 + \varepsilon_{xy})\right]^2 = 1^2 + (1 + \delta_x)^2 \tag{2-7}$$

$$2 + 4\varepsilon_{xy} + 2{\varepsilon_{xy}}^2 = 2 + 2\delta_x + {\delta_x}^2 \tag{2-8}$$

Second order terms can be neglected since strains are small and

$$\gamma_{xy} = \delta_x = 2\varepsilon_{xy}. \tag{2-9}$$

The shear modulus (G) for 7075 aluminum bars was measured to 26.8 GPa based on a measurement of shear elastic wave speed. The shear stress (τ) on the surface of the bar can be determined from the shear modulus and the shear strain.

$$\tau = G\gamma \tag{2-10}$$

The torque (T) in the bar is determined from the shear stress by this relation:

$$\tau = \frac{Tr}{J} \tag{2-11}$$

where r is the radius of the bar and J is polar moment of inertia ($= \frac{\pi}{2}r^4$). Equations 2-5, 2-9, 2-10, and 2-11 are combined to obtain torque histories of the incident, reflected and transmitted pulses from the measured voltage histories.

$$T = \frac{2VJG}{V_{ex}rf} \tag{2-12}$$

A moving average is taken of the measured voltages to smooth the curves for the torque pulses. The torque histories from the three pulses can be used to determine the shear stress and shear strain rate of the sample.

2.3.2 Torsional Wave Analysis

It is necessary to understand how torsional waves propagate through the cylindrical bars in order to analyze the loading and deformation of the sample. The infinitesimally thin section of the aluminum bar in Figure 2-9 is used to develop the equations and relations needed. Shear strain at surface of the bar can be represented as

$$\gamma = r\frac{\partial\phi}{\partial x} \tag{2-13}$$

where r is the radius of the bar, φ is the angle of twist of the bar in radians and x is the

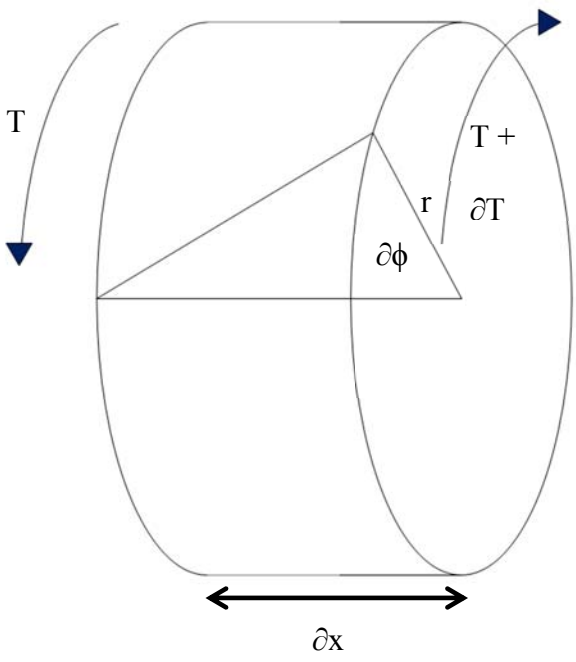

Figure 2-9 Section of the Bar with thickness δx

position on the bar in the axial direction. Taking the time derivative of both sides of equation 2-13 gives

$$\frac{\partial \gamma}{\partial t} = \frac{\partial}{\partial t}\left(r\frac{\partial \phi}{\partial x}\right) = r\frac{\partial}{\partial x}\left(\frac{\partial \phi}{\partial t}\right) = r\frac{\partial \omega}{\partial x} \tag{2-14}$$

where ω is the rotation rate of the bar in radians per second. For torsion in a cylinder:

$$\gamma = \frac{Tr}{GJ} \tag{2-15}$$

r is the radius of the bar and J is polar moment of inertia ($J = \pi r^4/2$). Equations 2-14 and 2-15 are combined to derive the following relation.

$$\frac{\partial \gamma}{\partial t} = \frac{\partial}{\partial t}\left(\frac{Tr}{GJ}\right) = \frac{r}{GJ}\frac{\partial T}{\partial t} = r\frac{\partial \omega}{\partial x} \tag{2-16}$$

Equation 2-16 can be simplified to:

$$\frac{\partial T}{\partial t} - GJ\frac{\partial \omega}{\partial x} = 0. \tag{2-17}$$

Equation 2-17 can be rewritten based on the definition of torsional impedance (K) of the bar and a shear wave speed (C_s) relation.

$$K = \rho J C_s \tag{2-18}$$

$$C_s = \sqrt{\frac{G}{\rho}} \tag{2-19}$$

$$\frac{\partial T}{\partial t} - KC_s\frac{\partial \omega}{\partial x} = 0 \tag{2-20}$$

ρ is the density of the bar. This equation will be used later; first another relation will developed from the thin section shown in Figure 2-9. Since the torque is not balanced across the section there is an angular acceleration (α) in the infinitesimal section.

$$\partial T = I\alpha \tag{2-21}$$

I is the moment of inertia and is calculated as

$$I = \frac{1}{2}Mr^2 = \frac{1}{2}\rho\pi r^2 \partial x r^2 = \rho J \partial x. \tag{2-22}$$

Therefore:

$$\frac{\partial T}{\partial x} = \rho J\alpha = \rho J \frac{\partial \omega}{\partial t} \tag{2-23}$$

Multiplying both sides of equation 2-23 by the shear wave speed and rearranging gives

$$C_s \frac{\partial T}{\partial x} - C_s \rho J \frac{\partial \omega}{\partial t} = 0, \tag{2-24}$$

and

$$C_s \frac{\partial T}{\partial x} - K \frac{\partial \omega}{\partial t} = 0 \tag{2-25}$$

For right travelling waves $C_s = \frac{dx}{dt}$, so equations (2-20 and 2-25 can rewritten as follows.

$$\frac{\partial T}{\partial t} dt - K \frac{\partial \omega}{\partial x} dx = 0 \tag{2-26}$$

$$\frac{\partial T}{\partial x} dx - K \frac{\partial \omega}{\partial t} dt = 0 \tag{2-27}$$

Adding equations 2-26 and 2-27 yields

$$\left(\frac{\partial T}{\partial x} - K\frac{\partial \omega}{\partial x}\right)dx + \left(\frac{\partial T}{\partial t} - K\frac{\partial \omega}{\partial t}\right)dt = 0 \tag{2-28}$$

or

$$d(T - K\omega) = 0. \tag{2-29}$$

Along a right going wave there is a characteristic equation:

$$(T - K\omega)\ is\ constant\ along\ C_s = \frac{dx}{dt} \tag{2-30}$$

For left going torsional waves, $C_s = -\frac{dx}{dt}$ is plugged into equations (2-20 and 2-25 yielding the characteristic equation for left going waves.

$$(T + K\omega)\ is\ constant\ along\ C_s = -\frac{dx}{dt} \tag{2-31}$$

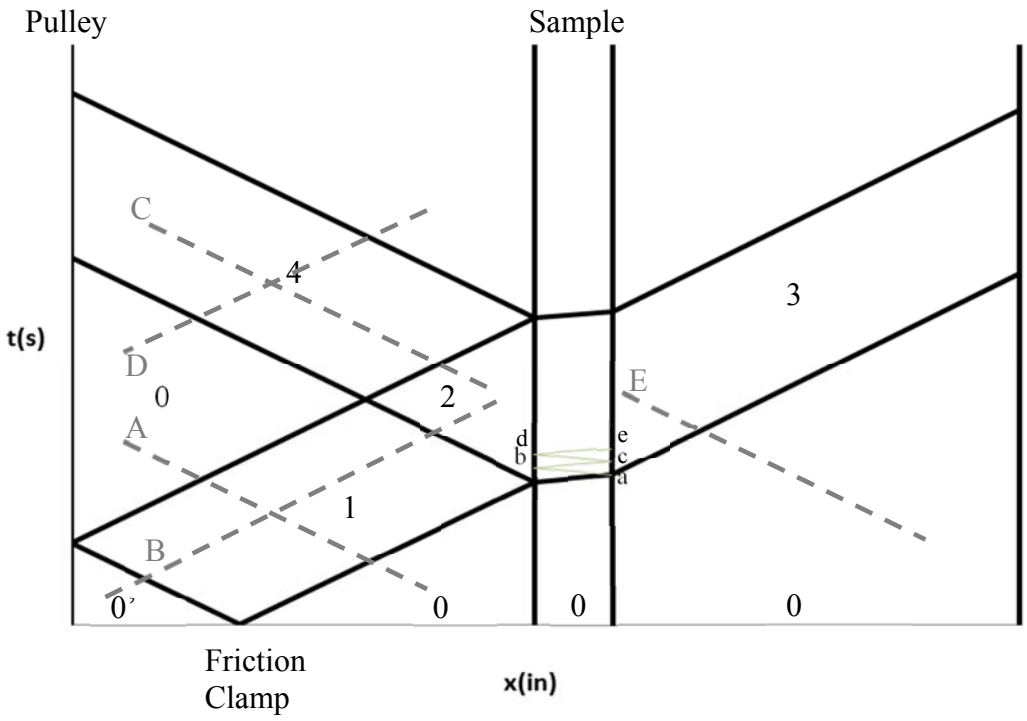

Figure 2-10 x-t diagram

With these characteristic equations developed the loading and deformation of the sample can be analyzed using an x-t diagram (Figure 2-10) and T-ω diagram (Figure 2-11). The x-t diagram shows the propagation of the waves through the bars and the sample. The length of the sample is exaggerated to show how the waves travel through the sample.

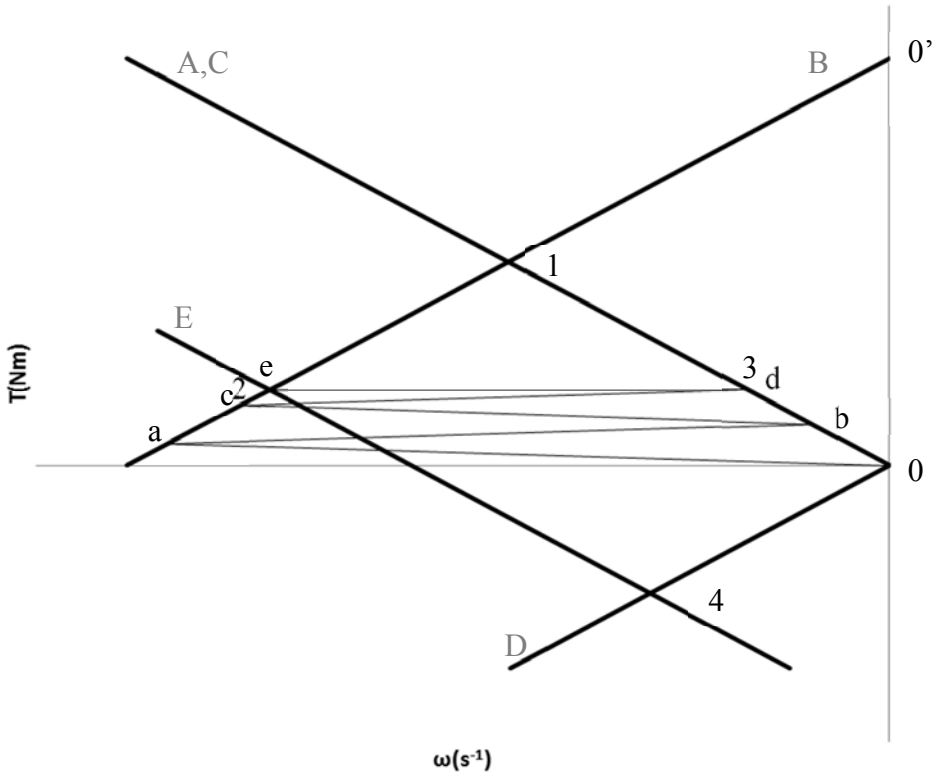

Figure 2-11: T-ω diagram

The T-ω diagram uses the known values for rotation speed (ω) and measured values for torque along with characteristic equations 2-30 and 2-31 for right and left going waves. Initially, to the right of the clamp it is initially unloaded and stationary, while to the left of clamp is loaded with the stored torque and also stationary.

$$\omega_0 = 0 \qquad T_0 = 0$$

$$\omega_{0'} = 0 \qquad T_{0'} = Stored\ Torque$$

Point 0 and 0' are plotted on the T-ω diagram. The dotted line A in Figure 2-10 is a line along $\frac{dx}{dt} = -C_s$, and therefore equation 2-31 applies and torques and rotation speed along line A in the x-t diagram can be found on line A in the T-ω diagram. The dotted line B in Figure 2-10 is a line where $\frac{dx}{dt} = C_s$, and therefore equation 2-30 applies and torques and rotation speed along line B in the x-t diagram can be found on line B in the T-ω diagram. The intersection of lines A and B in Figure 2-11 gives the incident torque and rotation speed as

$$T_1 = T_i = \frac{1}{2}T_{0'} = \frac{1}{2}\ stored\ torque \tag{2-32}$$

$$\omega_1 = -\frac{T_1}{K} = -\frac{T_i}{K} \tag{2-33}$$

where T_1 is the torque measured during incident torque (T_i) pulse. When the sample is loaded torsional waves traverse the sample increasing the load on the sample until the sample yields and can no longer support higher loads. The torsional impedance of the sample is less than that of the bar so the characteristic lines of the sample are less steep. Points a, b, c, d, and e in Figure 2-10 and Figure 2-11 show the load on the sample increasing to yielding. The deformation of the sample is calculated using the rotation speed on both sides of the sample (ω_3 and ω_2). Area and point 4 in Figure 2-10 and Figure 2-11 respectively represents the reflected pulse. Therefore T_4=the measured reflected torque (T_r) and

$$\omega_4 = \frac{T_4}{K} = \frac{T_r}{K}. \tag{2-34}$$

ω_2 can using the T-ω diagram at the intersection of characteristic lines B and C. Geometrically it is clear that $\omega_2=\omega_1+\omega_4$. Therefore using equations 2-33 and 2-34 gives

$$\omega_2 = \frac{-T_1+T_4}{K} = \frac{-T_i+T_r}{K}. \tag{2-35}$$

The measured transmitted pulse corresponds to area and point 3 in Figure 2-10 and Figure 2-11 respectively. Since both bars have the same torsional impedance (K) the characteristic lines A and E overlap. So T_3 is equal to the measured transmitted pulse (T_t) and

$$\omega_3 = -\frac{T_3}{K} = -\frac{T_t}{K}. \tag{2-36}$$

Now that the rotation speed of both ends of the sample has been determined, the shear strain rate ($\dot{\gamma}$) is calculated as follows

$$\dot{\gamma} = \frac{\omega_3-\omega_2}{L_s}\left(\frac{D_s}{2}\right), \tag{2-37}$$

where L_s is the sample length and D_s is average diameter as seen in Figure 2-6. Combining equations 2-35, 2-36, and 2-37 gives

$$\dot{\gamma} = \left(\frac{D_s}{2L_s}\right)\left(-\frac{T_t}{K} - \frac{-T_i+T_r}{K}\right). \tag{2-38}$$

Using the fact that the bars have the same impedance and that $T_i + T_r = T_t$, simplifies equation 2-38 to

$$\dot{\gamma} = \left(\frac{D_s}{2L_s}\right)\frac{-2T_r}{K}. \tag{2-39}$$

Shear strain rate history is developed from the reflected pulse using this relation and an example is show in **Error! Reference source not found.**. The shear strain history ($\gamma(t)$) is obtained by taking the integral of the shear strain rate history with respect to time.

$$\gamma(t) = \int_0^t \dot{\gamma}(t_1)dt_1 \tag{2-40}$$

The torque on the sample is taken from the torque measured in the transmitted pulse (T_r). The shear stress (τ) is calculated as

$$\tau = \frac{T_t r}{J} = \frac{2T_t}{\pi {D_s}^2 t}, \tag{2-41}$$

where t is the thickness and of the thin walled tube sample (seen in Figure 2-6) and $t \ll D_s$. The shear stress history is plotted with the shear strain rate history in **Error! Reference source not found.**. Plotting the shear stress history from equation 2-41 versus the shear strain history from equations 2-39 and 2-40 give the classic stress-strain plot as seen in **Error! Reference source not found.**3.

Table 2-1 Typical Values

Excitation Voltage(V_{ex})	36 V
Shear Strain Gauge Nominal Resistance(R)	1000Ω
Shear Strain Gauge Factor(f)	2.08
Bar Radius(r)	12.7mm
Bar Shear Modulus(G)	26.7 MPa**
Sample Average Diameter(D_s)	10mm
Sample Thickness(t)	1mm

Sample Length(L_s)	3mm

2.4 Results and Analysis

Figure 2-12: Sample shear strain rate history and shear stress history shows the ability of

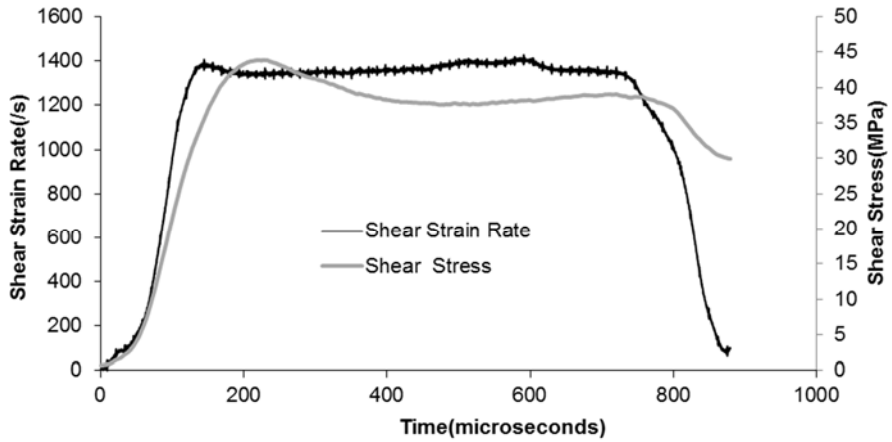

Figure 2-12: Sample shear strain rate history and shear stress history

the testing apparatus to achieve a nearly constant strain rate. The ability of the TKB method in that it can provide a pulse (about 700 micro seconds) with a nearly constant

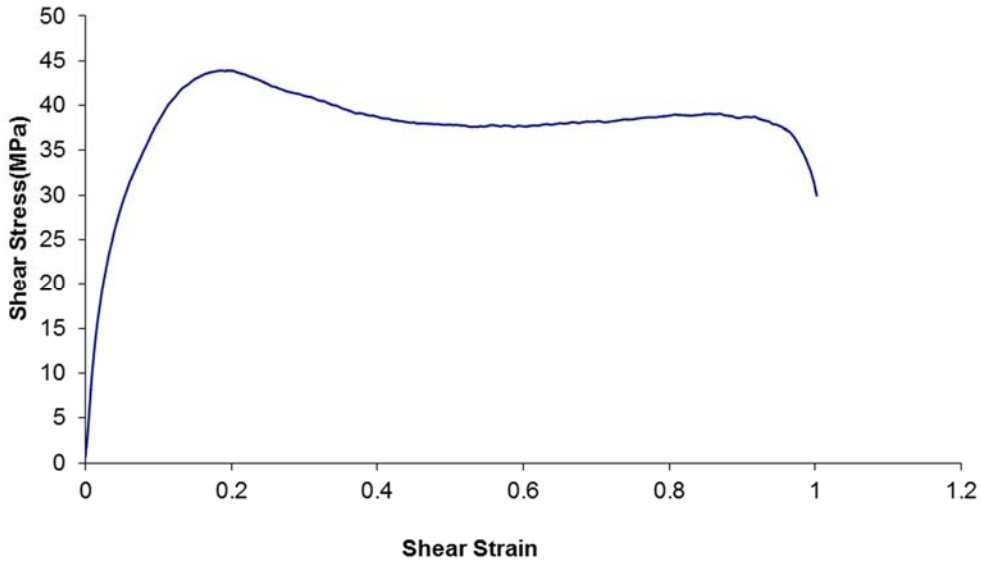

Figure 2-13: τ vs. γ plot

strain rate with a rise time of about 100 microseconds. The shear stress peaks after the shear strain rate has plateaued. The sample first demonstrates viscoelastic behavior as stress increases less than linearly with strain. As shear stress at what will be called the transient peak stress (τ_{peak}) the material behavior transitions to purely viscous flow behavior where stress is dependent on strain rate and independent of the accumulated strain. This is clear as stress levels out to a constant value that will be called the flow stress (τ_{flow}). For tests where more strain is allowed to develop the material begins to strain harden and eventually fracture (Fleck, Stronge, & Liu, 1990). This will be seen later in tests at a higher strain rates. Both the transient peak stress and flow stress are dependent on both temperature and strain rate. A matrix of temperatures and strain rates on PC using the TKB method was performed by Shen (Shen, 2007) and the results were fit with Ree-Eyring model (Ree & Eyring, 1955).

CHAPTER 3. SHEAR INDUCED AXIAL STRESS

3.1 Introduction

This TKB method was developed to measure the sample's axial response to shear stress to test the predictions of an isotropic non-linear elastic model for polycarbonate developed by Goel et al (Goel, Strabala, Negahban, & Turner, 2009). The model is applicable to early in the shearing where the deformation can be considered elastic with no plastic flow. The mathematical model for Cauchy stress tensor (**T**) (Goel, Strabala, Negahban, & Turner, 2009) is as follows:

$$\boldsymbol{T} = \kappa\frac{(J-1)}{J}\boldsymbol{I} + J^{-\frac{5}{3}}\left(\boldsymbol{B} - \frac{tr(\boldsymbol{B})}{3}\boldsymbol{I}\right) \tag{3-1}$$

where J is the volume ratio, which is equal to the determinant of the deformation gradient $\mathbf{F}$, $\mathbf{I}$ is the identity tensor, and $\mathbf{B}$ is the left Cauchy stretch tensor defined as $\mathbf{B} = \mathbf{F}\mathbf{F}^T$. The two material parameters κ and G are the bulk modulus and shear modulus at zero load and were taken from the ultrasonic measurements (Goel, Strabala, Negahban, & Turner, 2009) as

$$\kappa = 4760\ MPa, G = 1072\ MPa. \tag{3-2}$$

To set up and analyze these tensors it is necessary to set up a set of orthonormal base unit vectors $\mathbf{e_i}$. A cylindrical coordinate system works well for this thin walled tube sample. $\mathbf{e_1}$ is the direction of the shear or the circumferential direction. $\mathbf{e_2}$ is the axial direction and $\mathbf{e_3}$ is the radial direction. With these unit vectors it is possible to construct the deformation tensor (**F**) for the sample under shear can be written as

$$\boldsymbol{F} = \boldsymbol{e}_1\otimes\boldsymbol{e}_1 + \lambda\boldsymbol{e}_2\otimes\boldsymbol{e}_2 + \gamma\boldsymbol{e}_1\otimes\boldsymbol{e}_2, \tag{3-3}$$

where λ is the axial stretch, γ is the shear strain, and "$\otimes$" denotes the tensor product. From the deformation tensor shown above J, **B**, and tr(**B**) are

$$J = \det(\boldsymbol{F}) = \lambda, \tag{3-4}$$

$$\boldsymbol{B} = (1+\gamma^2)\boldsymbol{e}_1\otimes\boldsymbol{e}_1 + \boldsymbol{e}_2\otimes\boldsymbol{e}_2 + \lambda^2\boldsymbol{e}_3\otimes\boldsymbol{e}_3 + \gamma(\boldsymbol{e}_1\otimes\boldsymbol{e}_2 + \boldsymbol{e}_2\otimes\boldsymbol{e}_1), \tag{3-5}$$

$$tr(\boldsymbol{B}) = 2 + \lambda^2 + \gamma^2. \tag{3-6}$$

Applying these values for deformation to the model in equation 3-1 gives four non-zero stress values:

$$T_{11} = \kappa\frac{(\lambda-1)}{\lambda} + G\lambda^{-\frac{5}{3}}\frac{(1-\lambda^2+2\gamma^2)}{3}, \tag{3-7}$$

$$T_{22} = \kappa\frac{(\lambda-1)}{\lambda} + G\lambda^{-\frac{5}{3}}\frac{(1-\lambda^2-\gamma^2)}{3}, \tag{3-8}$$

$$T_{33} = \kappa\frac{(\lambda-1)}{\lambda} + G\lambda^{-\frac{5}{3}}\frac{(2\lambda^2-2-2\gamma^2)}{3}, \tag{3-9}$$

$$T_{12} = G\lambda^{-\frac{5}{3}}\gamma \tag{3-10}$$

where T_{11} is the Cauchy stress in the circumferential direction, T_{22} is the Cauchy stress in the axial direction, T_{33} is the Cauchy stress in the radial direction, and T_{12} is the Cauchy shear stress in the circumferential-radial plane. In the case, there are two potential simplifications can be used to describe shear deformation of the sample. The first is simple shear where the axial stretch (λ) is assumed to be one. The second is plane-stress simple shear where the radial stress (T_{33}) is assumed to be zero and λ is calculated as the value that makes T_{33} zero. This TKB method allows for the measurement of the shear

stress (T_{12}) and axial stress (T_{22}). The measured axial stress can be compared with the model predictions.

In addition to testing the predictions of the isotropic non-linear elastic model (Goel, Strabala, Negahban, & Turner, 2009), this method will allow the observation of axial stress of the sample under shear as the sample deforms past the elastic range into yielding and plastic flow.

3.2 Experimental Technique

Three modifications are made to standard TKB method to also measure the axial response of the material. An axial strain gauge bridge on the output bar is used to

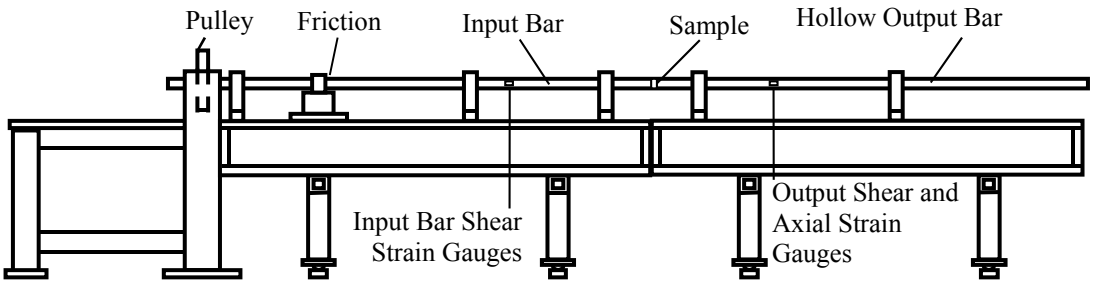

Figure 3-1: Kolsky bar set up for measuring shear induced axial stresses

measure the stress induce along the axis of the bar and sample. The axial stresses induced on the sample and transmitted to the output bar are very small. It is necessary to decrease the bar cross-sectional area to magnify resulting strains measured in the strain gauges. The clamped section of the bar is typically maximized to maximize the time duration of loading pulse with ensuring that the incident and reflected pulses don't overlap being the limiting factor in typical TKB tests. In this case, loading and release of the friction clamp has axial effects on the same order of magnitude of that of the sample.

The clamped section has to be significantly reduced to prevent that pulse from the clamp from overlapping the axial response of the sample.

3.2.1 Hollow Output Bar

The stresses induced along the axis of the sample are a couple orders of magnitude smaller than the shear stresses and cannot be detected with the strain gauges on a solid bar. The input bar has to be solid to withstand the friction clamp, but the 1 in. diameter solid output bar can be replaced by a hollow aluminum bar with an end cap for attaching the sample. The hollow output bar is 1 in. diameter thin walled tube with an approximately 1 mm thickness. The stresses experienced by the output bar are magnified by a factor of 8 by reducing the cross-sectional of the output bar. This makes it possible to measure the relatively small shear induced axial stress.

3.2.2 Output Bar Axial Strain Gauge Bridge

As the sample is loaded by the torsion pulse, the shear deformation introduces volume changes in the sample. For the sample to change dimensions in the axial direction, it has

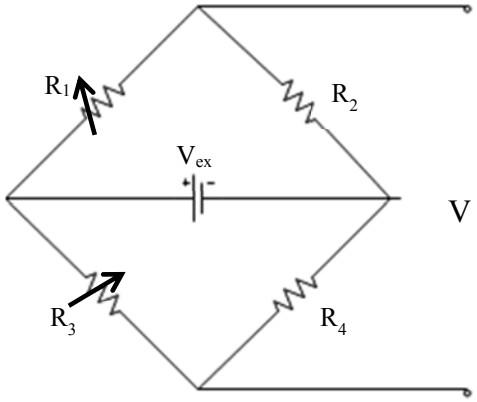

Figure 3-2 Wheatstone bridge where V_{ex}=Excitation Voltage, V= Measured Voltage, R_1 and R_3 are strain gauges, and R_2 and R_4 are resistors.

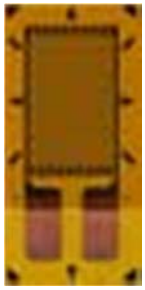

Figure 3-3: MicroMeasurement Strain Gauge

to exert a force on the aluminum bars. The force exerted on the aluminum bar result in pressure or tension pulses that travel down the bar. These pulses are measured using axial strain gauges. Two MicroMeasurement strain gauges (as seen in Figure 3-3) orientated along the axis of the bar are mounted in the same position along the bar as the shear strain gauges. The strain gauges are configured in a Wheatstone half bridge circuit as can be seen in Figure 3-2. The strain gauge bridge is excited with about 35 V and the output voltage is measured by the same Nicolet MultiPro digital oscilloscope use to measure the shear pulses.

3.2.3 Adjustment for Axial Effects of Initial Bar Loading

It was found that the release of the clamp results in axial stress on the same order of magnitude as the sample's axial response. The friction clamp introduces a complex stress

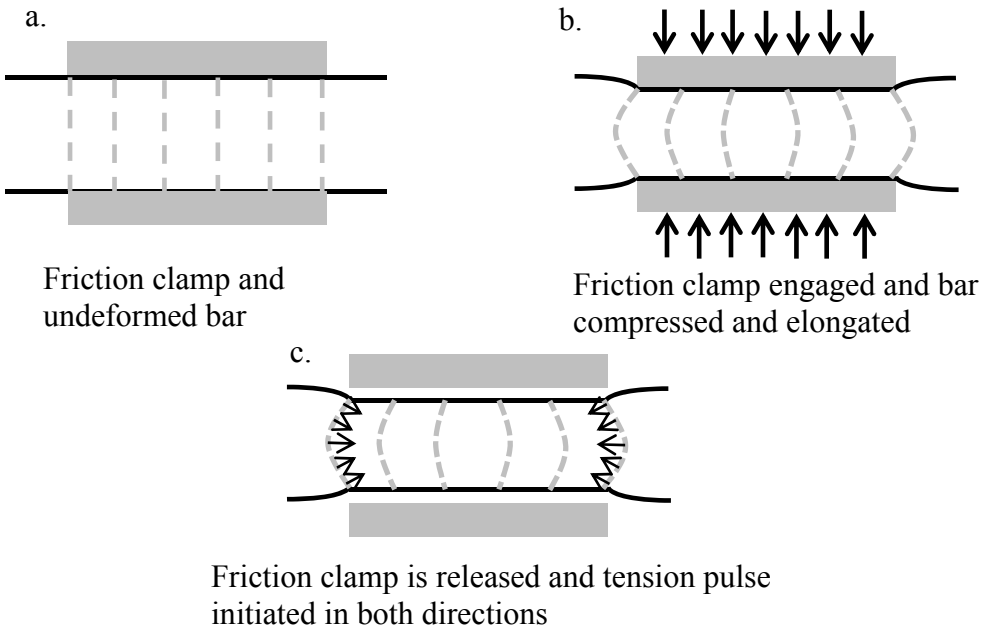

Figure 3-4: Effect of Friction Clamp on Clamped Portion of the Bar

state to the 3 inch section of the input bar that it clamps. The compression that acts perpendicular to the axis of the bar tends to cause elongation along the axis of the bar. That elongation is constrained due to friction at the interface of the surface of the bar and the friction clamp. Figure 3-4 b. shows an exaggeration of the constrained elongation. When the bolt breaks and the friction clamp is suddenly released the deformed bar will suddenly try to revert to its undeformed state. To get back to its initial state, it will pull against the bar initiating a tension pulses that travel in both direction from the friction clamp as seen in Figure 3-4 c. Also seen in Figure 3-4 c is that those tension stresses are not all directly oriented with the axis of the bar.

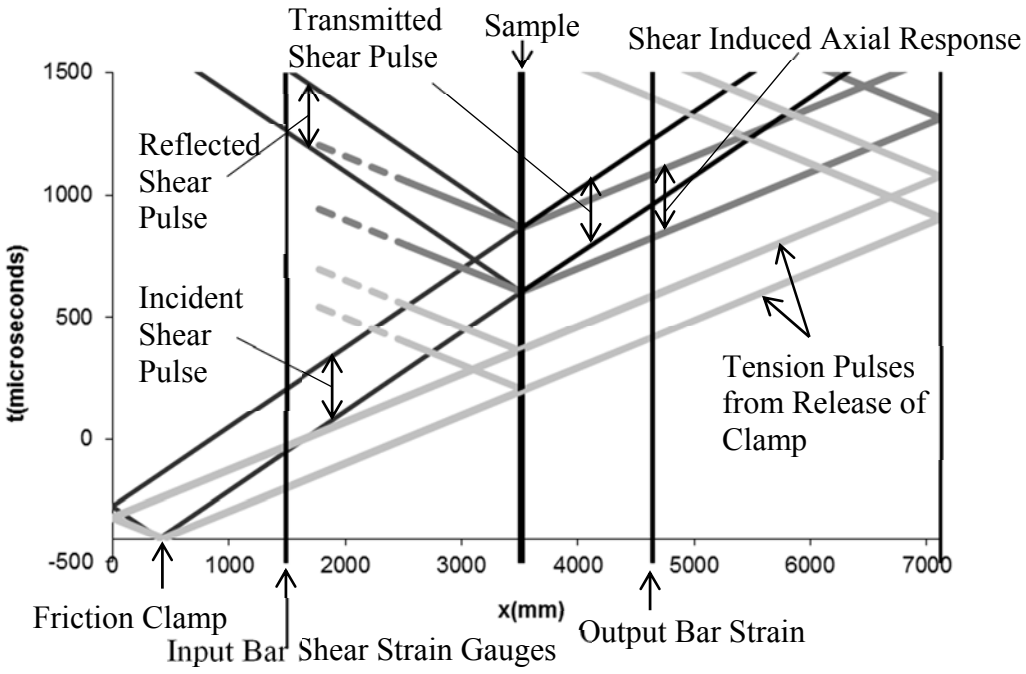

Figure 3-5: x-t diagram showing shear pulses, shear induced axial response, and effect of releasing the clamp.

It is important to note that in the x-t diagram in Figure 3-5 that the longitudinal waves such as the tension pulses from the clamp release and sample axial response travel at a higher speed than the shear wave. The shear waves are virtually invisible on the axial

strain gauges and the longitudinal waves are invisible on the shear gauges. In standard TKB tests the clamped section is maximized in order maximize the duration of the shear pulse. Having a long pulse ensures that yield and plastic flow have time to develop even for low strain rates. However, it was found that when a large clamped section was used the pulses from the release of the clamp overlap with the sample's axial response to shear stress. Reducing the clamped distance, to the 16 inches shown in Figure 3-5, results in adequate separation between the pulses from the clamp and sample axial response.

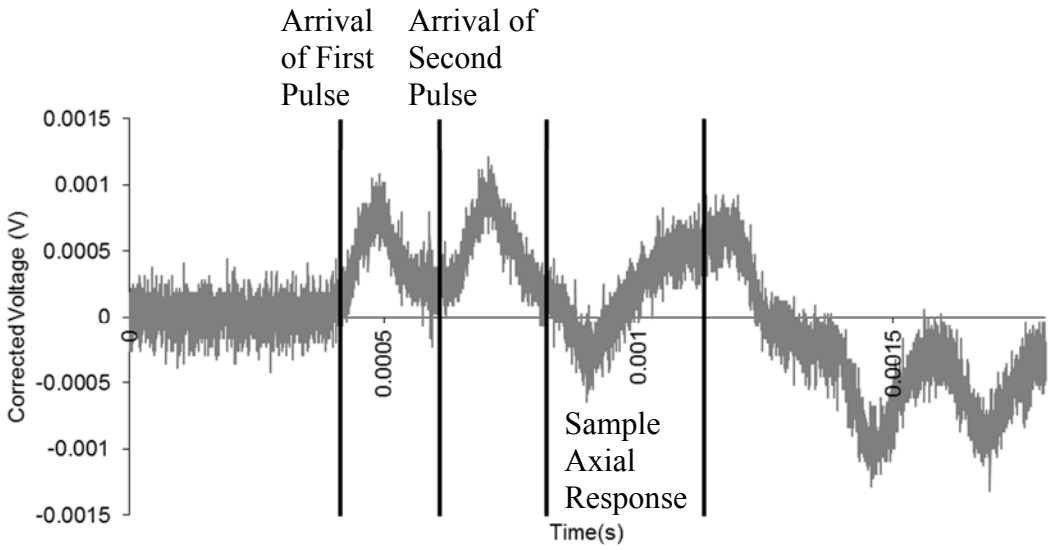

Figure 3-6: Axial strain gauge voltage history with arrival times based on x-t analysis.

Figure 3-6 shows the tension pulses created by the release of the clamp. They arrive at the exact time predicted by length of the bar and the longitudinal wave speed. However, the duration of these pulses is much longer than would be expected due to a 3 in compressed section. The reason for this goes back to the fact that not all of the stress is acting along the axis of the bar. The small amount of stress that is aligned with the axis of the bar reaches the output bar strain gauge at the predicted time. The stress that is at

small angles from the axis of the bar travels at small angles with axis of the bar and reflects off the surface bar as necessary. The larger the angle, the larger distance traveled by longitudinal stress waves and therefore travels slower down the bar. The complex stress profile in the input bar is transmitted through the sample as two pressure pulses. The voltage history when converted to force shows that the sample experiences two quick pulses of about 100 N or 20 lbf. This effect is inherent to the operation of the friction clamp. This small force will have a negligible effect on the sample and by reducing the clamped distance allows the clamp effects to be separated from the sample axial response to shear that is of interest in these experiments.

3.3 Experimental Analysis

The shear strain rate, shear strain, and shear stress histories are determined by the methods outlined in sections 2.3.1 and 2.3.2 with modifications shown below. For this experiment in addition to these histories, a history of axial stress is also needed.

3.3.1 Modifications to TKB Analysis Due to Hollow Output Bar

The different shape of the output bar results in modifications to the way torque in the output bar and the torsional wave analysis. In this case the input and output bars have unequal polar moments of inertia and therefore unequal torsional impedances. The input bar polar moment of inertia (J_i) and torsional impedance (K_i) have the same values as before. The polar moment of inertia for the hollow output (J_o) and torsional impedance for the hollow output bar (K_o) are calculated as follows:

$$J_o = \frac{\pi\left(r_{outer}^4 - r_{inner}^4\right)}{2} \tag{3-11}$$

$$K_o = \rho J_o C_s = \rho \frac{\pi(r_{outer}^4 - r_{inner}^4)}{2} C_s \quad (3\text{-}12)$$

where ρ is the density of the bar, r_{outer} and r_{inner} are the outer and inner radii of the bar, and C_s is the measured shear wave speed in the bar. This value for J_o will be used for the calculation of transmitted torque (T_t) and sample shear stress (τ) via equations 2-12 and 2-41. Equations 2-35 and 2-36 are still valid for the calculation of the rotational speeds of the input and output bars are still valid. However the torsional impedances in the two equations are no longer equal.

$$\omega_{input\ bar} = \frac{-T_{incident} + T_{reflected}}{K_i} \quad (3\text{-}13)$$

$$\omega_{output\ bar} = -\frac{T_{transmitted}}{K_o} \quad (3\text{-}14)$$

The shear strain rate is still calculated the same way it was in equation 2-37.

$$\dot{\gamma} = \frac{\omega_{output\ bar} - \omega_{input\ bar}}{L_s}\left(\frac{D_s}{2}\right) = \left(-\frac{T_{transmitted}}{K_o} + \frac{T_{incident} - T_{reflected}}{K_i}\right)\left(\frac{D_s}{2L_s}\right) \quad (3\text{-}15)$$

L_s and D_s are the sample length and average diameter respectively as shown in Figure 2-6. For balance bar analysis only the reflected pulse torque history is required to calculate the shear strain rate. The unbalanced bar analysis necessary for this experiment requires the incident, reflected, and transmitted pulses be lined up based on travel of the shear waves. With these modifications to the TKB method the shear stress and shear strain rate histories are determined from the shear strain gauge bridge voltage histories.

Table 3-1: Typical Values for Unbalanced Torsional Analysis

	Input Bar	Output Bar
Outer Radius(r_{outer})	12.7mm	12.7mm
Inner Radius(r_{inner})	N/A	11.8mm
Shear Wave Speed(C_s)	3087 m/s	3111 m/s
Polar Moment of Area(J)	4.09E-8 m^4	1.031E-8 m^4
Shear Modulus(G)	26.8 GPa	26.1 GPa
Torsional Impedance(K)	.354 Nms	.0865 Nms
Density(ρ)	2810 kg/m^3	2700 kg/m^3
Axial Wave Speed(C_a)	5128 m/s	5145 m/s
Cross-Sectional Area(A)	5.07E-4 m^3	6.85E-5 m^3

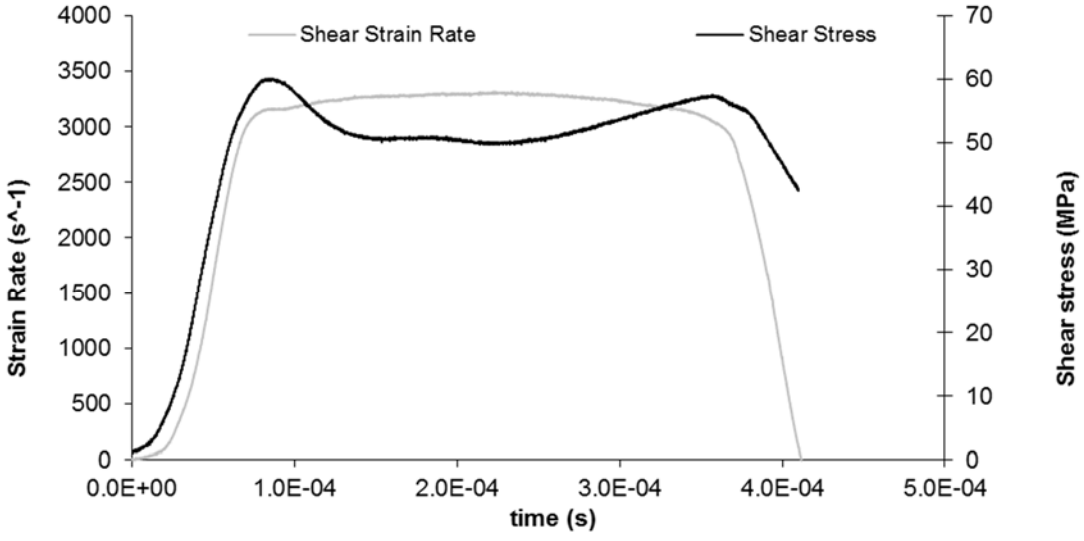

Figure 3-7: Shear Stress and Shear Strain Rate Histories

In the same way as before the shear strain rate can be integrated to give a shear strain history. This strain history can be plot both shear and axial stress vs. shear strain.

3.3.2 Measurement of Sample Induced Axial Stress

The axial stress induced in the sample is taken from the voltage history measured on the digital oscilloscope from the strain gauge half bridge on the output bar seen in Figure 3-8. Even with balancing the strain gauge bridges with a potentiometer, there tends to be some drift in the voltage signal from the time the bridge is balanced until the test is performed.

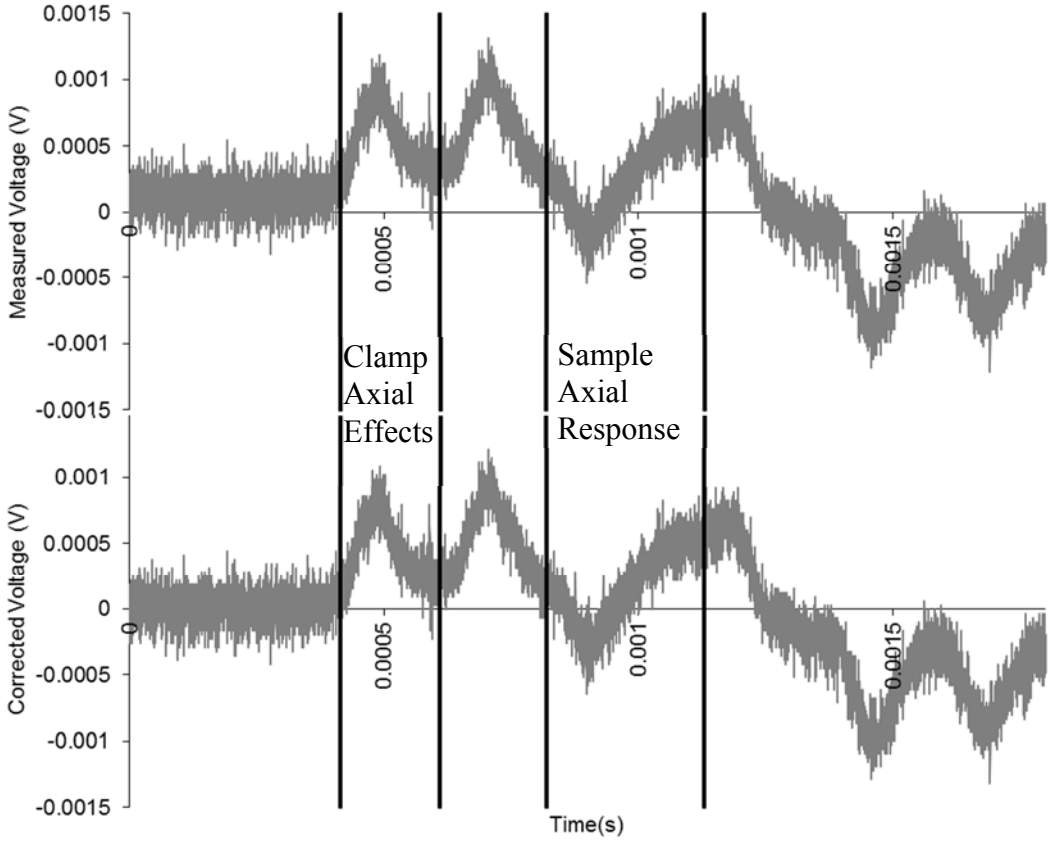

Figure 3-8: Voltage History Recorded by Digital Oscilloscope and Corrected Signal

The average of the flat part is taken and subtracted from the signal. This corrected voltage is used in the analysis. Strain gauge and Wheatstone bridge analysis is necessary

to use this voltage history to derive an axial stress history of the sample. The general equation for Wheatstone bridge is

$$V = V_{ex}\left[\frac{R_3}{R_3+R_4} - \frac{R_2}{R_1+R_2}\right]. \tag{3-16}$$

The active gauges and the resistors have the same nominal resistance(R) of 1000 Ω. The resistance of active gauges changes with strain(ε) in the bar.

$$R_1 = R_3 = R + f\varepsilon \; and \; R_2 = R_4 = R \tag{3-17}$$

Combining equations 3-16 and 3-17 gives

$$V = V_{ex}\left(\frac{R+f\varepsilon}{2R+f\varepsilon} - \frac{R}{2R+f\varepsilon}\right) = \frac{V_{ex}f\varepsilon}{2R+f\varepsilon}. \tag{3-18}$$

For small values of strain equation 3-18 can be simplified to

$$V \approx \frac{V_{ex}f\varepsilon}{2R} \tag{3-19}$$

and strain can be solved for as

$$\varepsilon = 2\frac{VR}{V_{ex}f}. \tag{3-20}$$

Since the bar is elastic 7075 Aluminum the force(F) in the bars and therefore on the sample can be computed.

$$F = A_{bar}\sigma = A_{bar}E\varepsilon = 2\frac{A_{bar}EVR}{V_{ex}f} \tag{3-21}$$

Dividing that force history from the output bar by the cross-sectional area (A_{sample}) of the sample gives the axial stress (σ_{axial}) in the sample.

$$\sigma_{axial} = \frac{F}{A_{sample}} = \frac{F}{2\pi D_s t} = 2\frac{A_{bar}EVR}{V_{ex}f2\pi D_s t} \quad (3\text{-}22)$$

Table 3-2: Values for Calculation of Axial Strain Gauge Analysis

Excitation Voltage(V_{ex})	~35V
Gauge Factor(f)	2.08
Sample Average Diameter(D_s)	18.58 mm
Sample Thickness(t)	.58 mm
Bar Elastic Modulus(E)	72.84 GPa
Nominal Resistance(R)	1000Ω
Sample Cross-sectional Area(A_{sample})	3.41E-5 m^2
Bar Cross-sectional Area(A_{bar})	6.58E-5 m^2

The axial stress history for the period of the shearing of the sample is found using equation 3-22 and shown in Figure 3-9.

$$\sigma_{axial} = \frac{F}{A_{sample}} = \frac{F}{2\pi D_s t} = 2\frac{A_{bar}EVR}{V_{ex}f2\pi D_s t} \quad (3\text{-}22)$$

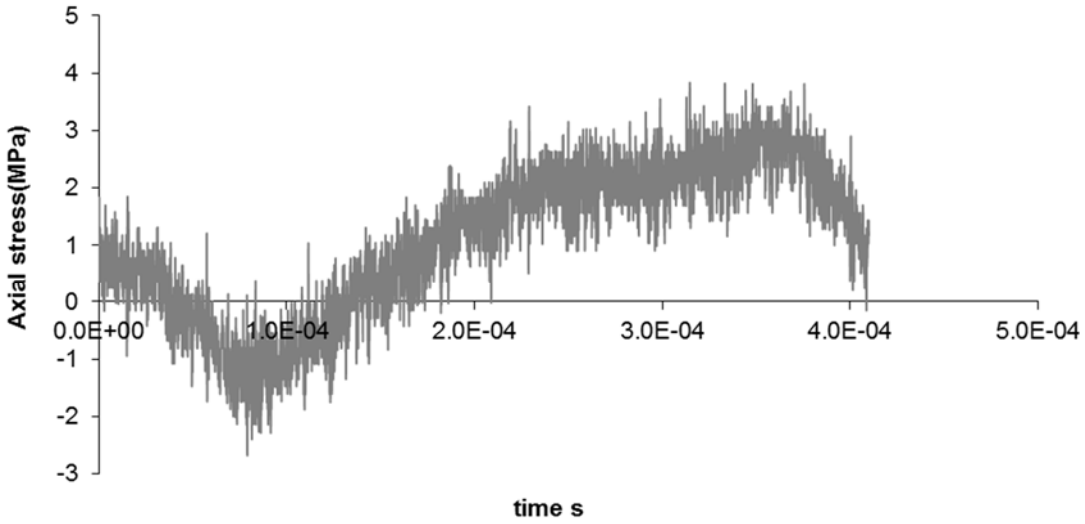

Figure 3-9: Sample Axial Stress History

3.4 Experimental Results

3.4.1 General Axial Stress Response

The shear strain rate shown in Figure 3-7 is integrated as shown in equation 2-40 to get

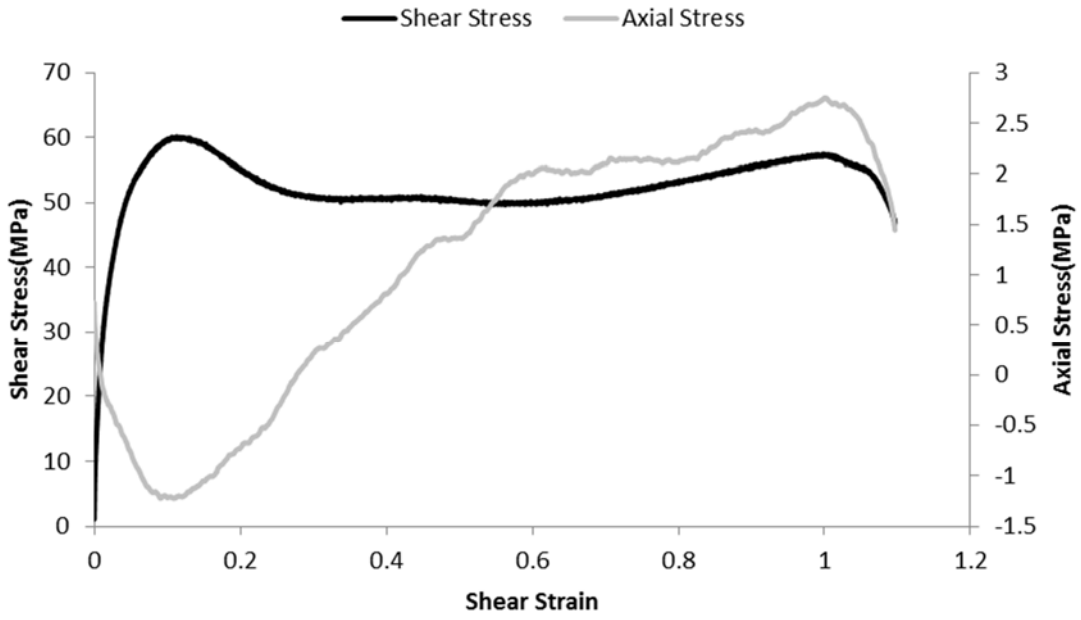

Figure 3-10: Shear and Axial Stress vs. Shear Strain

the shear strain history. Combining the shear strain history with the shear stress history in Figure 3-7 and the axial stress history in Figure 3-9 gives a shear and axial stress vs. shear strain as shown in Figure 3-10. While the sample is being deformed visco-elastically the sample expands in the axial direction, but is constrained by the bar. Therefore a compressive stress is induced in the sample and transmitted to the output bar. The sample attempts to expand in the axial direction up to the point of yielding. At the yield point the sample stops expanding and starts contracting in the axial direction. Since once again the sample is constrained in the axial direction by the bars so as the sample contracts, the compression relaxes and turns to tension as the sample undergoes plastic deformation. When the sample begins the process of strain hardening the axial contraction of the expansion of the sample slows, seen as the axial tension while continuing increase, its increase slows. Appendix A show the results of four of these TKB tests measuring sample axial response including the one

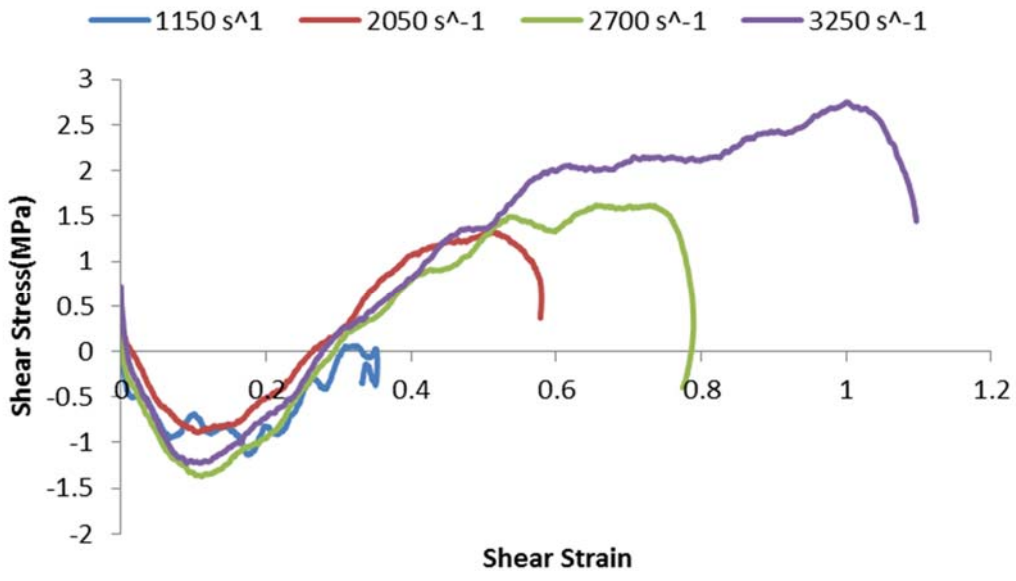

Figure 3-11: Sample axial response plotted versus shear strain over a range of strain rates

shown in the previous examples (Figure 3-6, Figure 3-7, Figure 3-8, Figure 3-9, and

Figure 3-10). These tests cover a range of strain rates. The axial stress from all from all four tests are plotted together in Figure 3-11, and this shows the repeatability of these results. While the magnitude of shear stress changes with strain rate, the strains at which yielding, plastic flow, and all characteristic deformation behavior changes little with strain rate. Thus the axial responses of the four tests line up when plotted versus shear strain. If there is any effect of strain rate on this axial response in this range of strange rates; it is too small to be detected by this method.

3.4.2 Comparisons with Isotropic Non-Linear Elastic Model

At this point the isotropic non-linear elastic model (Goel, Strabala, Negahban, & Turner, 2009) is tested versus the experimental results. Both the simple shear and the plane-stress simple shear forms of the model will be compared to the tests data. Since the model is an elastic model it should only predict the shear and axial stress in the elastic range of deformation. The model will be compared to test at a shear strain rate of

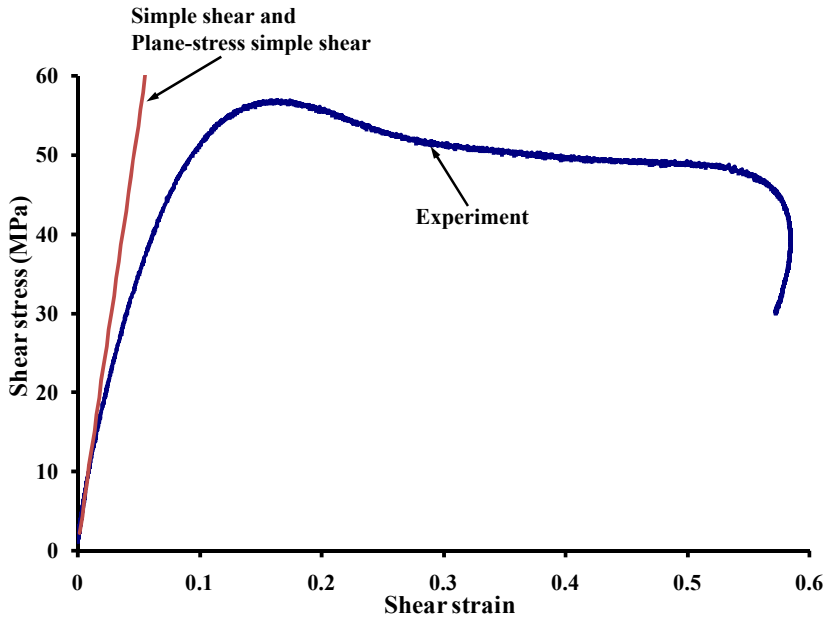

Figure 3-12: Comparison of experimental results and model prediction for shear stress vs. shear strain.

2050 s^{-1}. There is no practical difference in the model predictions for the shear stress by the model using equation 3-10 for simple shear and plane-stress simple shear. They form a single line in Figure 3-12. The model appears to be very close to the experimental results up to about .03 in shear strain. The model predictions for axial stress vary on whether the sample deformation can be considered simple shear or plane- stress simple shear. Up to .03 shear strain the experimental result follow the simple shear curve closest. From the .03 to .08 the experimental results fall between the curves. The isotropic non-

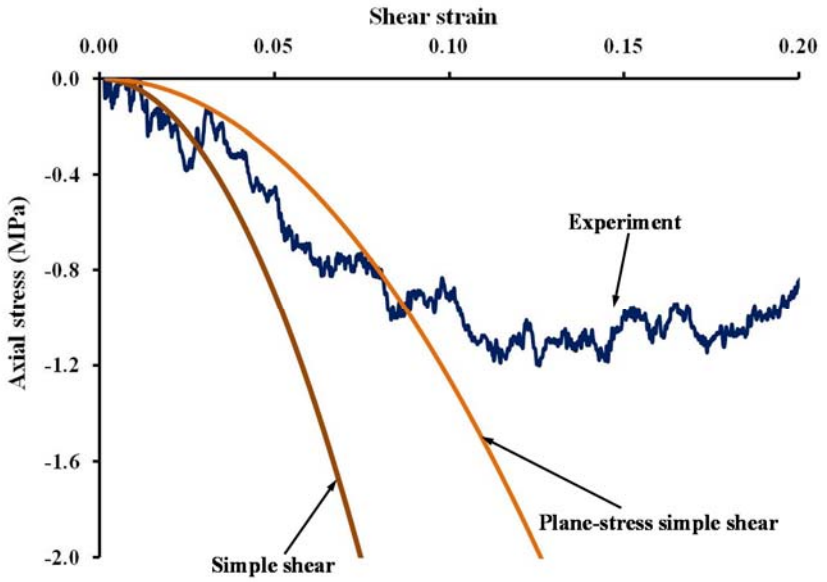

Figure 3-13: Experimental results for axial stress compared with model predictions

linear elastic model developed using ultrasonic tests (Goel, Strabala, Negahban, & Turner, 2009) accurately predicts the high rate deformation behavior of the TKB test both in terms of shear and axial stress up to .03 shear strain when simple shear is assumed.

3.4.3 Conversions to Invariant Stress and Strain

In appendix A, the deformation is shown in terms of deviatoric invariant stress, mean stress, and deviatoric invariant strain. This allows for the better understanding of the

stress state when both shear and compressive stress are present and allows for comparing shear, compressive and combined loading tests. These pure shear tests will be compared with results from the combined loading tests and compressive tests.

CHAPTER 4. DYNAMIC TORSION WITH STATIC AXIAL COMPRESSION

4.1 Introduction

Polycarbonate is an amorphous polymer, meaning that it is composed of long polymeric chains randomly arranged and has no crystal structure. The amorphous structure of the

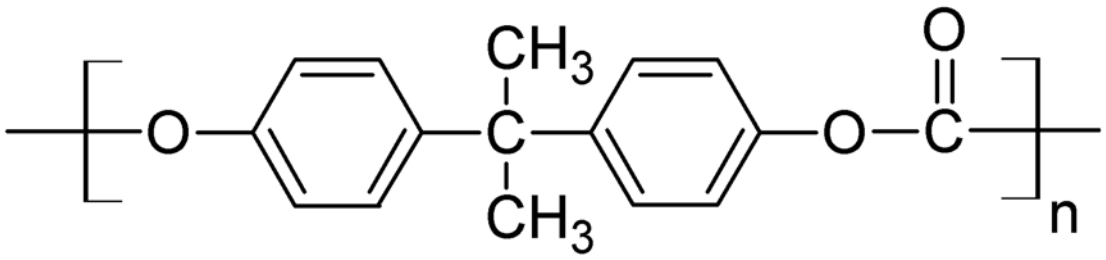

Figure 4-1: Polycarbonate from Biphenyl A Chemical Structure

material leads to it transparency. The chemical structure of this polymer leads to its stiffness and thermal stability (Mehta & Prakas, 2009) and therefore its engineering utility. The yield and flow behavior are heavily dependent on how these molecules move past one another. Shen (Shen, 2007) and Reitsch and Bouette (Rietsch & Bouette, 1990) studied the effects of both strain rate and temperature on the flow stress and yield stress. In both cases, the results were fit to variations of the Ree-Eyring model (Ree & Eyring, 1955):

$$\dot{\gamma} = 2\dot{\gamma}_o exp\left(-\frac{\Delta H}{kT}\right)\sinh\left(\frac{v\tau}{kT}\right) \tag{4-1}$$

where $\dot{\gamma}_o$ is a reference shear strain rate, ΔH is the activation energy for molecular motion, v is the activation volume, k is the Boltzmann constant, T is the absolute temperature and τ is the yield stress. If only shear is occurring, the stresses are purely deviatoric. However, if axial compression is added, volumetric stresses are also present in the

sample. These volumetric stresses can potentially also affect the ability of molecules move past one another. The magnitude of the volumetric stresses can potentially affect the deviatoric stress at which yield and plastic flow occur. This will be investigated in this chapter.

4.2 Experimental Set-up

The TKB experimental method is versatile enough to allow a static compression to the sample, with minimal modification to the experimental method and analysis. Figure 4-2 shows the experimental set up for this series experiments. Both bars and the sample are compressed by the axial piston and stopped by the end stop. It was found that scissor jack could better maintain pressure on the bars and sample than the axial piston. Most of the

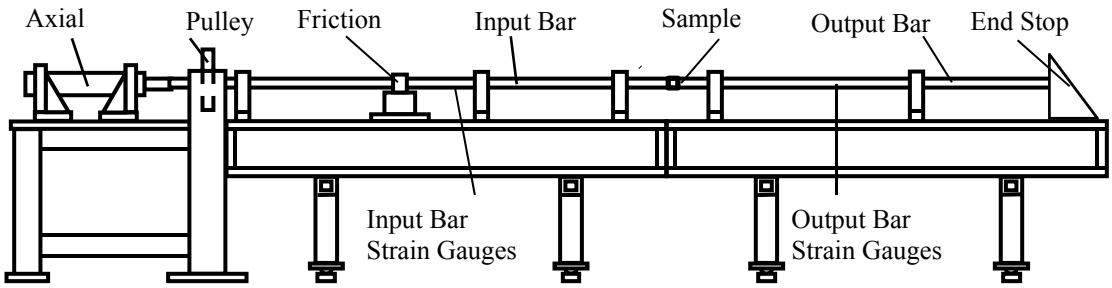

Figure 4-2 Combined loading TKB Set-up

tests were performed with a jack rather the axial piston. Only shear strain gauges are used in the pure TKB tests. Strain gauges oriented along the axis of the bars are also utilized in this test. These axial strain gauges are in the same position along the bar as the shear gauges. The test is performed using the same method described in section 2.3, only that before the clamp is engaged the sample and entire assembly is compressed. When the tests were performed with the axial hydraulic piston, the axial load could be estimated using the pressure on the axial piston. However, the hydraulic piston tended to unload

some before the torsion pulse could be stored and released. When the jack was used, it was necessary to use a strain gauge amplifier with a digital read out to give an indication of the applied compression. Once the axial compression is applied, the torsion pulse is stored using the pulley and friction clamp. The friction clamp bolts breaks and the torsion pulse is released and loads the sample and the output of the strain gauges is recorded.

4.3 Experimental Analysis

4.3.1 Axial Strain Gauge Analysis

The strain gauge analysis for this series of experiments is the same as the analysis described in section 3.3.2 only that in this case the bar is solid and the bar is initially loaded. The axial stress history for the sample shown in Figure 4-3: Sample Axial Stress History is determined from the measured voltage from the output bar axial strain gauge $\sigma axial=FAsample=F2\pi Dst=2AbarEVRVexf2\pi Dst$ (3-22) with the values in Table 2-1. The initial flat section of the history is used to find the initial load of the sample. Even with strain gauge bridges zeroed before test, strain gauge bridges voltages drift in the amount of time it takes to

Table 4-1: Typical Values Combined Loading Axial Strain Gauge Analysis

Bar Cross-sectional Area(A_{bar})	5.07cm^2
Gauge Factor(F)	2.08
Excitation Voltage(V_{ex})	Typically 25 V
Young's Modulus(E)	72.84 GPa

Sample Cross-Sectional Area(A_{sample})	3.68173E-05 m^2

load the bar, clamp, store torque, and release. In cases where the bar is initially unloaded

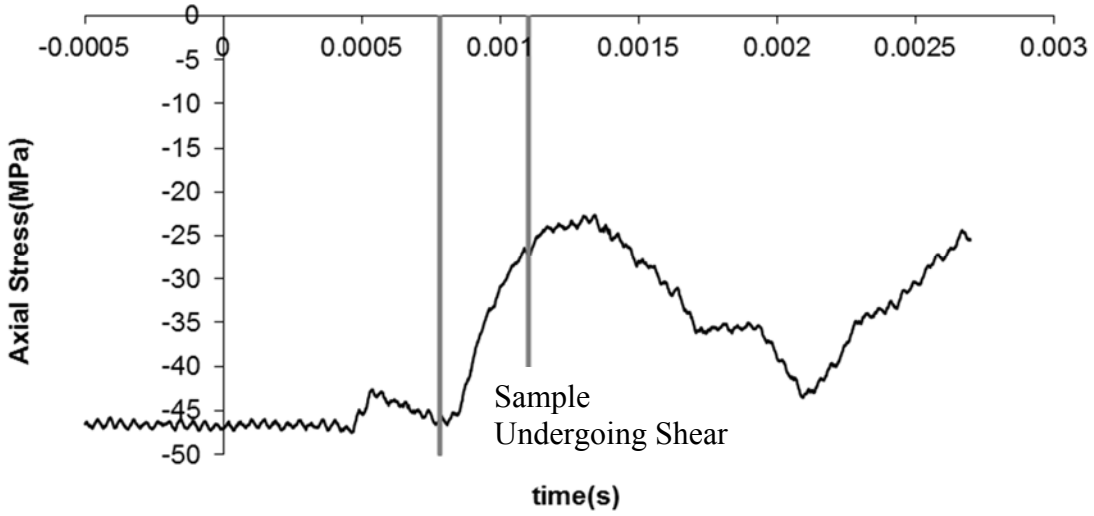

Figure 4-3: Sample Axial Stress History

the drift can be corrected by the initial average voltage or stress, but cannot for non-zero initial loads.

4.3.2 Sample Dimensional Changes Due to Compression

The compression of sample changes the dimensions of the sample critical for TKB analysis, including sample length (L) and second moment of area (J). Data from quasi-static compression test using a hydraulic material testing system along with strain gauge measurement for initial loading are used to obtain the new sample dimensions. The hydraulic test was performed by P. Moy et. al. (Moy, Weerasooriya, Hsieh, & Chen, 2009) at the Army Research Laboratory. The data is given as engineering stress (σ_e) and engineering strain (ε_e). For simplicity both the compressive stress and strain are denoted as positive. Engineering stress is calculated as

$$\sigma_{engr} = \frac{F}{A_o} \tag{4-2}$$

where A_o is initial cross-sectional area of the sample. The engineering stress is used to find a corresponding engineering strain from the data set. The compressed sample length (L) can be found from the initial length (L_o) using the engineering strain as

$$L = L_o(1 - \varepsilon_e). \tag{4-3}$$

Incompressibility is assumed to compute true stress and the other compressed sample dimensions. The length (L) changes by a factor of $(1 - \varepsilon_e)$ the cross-sectional area changes by a factor of $1/(1 - \varepsilon_e)$.

$$\frac{actual\ area}{intial\ area} = \frac{A}{A_0} = \frac{1}{(1-\varepsilon_e)} \tag{4-4}$$

The true axial stress (σ_{true}) of the sample can be computed with this ratio as

$$\sigma_{true} = \sigma_e \frac{A_o}{A} = \sigma_e(1 - \varepsilon_e). \tag{4-5}$$

The thin walled tube can be estimated as rectangular prism with cross-sectional area (A) equal to $2\pi D_s$*t. The thickness and circumference change by the same factor.

$$t = t_o \frac{1}{\sqrt{1-\varepsilon_e}} \tag{4-6}$$

$$\pi D_s = \pi D_{so} \frac{1}{\sqrt{1-\varepsilon_e}}\ therefore\ D_s = D_{so} \frac{1}{\sqrt{1-\varepsilon_e}} \tag{4-7}$$

The sample dimensions L_o, t_o, and D_{so} are measured from the unloaded sample before the test and the loaded sample dimensions L, t, and D_s are used in the dynamic shear analysis described in section 2.3.2. Based on the compressed sample's dimensions, the sample

axial stress history can be found from axial strain gauge analysis, and the shear stress and shear strain rate history are found using shear strain gauge and torsional wave analysis.

The three histories for a typical test are shown in Figure 4-4.

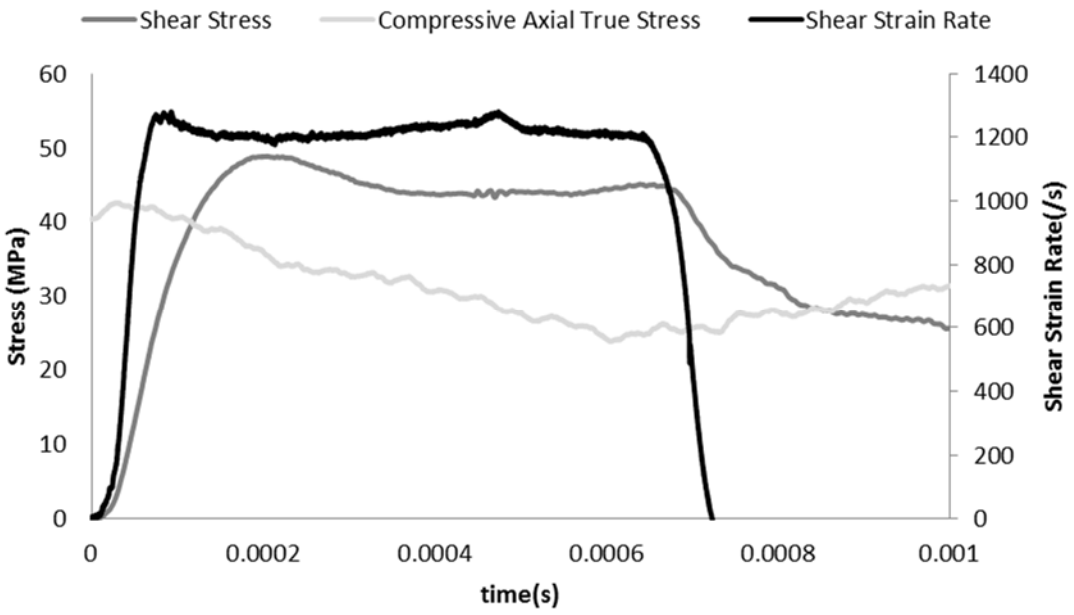

Figure 4-4: Shear Stress, Axial Stress and Shear Strain Rate Histories

4.3.3 Pressure and Deviatoric Invariant Stress

For simplicity the thin walled tube of the sample can be thought of as a rectangular prism

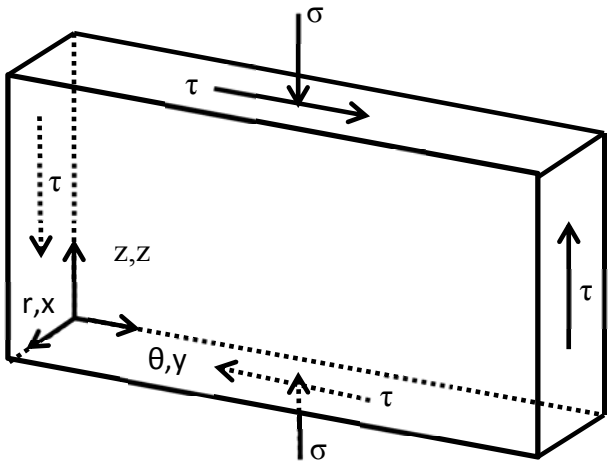

Figure 4-5 Rectangular Prism as Simplification of Thin Walled Tube

with the r, θ, and z axes replaced with x, y, and z axes. The sample can be thought of having a uniform stress state as defined with the stress tensor **T** as follows

$$\boldsymbol{T} = \begin{bmatrix} \sigma_x & \tau_{xy} & \tau_{xz} \\ \tau_{yx} & \sigma_y & \tau_{yz} \\ \tau_{zx} & \tau_{zy} & \sigma_z \end{bmatrix} = \begin{bmatrix} 0 & 0 & 0 \\ 0 & 0 & \tau \\ 0 & \tau & \sigma \end{bmatrix}. \tag{4-8}$$

σ is the measured axial stress history form the axial strain gauge and τ is shear stress measured using the TKB method. τ_{xy}, τ_{xz}, τ_{yx}, and τ_{zx} can reasonably assumed to be zero. Since the sample is compressed in z direction and constrained in x and y directions, σ_x and σ_y will not be zero, but will likely be small enough to be neglected. It is necessary to separate the mean stresses or pressure and the deviatoric stress that cause yielding and plastic flow. Many traditional yield criteria such as octahedral shear stress (or von Mises) yield criterion take into account only deviatoric stresses. However, we wish to test the effects of pressure or volumetric stress on the deviatoric stress at which yielding and plastic flow occurs. The measure for the volumetric stress is the pressure (P), calculated as

$$\mathrm{P} = -\frac{tr(\boldsymbol{T})}{3} = -\frac{\sigma}{3}. \tag{4-9}$$

Subtracting the mean stress (-P) from the stress tensor ($\boldsymbol{T}$) yields the deviatoric stress tensor ($\boldsymbol{T}_d$).

$$\boldsymbol{T}_d = \boldsymbol{T} - \sigma_{mean}\boldsymbol{I} = \begin{bmatrix} \frac{-\sigma}{3} & 0 & 0 \\ 0 & \frac{-\sigma}{3} & \tau \\ 0 & \tau & \frac{2\sigma}{3} \end{bmatrix} \tag{4-10}$$

A deviatoric invariant stress (s) is needed to give a single value to represent the deviatoric stress in the sample. The invariant chosen is

$$s = \sqrt{tr\left(\boldsymbol{T}_d{}^2\right)}. \tag{4-11}$$

$$\boldsymbol{T}_d{}^2 = \begin{bmatrix} \frac{\sigma^2}{9} & 0 & 0 \\ 0 & \frac{\sigma^2}{9} + \tau^2 & \frac{\sigma\tau}{3} \\ 0 & \frac{\sigma\tau}{3} & \frac{4\sigma^2}{9} + \tau^2 \end{bmatrix} \tag{4-12}$$

$$s = \sqrt{tr\left(\boldsymbol{T}_d{}^2\right)} = \sqrt{\frac{2}{3}\sigma^2 + 2\tau^2}. \tag{4-13}$$

The deviatoric invariant stress is proportional to the von Mises stress.

$$s = \sqrt{\frac{2}{3}}\tau_{von\ Mises} \tag{4-14}$$

From the axial and shear stress histories, deviatoric invariant and pressure histories are derived. The effect of the pressure on the deviatoric stress at which yield and flow occur will be studied.

4.3.4 Deviatoric Invariant of Left Cauchy Stretch Tensor

To match the deviatoric invariant of stress, a deviatoric invariant of strain is needed. This strain invariant starts with the deformation tensor (**F**).

$$\boldsymbol{F} = \begin{bmatrix} \frac{\partial x}{\partial X} & \frac{\partial x}{\partial Y} & \frac{\partial x}{\partial Z} \\ \frac{\partial y}{\partial X} & \frac{\partial y}{\partial Y} & \frac{\partial y}{\partial Z} \\ \frac{\partial z}{\partial X} & \frac{\partial z}{\partial Y} & \frac{\partial z}{\partial Z} \end{bmatrix} \tag{4-15}$$

The upper case coordinates represent the undeformed sample, while the lower case coordinates represent the sample in a deformed state. Due to the axial compression in z direction $\frac{\partial z}{\partial Z} = \left(1 - \varepsilon_{engr}\right) = \lambda$. Unfortunately there is no way of measuring the change in that strain during the experiment. The strain used is the same strain used to determine the sample dimensions is section 0. It is assumed that the strain in the z direction remains relatively unchanged. Incompressibility is assumed so $\frac{\partial x}{\partial X} = \frac{\partial y}{\partial Y} = \frac{1}{\sqrt{\lambda}}$. $\frac{\partial y}{\partial Z}$ is the shear strain (γ) determined through the TKB method. The rest of the terms can be assumed to be zero.

$$\boldsymbol{F} = \begin{bmatrix} \frac{1}{\sqrt{\lambda}} & 0 & 0 \\ 0 & \frac{1}{\sqrt{\lambda}} & \gamma \\ 0 & 0 & \lambda \end{bmatrix} \tag{4-16}$$

The Left-Cauchy stretch tensor (**B**) is calculated.

$$\boldsymbol{B} = \boldsymbol{F}\boldsymbol{F}^{\boldsymbol{T}} = \begin{bmatrix} \frac{1}{\lambda} & 0 & 0 \\ 0 & \frac{1}{\lambda} + \gamma^2 & \lambda\gamma \\ 0 & \lambda\gamma & \lambda^2 \end{bmatrix} \tag{4-17}$$

The volumetric strain are subtracted out to make the Left-Cauchy stretch tensor deviatoric ($\mathbf{B}_d$).

$$\boldsymbol{B_d} = \boldsymbol{B} - \frac{tr(\boldsymbol{B})}{3}\boldsymbol{I} = \begin{bmatrix} \frac{\frac{1}{\lambda} - \lambda^2 - \gamma^2}{3} & 0 & 0 \\ 0 & \frac{\frac{1}{\lambda} - \lambda^2 + 2\gamma^2}{3} & \lambda\gamma \\ 0 & \lambda\gamma & \frac{-2\frac{1}{\lambda} + 3\lambda^2 - \gamma^2}{3} \end{bmatrix} \tag{4-18}$$

The deviatoric invariant strain (η) is calculated from the deviatoric Left Cauchy stretch tensor by

$$\eta = \sqrt{tr(\boldsymbol{B}_d^2)} = \sqrt{\frac{2}{3}\left(\gamma^4 - \gamma^2\lambda^2 + \frac{4\gamma^2}{\lambda} + \lambda^4 - 2\lambda + \frac{1}{\lambda^2}\right)}. \quad (4\text{-}19)$$

This deviatoric invariant strain will be used to compare the results of the combined loading TKB tests to the pure shear TKB tests and the CKB tests. A deviatoric invariant strain rate ($\dot{\eta}$) can be found from the deviatoric invariant strain history. The Δt is 10^{-7} seconds.

$$\dot{\eta} = \frac{d\eta}{dt} \approx \frac{\Delta\eta}{\Delta t} \quad (4\text{-}20)$$

4.4 Results and Analysis

4.4.1 Typical Test Results

For this test, the entire set up is compressed so that sample experience about 45 MPa of axial compressive stress. The torque applied on the pulley in order to achieve shear strain

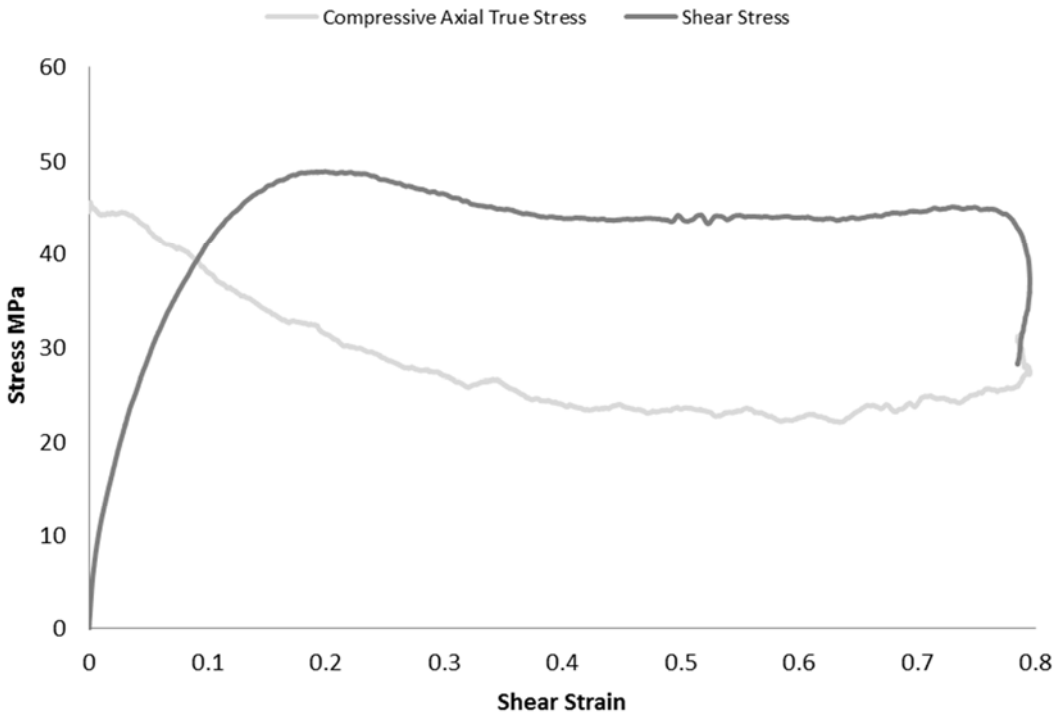

Figure 4-6: Stress vs. Strain Plot

rate of 1200 s^{-1}. The axial strain gauge records an engineering stress in the sample of 46.5 MPa. Based on the analysis done in section 4.3.1, the true stress is calculated as 45.5 MPa and the compressed sample dimensions are found. The outputs from the shear strain gauges and the TKB analysis described in section 2.3.2 give the shear stress and shear strain rate histories seen in Figure 4-4. The plateau of strain rate is averaged to give the nominal value of 1220 $^{s-1}$. In addition to giving the applied stress, the axial strain gauges give a history of the axial stress in the sample also shown in Figure 4-4. It is observed that the sample while undergoing shear partially unloads in the axial direction. Given that in this paper it is shown that shear will induce axial stresses, it should be no surprise that there are axial effects in the compressed TKB tests. As before, the strain rate history is integrated to give a strain history and therefore a stress-strain plot, as seen in Figure 4-6.

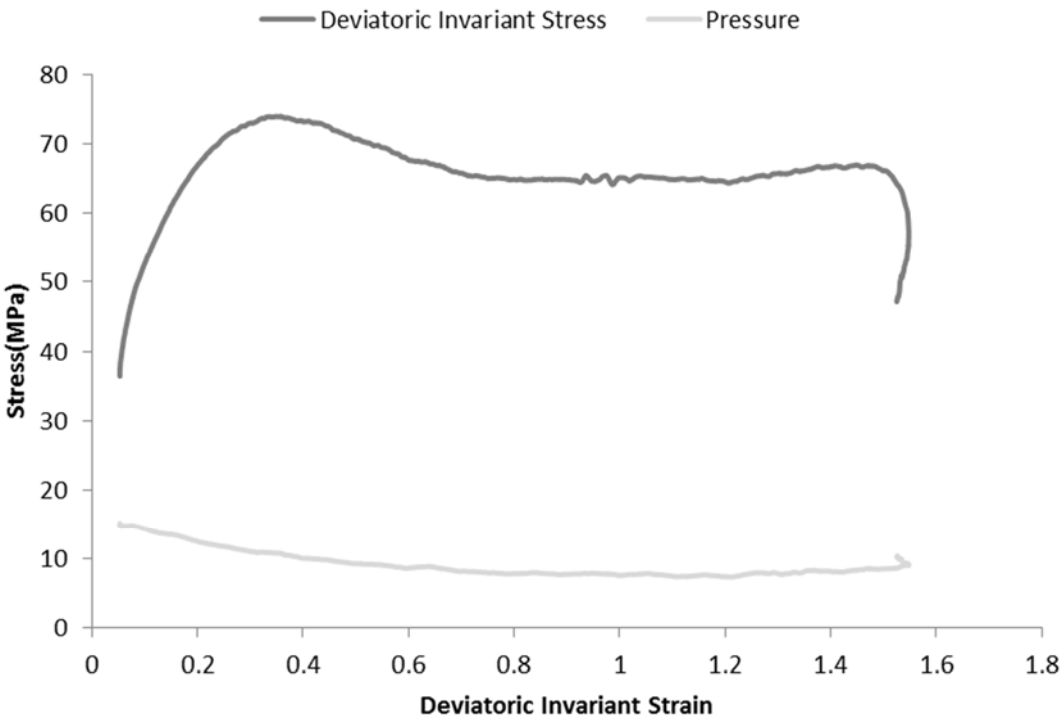

Figure 4-7 Deviatoric Invariant Stress and Mean Pressure vs. Deviatoric Invariant Strain

The deviatoric stress shows classic deformation behavior. First comes visco-elastic deformation, yielding, and then plastic flow and the axial stress declines as the sample deforms. The deviatoric invariant stress (equation 4-13) and pressure (equation 4-9) are calculated and plotted vs. deviatoric invariant strain (equation 4-19) in Figure 4-7. It is desired to understand the effect of pressure on the deviatoric stress at which yielding and

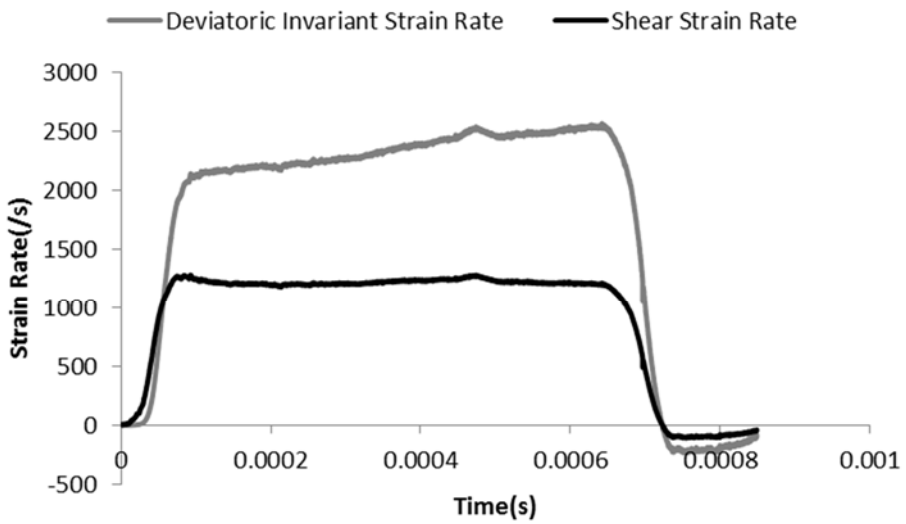

Figure 4-8: Deviatoric Invariant Strain Rate Compared with Shear Strain Rate

plastic flow occurs. The yielding stress is the peak deviatoric invariant stress, in this case 74.0 MPa and the mean stress when yielding occurs is 10.8 MPa. The flow stress is the stress that it levels out to. For consistency the flow stress was chosen as minimum stress after the yielding peak and before the final unloading. For this test the flow stress was found to be 64.1 MPa and the mean stress at that point is 7.74 MPa. The deviatoric invariant strain rate is found from the derivative of deviatoric invariant strain history and is seen in Figure 4-8. Unlike the shear strain rate, the deviatoric invariant strain rate does change significantly over the duration of the test. The rates at the point of yielding and flow are found to be 2204 s^{-1} and 2523 s^{-1} respectively.

4.4.2 Analysis of the Series of Compressed TKB Experiments

The yield stress and flow stress are known to vary with strain rate and temperature. It is desired to determine whether pressure also affects both yield stress and flow stress. Tests were performed at a variety of strain rates and applied axial stresses. Temperature was held constant at room temperature to remove the effect of another variable. The table below contains the nominal shear strain rate, deviatoric invariant yield and flow stresses, deviatoric invariant strain rates at yielding and flow, and the mean stress at yielding and flow for seven combined loading test as well as the four tests (Tests 1-4) from the previous chapter. The tests from the previous chapters are included because the tests with various axial loads have to be compared to tests where the only axial stress is the induced axial stress. Deviatoric invariant stress and mean stress vs deviatoric invariant strain and deviatoric invariant strain rate and engineering strain rate histories for tests 5-11 are shown in Appendix B.

Table 4-2: Experimental Results for Combined Loading TKB Tests

	Shear Strain Rate(/s)	Deviatoric Invariant Yield Stress (MPa)	Deviatoric Invariant Strain Rate at Yield (/s)	Pressure at Yield (MPa)	Deviatoric Invariant Flow Stress (MPa)	Deviatoric Invariant Strain Rate at Flow (/s)	Pressure at Flow (MPa)
1	3251.904	85.0689	5779.601	-0.40174	70.31473	6611.702	0.626496
2	1146.186	78.70324	2284.735	-0.32663	68.76775	2266.735	0.018007
3	2717.268	88.29	5123.175	-0.36153	74.53633	5586.807	0.210166
4	2046.999	80.47927	3734.353	-0.27258	68.97382	3783.074	-0.24272
5	1171.544	82.29349	2104.656	15.22414	72.05861	2273.477	9.581812
6	1219.982	73.99529	2204.215	10.846	64.14551	2523.356	7.741651
7	1283.342	79.45286	2286.946	14.9348	66.97579	2561.269	9.068956
8	1984.266	85.15725	3622.514	9.244085	74.17111	4033.732	5.546451
9	603.7499	90.01289	3345.287	20.63108	84.28719	3425.419	17.62865
10	1177.964	76.24302	2134.67	3.587578	68.2731	2367.475	3.437677
11	1166.647	72.13709	2130.46	9.068263	61.7600	2356.686	5.383052

4.4.3 Regression Analysis

For these tests, both strain rate and pressure are varied. Linear regression analysis will be used to separate and quantify the effects of strain rate and pressure. Based on results and models developed by (Shen, 2007) and (Rietsch & Bouette, 1990), flow stress and yield stress for a given temperature can be modeled as constant plus a term proportional to the natural logarithm of strain rate based on the Eyring model (Eyring, 1936) shown in equation $\frac{\tau}{T} = A\left[\ln(2C\dot{\gamma}) + \frac{\Delta H}{kT}\right]$(1-3. In order that data from the compression experiments in the next chapter can be added to the current data set stresses and strain rates will be deviatoric invariant stresses and deviatoric invariant strain rates. Since the effect of pressure is believed to be due to friction, a linear effect due to friction will be assumed. The model which will be used to fit the data for yield and flow stress is as follows:

$$s_{yield/flow} = C_0 + C_1 \ln(\dot{\eta}) + C_2 P \tag{4-21}$$

The coefficients C_0, C_1, and C_2 will be calculated by regression analysis in Microsoft Excel. From the P-value, t it will be possible to verify a dependence on strain rate and pressure. Generally, the P-value should be less than .05 to show that correlation with the given variable has a less than 5% probability of being due to chance. Table 4-3 and Table 4-4 show the regression analysis for both the yield and flow stress. It should be noted that the intercept is a combination of material constants, a physical constant and temperature from equation $\frac{\tau}{T} = A\left[\ln(2C\dot{\gamma}) + \frac{\Delta H}{kT}\right]$ (1-3).

$$C_0 = A\left[\ln(2C) + \frac{\Delta H}{kT}\right] \tag{4-22}$$

Table 4-3: Regression Analysis for Deviatoric Invariant Yield Stress

		Coefficients	*Standard Error*	*P-value*	*Lower 95%*	*Upper 95%*
C_0	Intercept	-36.342	25.49507	0.191854	-95.1338	22.44973
C_1	$\ln(\dot{\eta})$	14.34372	3.122722	0.001771	7.142708	21.54473
C_2	Pressure	0.376638	0.155971	0.042191	0.016969	0.736308

Table 4-4: Regression Analysis for Deviatoric Invariant Flow Stress

		Coefficients	*Standard Error*	*P-value*	*Lower 95%*	*Upper 95%*
C_0	Intercept	-12.8247	32.3632	0.702263	-87.4544	61.80497
C_1	$\ln(\dot{\eta})$	9.830731	3.943629	0.037358	0.736706	18.92476
C_2	Pressure	0.722104	0.273964	0.029909	0.090342	1.353867

This intercept according to the data set could be positive, negative, or zero. The dependence of yield and flow stress on strain rate and pressure is shown to be significant (P-value<.05) and positive. This shows that increasing pressure increases the deviatoric invariant stress at which yield and flow occur. Large pressures are not achievable in these combined loading tests, because large stresses would deform the sample too much and it would not be possible to estimate their dimensions. Also, samples unload while deforming under torsion. Compression tests will allow for comparison of the very small induced volumetric stress of the pure torsion tests, the moderate pressures of the combined loading torsion tests, and high pressures of the compression tests.

CHAPTER 5. COMPRESSION TESTING

5.1 Introduction

Split-Hopkinson pressure bar tests have traditionally been performed with a fast moving striker bar used to initiate the pulse. There are practical limits to the length of striker bars and therefore pulse duration. With limited pulse durations, there is little time for yielding and flow behavior to develop in strain rates in the low thousands and lower. Figure 5-1 from Moy et al (Moy, Weerasooriya, Hsieh, & Chen, 2009) show the gap between traditional SHPB tests and hydraulic testing machines. The tests at 4600/s, 3300/s, 2300/s and 600/s are SHPB tests; the time duration is limited by the length of the striker

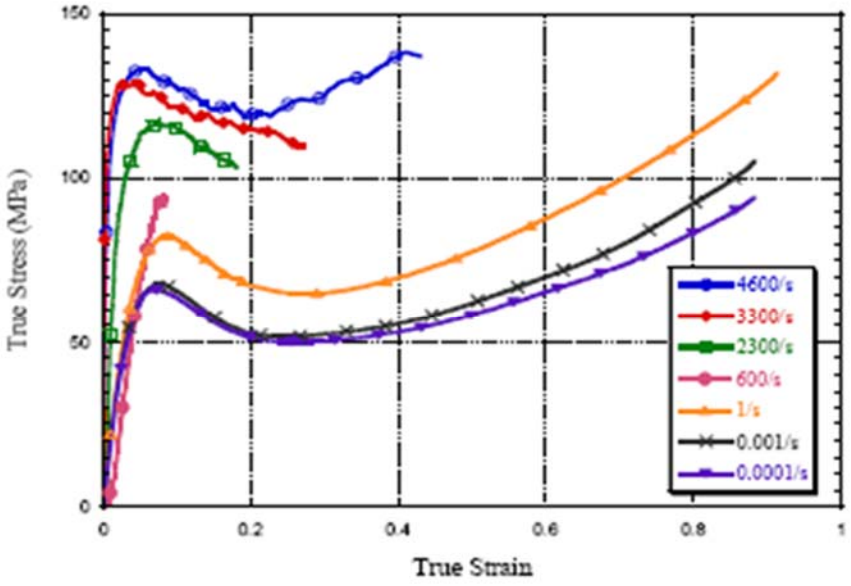

Figure 5-1: True Stress vs. True Strain Based on SHPB and Hydraulic Tests (Moy, Weerasooriya, Hsieh, & Chen, 2009)

bar. Since duration of the pulse is constant, decreasing the strain rate decreases the total amount of strain developed. For strain rates in the low thousands, flow behavior does not develop. Yielding is not observed at strain rates in the hundreds. A gap exists between

the strain rates achievable with SHPB and hydraulic testing machines. The friction clamp type compressional Kolsky bar (CKB) method allows for 50 inches of clamped bar section and nearly 500 μs of pulse duration. It would be very impractical to get the equivalent striker bar for a SHPB test. This CKB method also produces a pulse of relatively constant strain rate with no need for pulse shaping which is typically necessary for SHPB tests. It will be demonstrated that CKB method presented here can effectively bridge the gap between SHPB and hydraulic tests by covering strain rates. The temperature and strain rate dependence of both yield and flow stress was shown for during dynamic shear in TKB tests by Shen (Shen, 2007). The effect of rate and temperature on the yielding and plastic flow of polycarbonate will be studied. An array of strain rates (400/s, 800/s, and 1200/s) and temperatures (20 C, 40 C, 60 C, 80 C, and 100 C) will be performed.

The results from this series of tests can be converted to deviatoric invariant stress and strain and be compared TKB with axial response and combined loading tests. When the sample is being compressed the mean stress is 1/3 the compressive stress.

5.2 Compressional Kolsky Bar Experimental Technique

5.2.1 Experimental Set-up

This is the fourth application of striker-less Kolsky bar apparatus will be referred to as compressional Kolsky car (CKB) method. In this configuration, the friction clamp is applied, and the axial piston is used to compress the section of the bar between the clamp and the pulley. When the desired compression is applied, more pressure is applied to friction clamp until the bolt breaks. This releases the stored compression in that section

of the bar and initiates a compression pulse. This pulse travels faster than the torsional

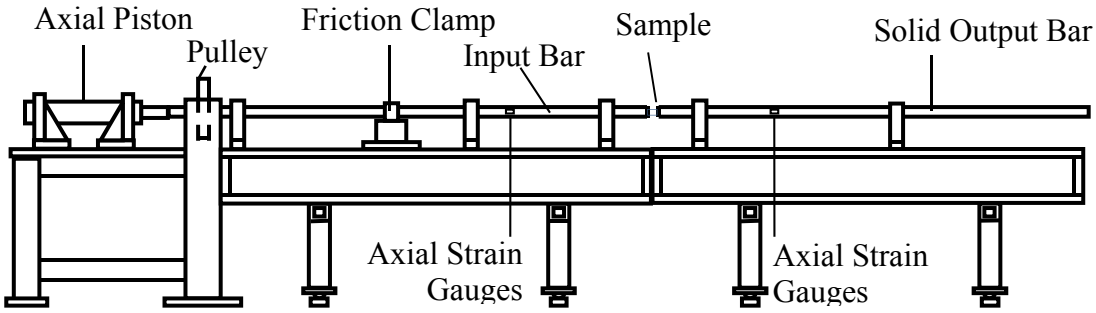

Figure 5-2: Experimental Set-up for Compressional Kolsky Bar Method

pulse described in Chapter 2. since it is a longitudinal wave rather than a shear wave. Like the previously described torsion wave, the compression pulse is partially

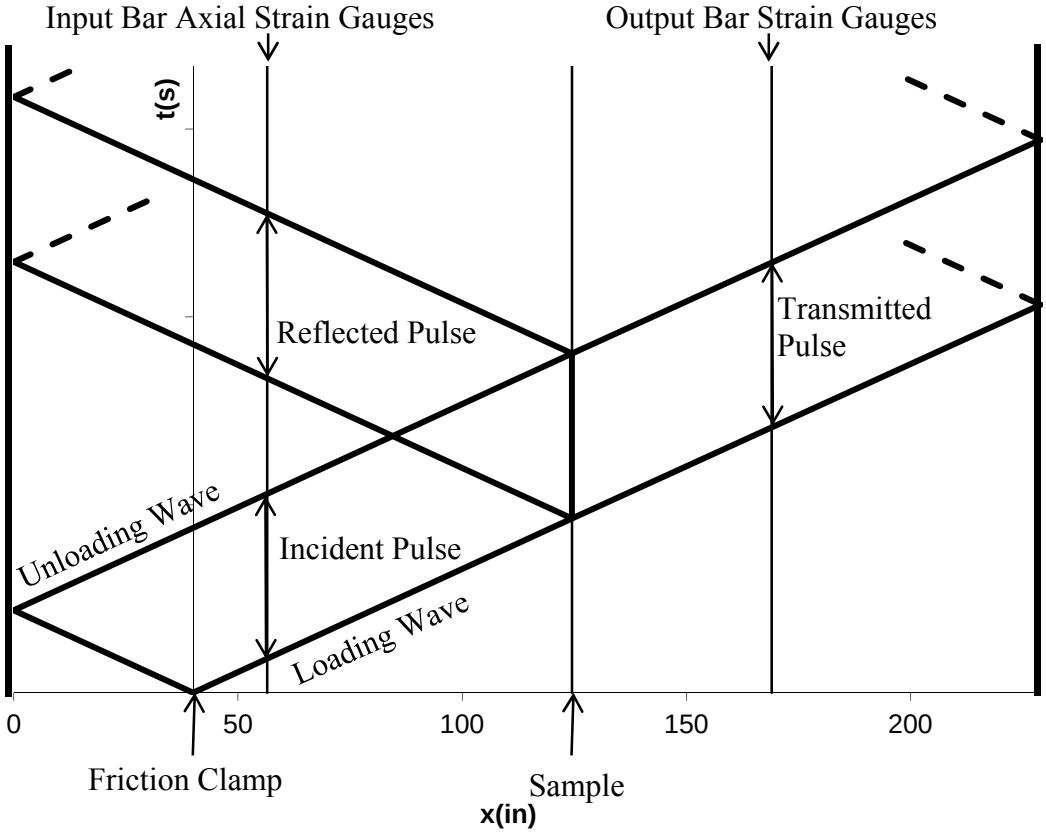

Figure 5-3: X-T Diagram

transmitted through the sample and partially reflected as seen in **Error! Reference source not found.**. The polycarbonate sample is a small cylinder as seen in Figure 5-4.

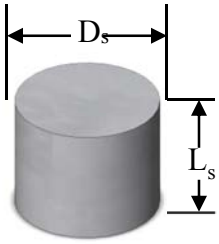

Figure 5-4: Compression Sample: where D_s = sample diameter, L_s = sample length, A_s = sample cross-sectional area

The sample is placed between the two bars and the ends are lubricated to minimize lateral stress due to friction as the sample expands in the lateral direction.

5.2.2 Thermal Chamber

To observe the effects of temperature on the deformation on polycarbonate, elevated

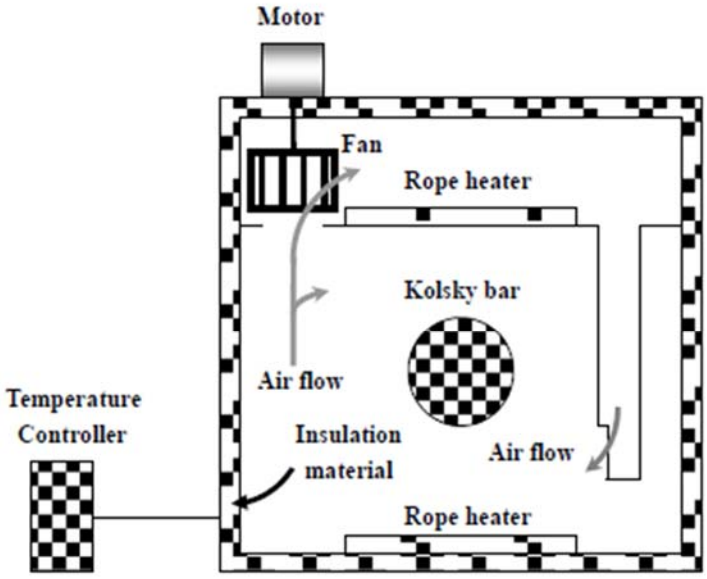

Figure 5-5: Schematic of Thermal Chamber (Shen, 2007)

temperatures are needed. The thermal chamber used for this series of compression tests is the same device used by Shen (Shen, 2007) in his series of torsion tests. The

temperature controller controls based on the input of a thermocouple that is placed directly to the surface of the sample. Shen found good uniformity in temperature at multiple points along the sample surface (Shen, 2007), so uniformity in temperature can be assumed.

5.3 CKB Experimental Analysis

5.3.1 Strain Gauge Analysis

The three stress pulses are measured using MicroMeasurments strain gauges shown in

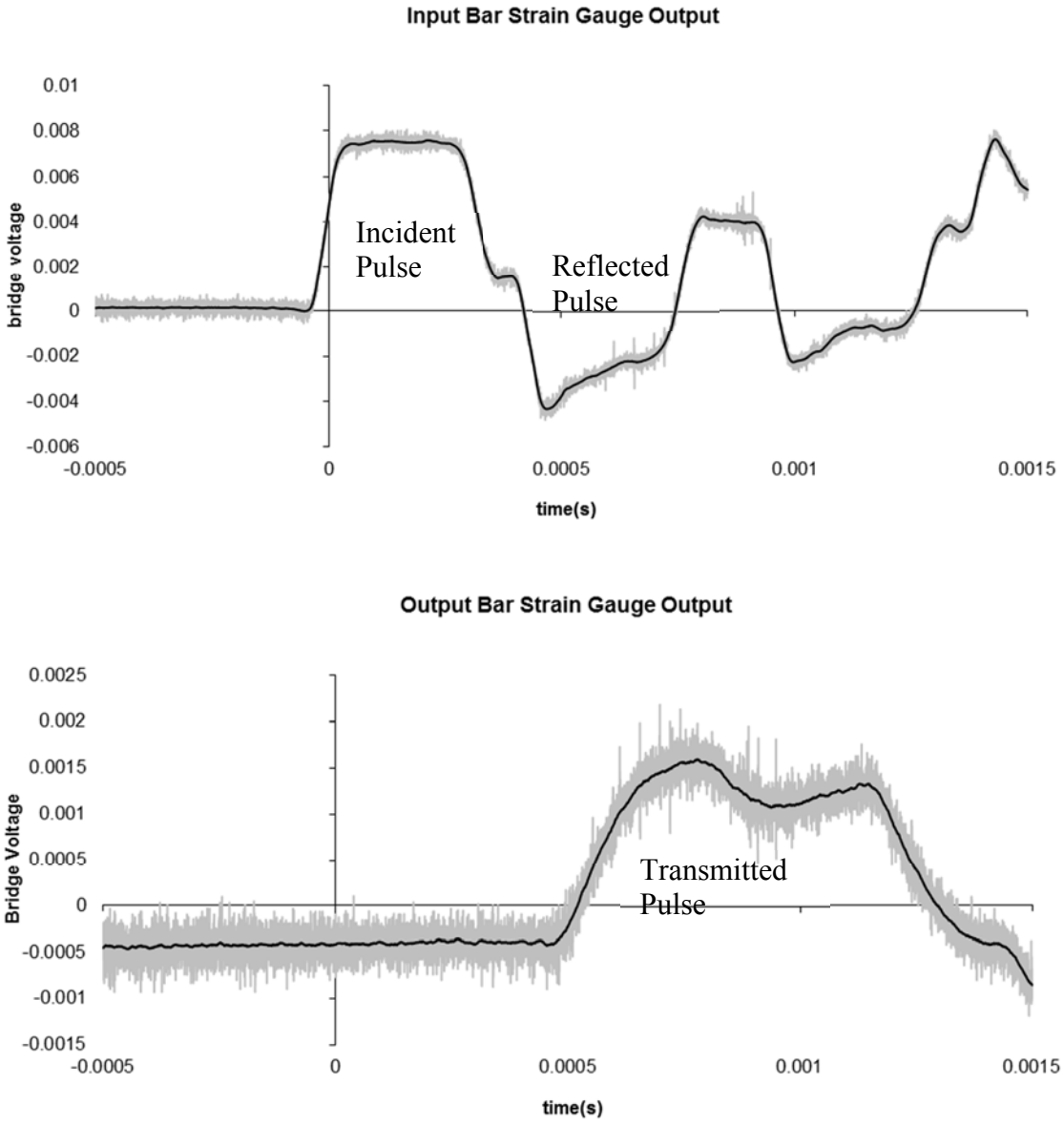

Figure 5-6: Outputs of Strain Gauge Bridges on Input Bar and Output Bar

Figure 3-3 configure in a half-Wheatstone bridge configuration as seen in Figure 3-2. The voltage history of the two bridges is recorded using a digital oscilloscope and typical voltage histories are shown in Figure 5-6. Although the strain gauge bridge is balanced before the tests, by the time the test is run there is some drift. An average of the first few thousand points is taken and subtracted from the data to ensure the voltage is zero when the bars are unloaded. Also it can be seen that the incident does not fully unload, and therefore, the reflected pulse is obscured. Adjustments are made to the analysis to deal with the unusable reflected pulse. The strain gauge analysis for the axial strain gauge bridges, as described in earlier chapters, is used to convert the voltage history to a stress history.

5.3.2 CKB Longitudinal Wave Analysis

The analysis for the longitudinal wave analysis resembles the torsional wave analysis described in section 2.3.2. The deformation on an infinitesimally thin section of the aluminum bar as shown in **Error! Reference source not found.** is considered. The difference of the velocities on the two sides results in a deformation rate of

$$\frac{\partial \varepsilon}{\partial t} = \frac{\partial v}{\partial x}. \tag{5-1}$$

where ε is compressive strain, v is material velocity, and x is the position on the bar in the axial direction. The strain is related to stress or pressure by Hooke's law

$$\varepsilon = \frac{P}{E} \tag{5-2}$$

where ε is compressive strain, v is material velocity and x is the position on the bar in the axial direction. The strain is related to stress or pressure by Hooke's law

$$\varepsilon = \frac{P}{E} \tag{5-3}$$

where E is the Young's Modulus. The following relation is derived by combining

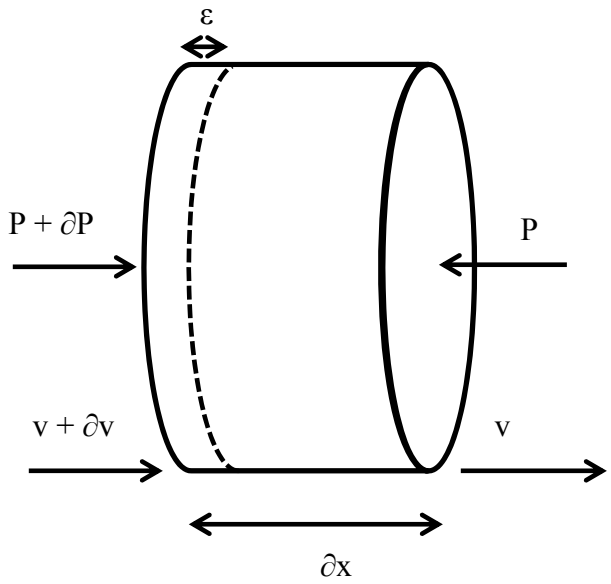

Figure 5-7: Section of bar with thickness ∂x, where P is pressure or compressive stress and v is material velocity

equations 5-1 and the derivative of equation 5-3.

$$\frac{\partial \varepsilon}{\partial t} = \frac{1}{E}\frac{\partial P}{\partial t} = \frac{\partial v}{\partial x} \tag{5-4}$$

Equation 5-4 can be simplified to:

$$\frac{\partial P}{\partial t} - E\frac{\partial v}{\partial x} = 0 \tag{5-5}$$

Based on the following relations for wave impedance (Z) of the bar and the axial wave

$\partial P \partial t - E \partial v \partial x = 0$ (5-5 can be rewritten as

$$Z = \rho C_a \tag{5-6}$$

$$C_a = \sqrt{\frac{E}{\rho}} \tag{5-7}$$

$$\frac{\partial P}{\partial t} - Z C_a \frac{\partial v}{\partial x} = 0 \tag{5-8}$$

ρ is the density of the bar. This equation will be used later; first another relation will developed from the section shown in Figure 5-4. Since the pressures on each side are not equal, the section of the bar is accelerating. By Newton's 1st law of motion

$$F = \partial P A = mass * acceleration = \rho A \partial x \frac{\partial v}{\partial t}. \tag{5-9}$$

Dividing both sides of equation 5-9 by ∂x and cross-sectional area yields

$$\frac{\partial P}{\partial x} = \rho \frac{\partial v}{\partial t}. \tag{5-10}$$

Multiply both sides of equation by the axial wave speed and rearranging gives

$$C_a \frac{\partial P}{\partial x} - C_a \rho \frac{\partial v}{\partial t} = 0 \; or \tag{5-11}$$

$$C_a \frac{\partial P}{\partial x} - Z \frac{\partial v}{\partial t} = 0. \tag{5-12}$$

For a right travelling wave $C_a = \frac{dx}{dt}$, so equations 5-8 and 5-12 can rewritten as

$$\frac{\partial P}{\partial t} dt - Z \frac{\partial v}{\partial x} dx = 0 \tag{5-13}$$

and

$$\frac{\partial P}{\partial x}dx - Z\frac{\partial v}{\partial t}dt = 0 \tag{5-14}$$

respectively. Adding equations 5-13and 5-14 yields

$$\left(\frac{\partial P}{\partial x} - Z\frac{\partial v}{\partial x}\right)dx + \left(\frac{\partial P}{\partial t} - Z\frac{\partial v}{\partial t}\right)dt = 0 \tag{5-15}$$

or

$$d(P - Zv) = 0 \tag{5-16}$$

Along a right going wave there is a characteristic equation:

$$(P - Zv)\ is\ constant\ along\ C_a = \frac{dx}{dt}. \tag{5-17}$$

For left going torsional the $C_a = -\frac{dx}{dt}$ can be plugged into equations 5-8 and 5-12 yielding the characteristic equation for left going waves.

$$(P + Zv)\ is\ constant\ along\ C_a = -\frac{dx}{dt} \tag{5-18}$$

The loading and deformation of the sample can be analyzed using an x-t diagram (Figure 5-8) and T-ω diagram (Figure 5-9) with those characteristic equations. The x-t diagram shows the propagation of the waves through the bars and the sample. The length of the sample is exaggerated to show how the waves travel through the sample. The P-v diagram uses the known values for velocity (ω) and measured values for pressure along with characteristic equations 5-17 and 5-18 for right and left going waves to calculate the desired values of pressure and velocity. To the right of the clamp it is initially unloaded and stationary, while to the left of clamp is loaded with the stored pressure and stationary.

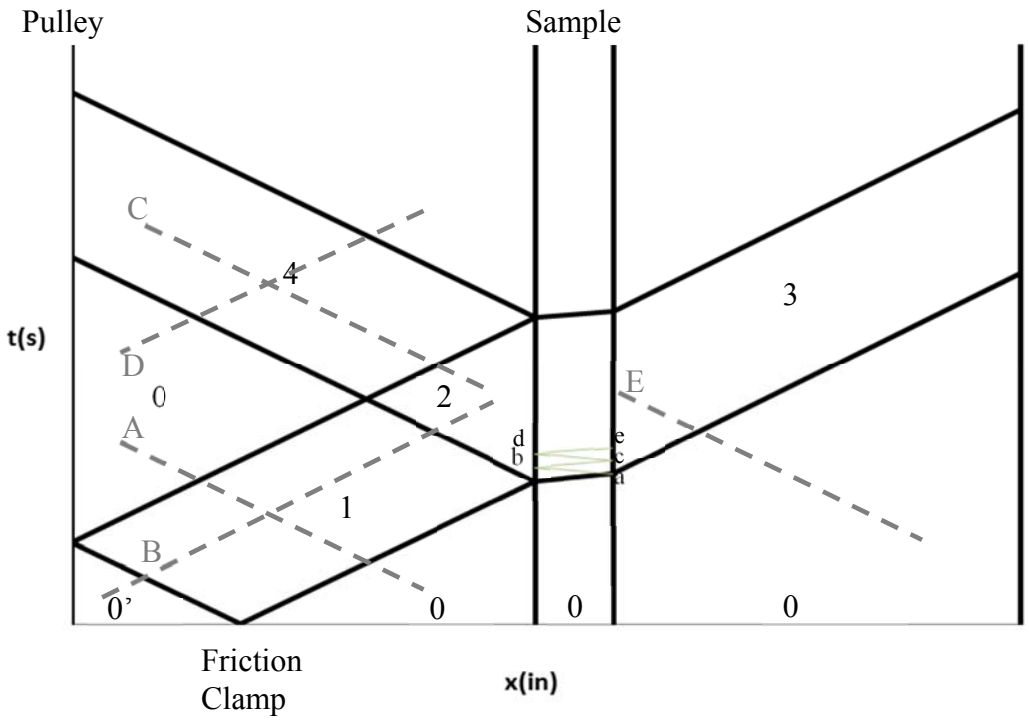

Figure 5-8 x-t diagram

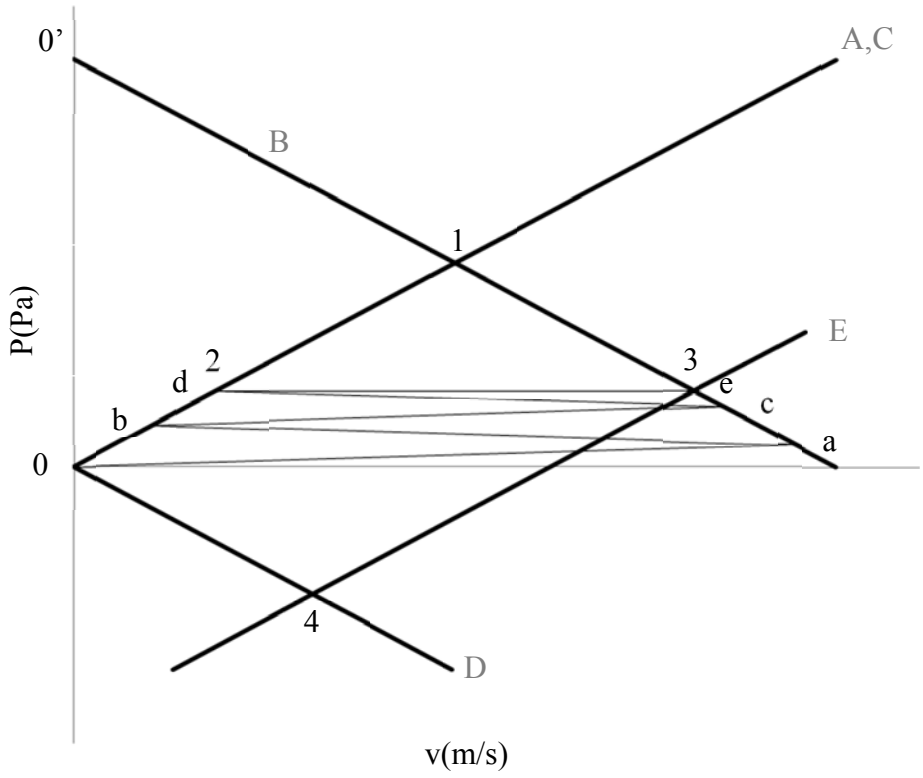

Figure 5-9: P-v Diagram

$$v_0 = 0 \qquad P_0 = 0$$

$$v_{0'} = 0 \qquad P_{0'} = Stored\ Pressure$$

Point 0 and 0' are plotted on the T-ω diagram. The dotted line A in Figure 5-8 is a line where $\frac{dx}{dt} = -C_a$, and therefore equation 5-18 applies, and pressures and velocities along line A can be found on line A in the P-v diagram. The dotted line B in Figure 5-8 is a line where $\frac{dx}{dt} = C_s$, and therefore equation 5-17 applies, and pressures and velocities along line B can be found on line B in the P-v diagram. The intersection of lines A and B in Figure 5-9 gives incident pressure (P_i) or the pressure measured during the incident pulse is given as

$$P_1 = P_i = \frac{1}{2}P_{0'} = \frac{1}{2}\ stored\ pressure \tag{5-19}$$

and the velocity in area 1 is

$$v_1 = -\frac{P_1}{Z} = -\frac{P_i}{Z}. \tag{5-20}$$

When the sample is loaded, compressive waves traverse the sample increasing the load on the sample until the sample yields and can no longer support higher loads. The axial impedance of the sample is less than that of the bar so the characteristic lines of the sample are less steep. Points a, b, c, d, and e in Figure 5-8 and Figure 5-9 show the load on the sample increasing to yielding. The deformation rate will be proportional to the difference of the velocities of the bar on each side of the sample (v_3-v_2). These values have to be calculated from the three measured pressure pulses. Area 4 and point 4 in and

represent the reflected pulse. From P_4, the measured reflected pressure (P_r), the velocity of section 4 can be calculated

$$v_4 = \frac{P_4}{Z} = \frac{P_r}{Z}. \tag{5-21}$$

v_2 can using the P-v diagram at the intersection of characteristic lines B and C. Geometrically, it is clear that $v_2=v_1+v_4$. Therefore, using equations 5-20, 2-33, and 5-21 gives

$$v_2 = \frac{-P_1+P_4}{Z} = \frac{-P_i+P_r}{Z}. \tag{5-22}$$

The measured transmitted pulse corresponds to area and point 3 in Figure 5-8 and Figure 5-9 respectively. Since both bars have the same axial impedance (Z), the characteristic lines A and E overlap. P_3 is equal to the measured transmitted pulse (P_t) and

$$v_3 = -\frac{P_3}{Z} = -\frac{P_t}{Z}. \tag{5-23}$$

Since the speed of both ends of the sample has been determined, the strain rate ($\dot{\varepsilon}$) is calculated as follows

$$\dot{\varepsilon} = \frac{v_3-v_2}{L_s}, \tag{5-24}$$

where L_s is the sample length as seen in Figure 5-4. Combining equations 5-22, 5-23, 2-36, and 5-24 gives

$$\dot{\varepsilon} = \left(\frac{1}{L_s}\right)\left(-\frac{P_t}{Z} - \frac{-P_i+P_r}{Z}\right). \tag{5-25}$$

It was shown in Figure 5-6 that the transmitted pulse is unusable. Using the fact that the bars have the same impedance and that $P_i + P_r = P_t$, simplifies equation 5-25 to

$$\dot{\varepsilon} = \left(\frac{1}{L_s}\right)\frac{2(P_i - P_t)}{Z}. \tag{5-26}$$

Using this relation, a shear strain rate history is developed from the reflected pulse and an example is show in Figure 5-10.

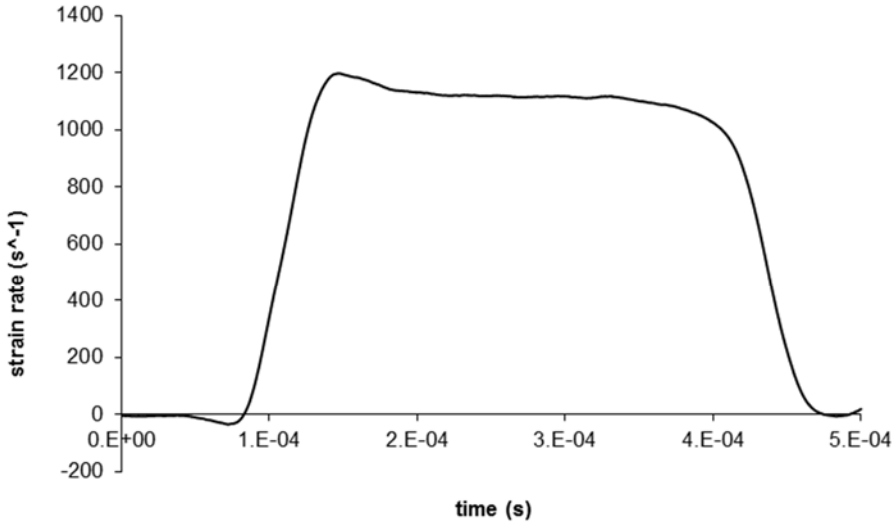

Figure 5-10: Strain Rate History

The engineering shear strain history ($\varepsilon_{engr}(t)$) is obtained by taking the integral of the shear strain rate history with respect to time.

$$\varepsilon_{engr}(t) = \int_0^t \dot{\varepsilon}(t_1)dt_1 \tag{5-27}$$

The axial stress on the sample is taken from the transmitted pulse (P_r). Therefore, the compressive engineering stress (σ_{engr}) is calculated as

$$\sigma_{engr} = \frac{P_t A_{bar}}{A_{s0}} \tag{5-28}$$

where A_{bar} is the cross-sectional area of the bar and A_{s0} is the initial cross-sectional area of the sample. With both an engineering stress and engineering strain history, stress can be plotted versus strain in Figure 5-11.

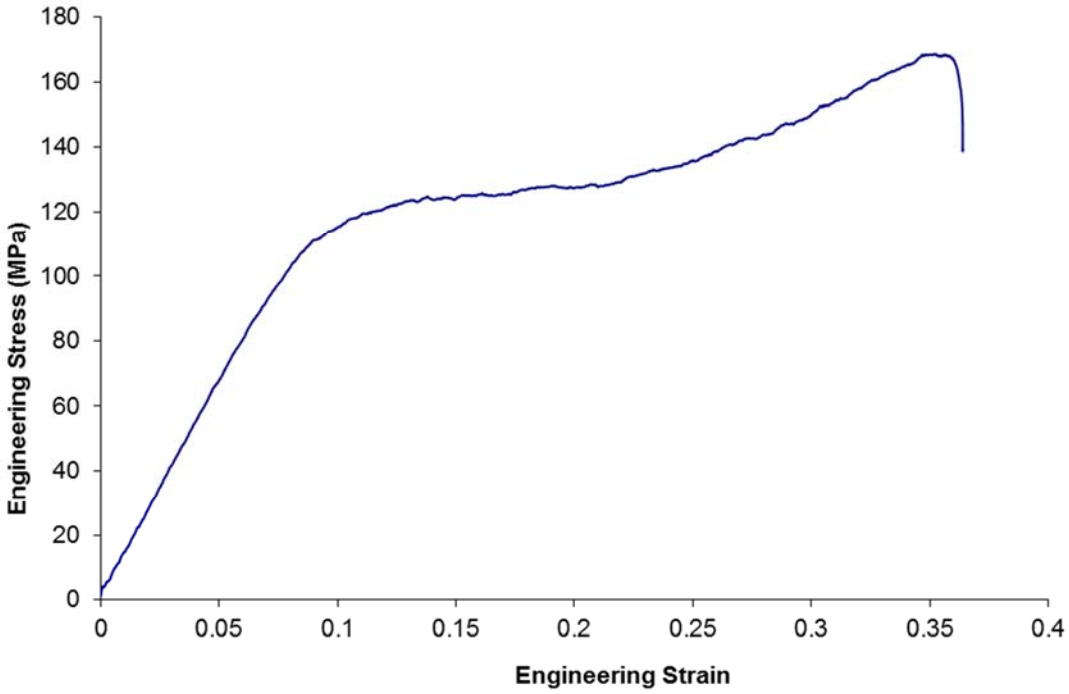

Figure 5-11: Engineering Stress vs. Engineering Strain

Table 5-1: Typical Values for Strain Gauge and Stress Analysis

Excitation Voltage(V_{ex})	35 V
Shear Strain Gauge Nominal Resistance(R)	1000Ω
Shear Strain Gauge Factor(f)	2.08
Bar Radius(r)	12.7mm
Bar Shear Modulus(G)	26.7 MPa
Sample Diameter(D_s)	5 mm
Sample Length(L_s)	2-4 mm

5.3.3 Converting to True Stress and Strain

Unlike the torsion test, the dimensions of the sample change significantly as the sample deforms. Engineering stress (σ_{engr}) is the force applied to the sample divided by the original sample cross-sectional area (A_{s0}) while true stress (σ_{true}) is the force divided by actual cross-sectional area (A_s).

$$\sigma_{engr} = \frac{F}{A_{s0}} \tag{5-29}$$

$$\sigma_{true} = \frac{F}{A_s} \tag{5-30}$$

To calculate the actual cross-sectional area, the sample is assumed to be incompressible. If volume remains constant, cross-sectional area can be found as a function of engineering strain.

$$A_{s0}L_{s0} = A_sL_{s0}(1 - \varepsilon_{engr}) \tag{5-31}$$

$$A_s = \frac{A_{s0}}{(1-\varepsilon_{engr})} \tag{5-32}$$

True stress can be calculated from engineering stress by

$$\sigma_{true} = \sigma_{engr}(1 - \varepsilon_{engr}). \tag{5-33}$$

Engineering strain does not take into account the change in length of the sample as the sample is compressed. True strain or logarithmic strain is calculated as

$$\varepsilon_{true} = ln(1 - \varepsilon_{engr}) \tag{5-34}$$

Using equations 5-33 and 5-34, true stress vs. true strain can be shown.

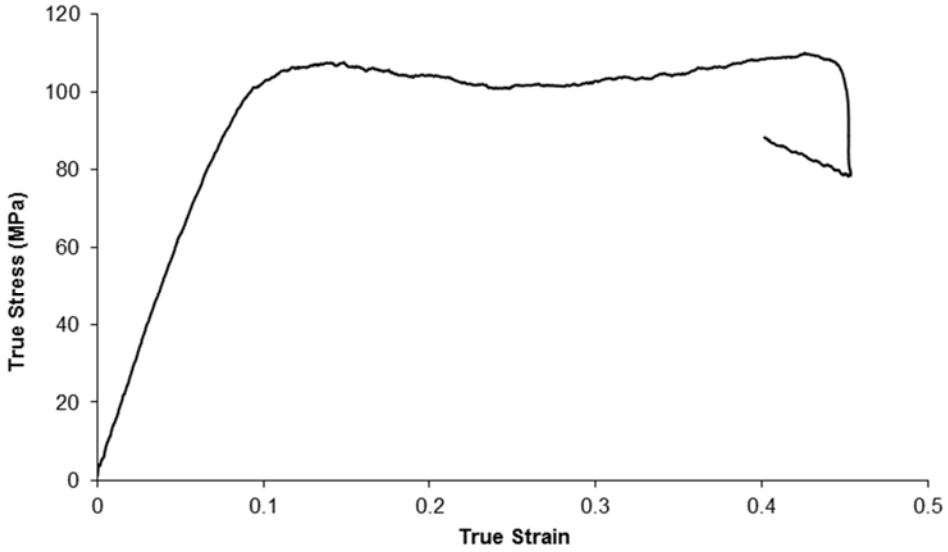

Figure 5-12: True Stress vs. True Strain

5.4 Experimental Results

5.4.1 Strain Rate Range

The longer duration pulse achieved in the CKB method allows for tests at strain rates that range from the mid hundreds to lower thousands per second. Figure 5-13 shows these tests plotted with results from hydraulic testing machines. 100/s is the upper limit of hydraulic testing. The CKB tests are able to test in the strain rate range between hydraulic tests and SHPB tests.

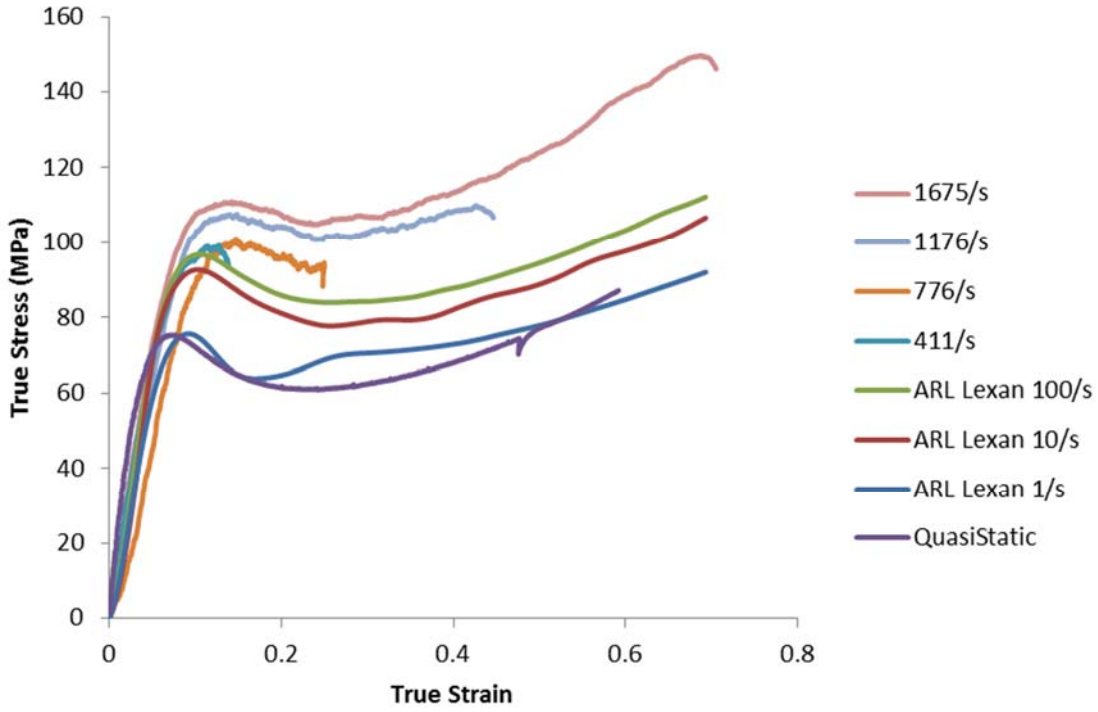

Figure 5-13: CKB Tests Compared with Hydraulic Test Machine Results from the Army Research Lab (Moy, Weerasooriya, Hsieh, & Chen, 2009)

5.4.2 Temperature and Strain Rate Dependence

Tests are performed along the matrix of temperatures (20 C, 40 C, 60 C, 80 C, and 100 C)

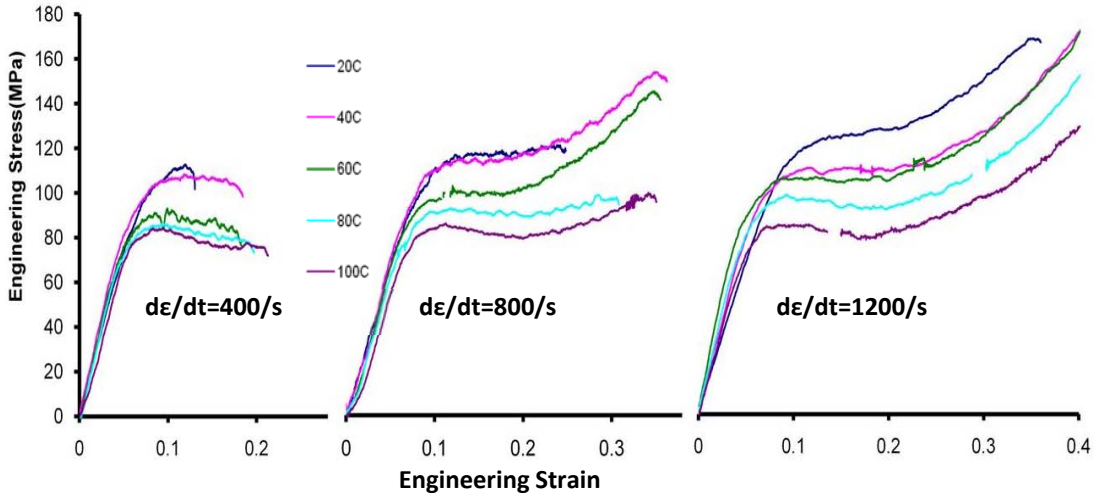

Figure 5-14: Effect of Temperature on Engineering Stress at Strain Rates of 400/s, 800/s, and 1200/s.

and strain rates (400 s^{-1}, 800 s^{-1}, and 1200 s^{-1}). Higher strain rates and lower

temperatures result in higher yield stresses and flow stress. This can be observed in both engineering stress (Figure 5-14) and true stress (Figure 5-15 and Figure 5-16).

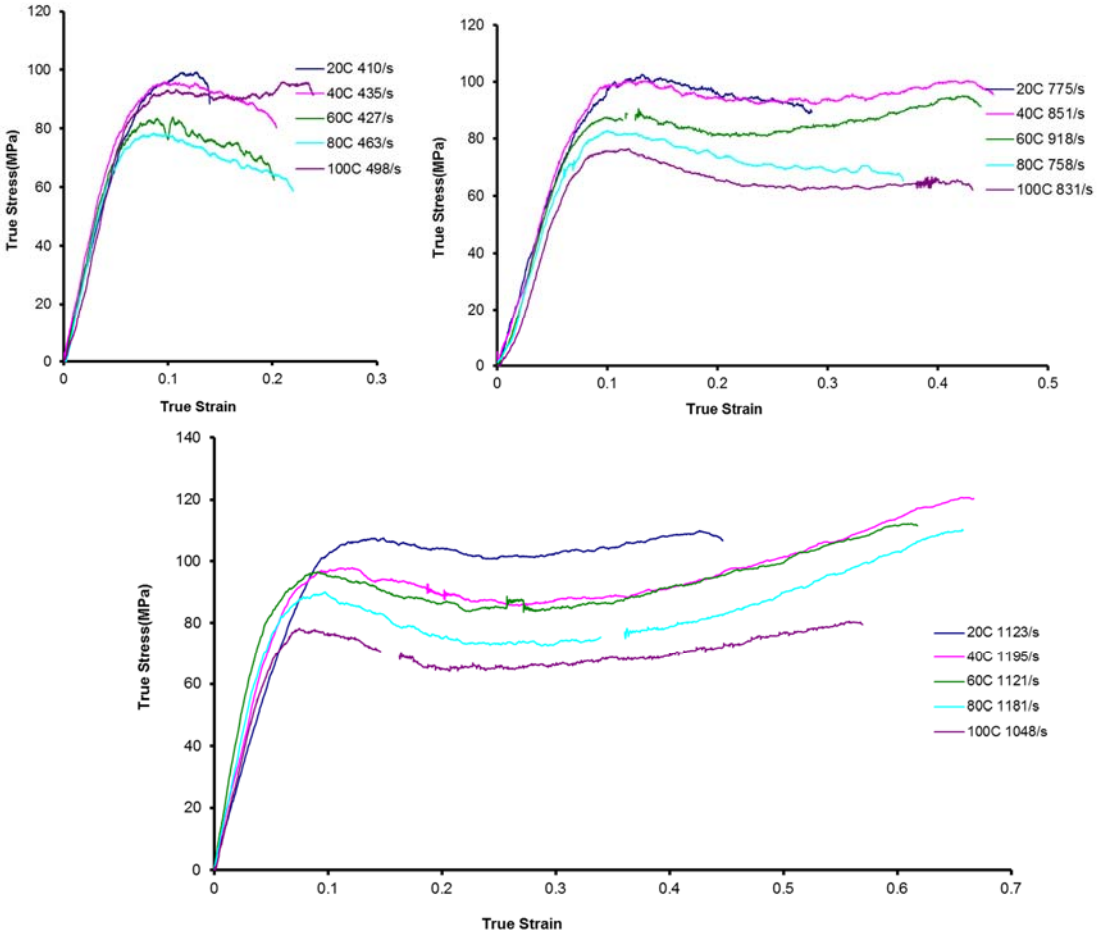

Figure 5-15: Effect of Temperature on True Stress with Strain Rates of

Figure 5-15 shows that temperature tends to have a greater effect on the yield stress and the stress at which flow occurs when strain rates are higher.

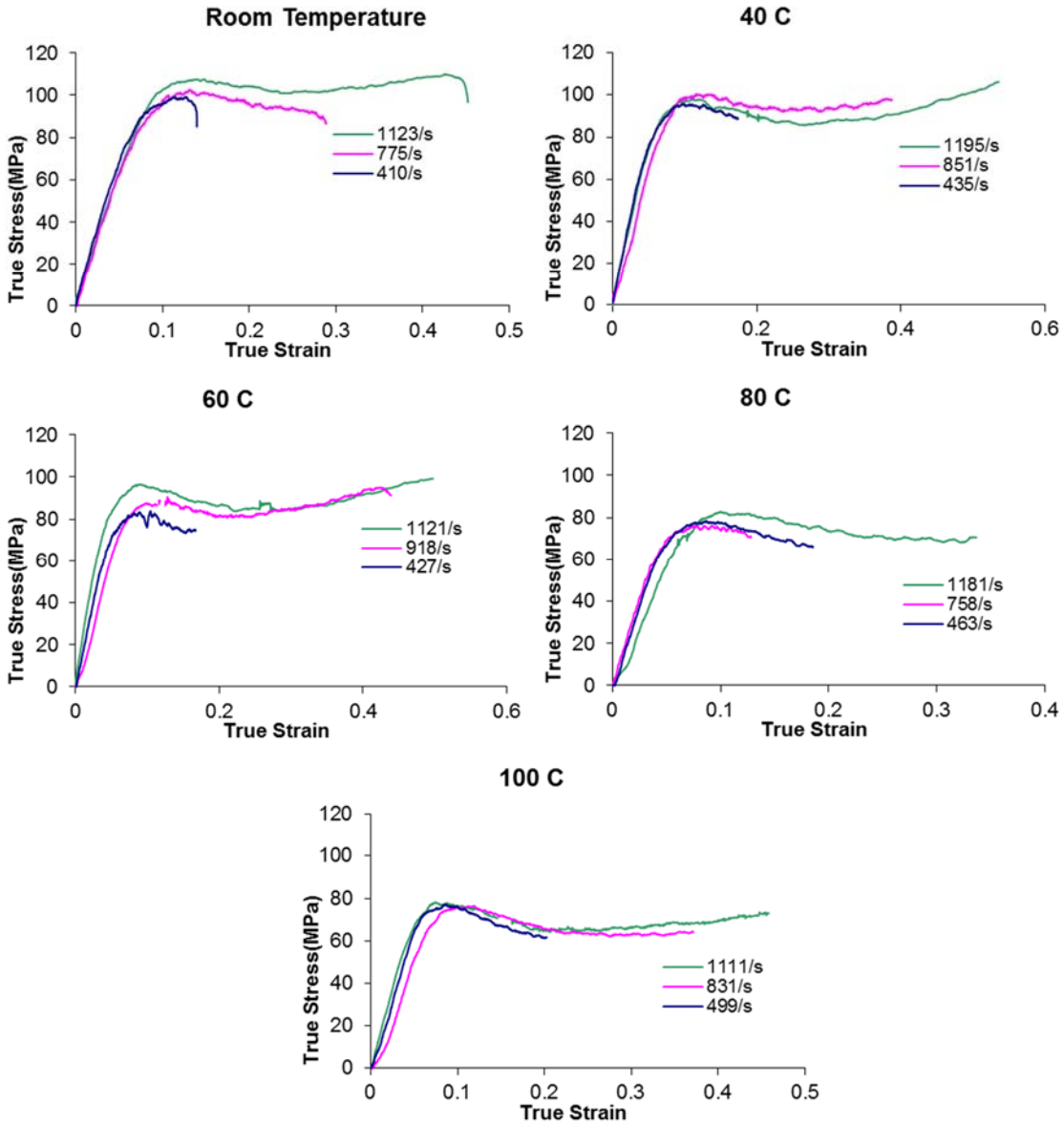

Figure 5-16: Effect of Strain Rate on True Stress at Temperatures of 20 C, 40 C, 60 C, 80 C and 100 C

Yield and flow stress tends to increase with increasing strain rate, but the effect is much smaller than that of temperature in this range. The yield stress is found as the initial peak and the flow stress is chosen as the minimum after the initial peak. Table 5-2 displays those values as well as the strain rate.

Table 5-2: True Yield and Flow Stress Results (Flow behavior did not develop)**

T / $\dot{\varepsilon}$	20 C	40 C	60 C	80 C	100 C
400/s	411/s	435/s	424/s	459/s	492.9/s
Yield Stress	99.1 MPa	95.8 MPa	83.8 MPa	78.4 MPa	77.2 MPa
Flow Stress	**	89.3 MPa	77.1 MPa	66.5 MPa	73.6 MPa
800/s	776/s	855/s	924/s	757/s	832/s
Yield Stress	103.6 MPa	100.6 MPa	86.5 MPa	83.3 MPa	76.5 MPa
Flow Stress	94.1 MPa	93.1 MPa	79.5 MPa	68.7 MPa	61.6 MPa
1200/s	1123/s	1198/s	1123/s	1185/s	1054/s
Yield Stress	107.7 MPa	98.0 MPa	96.6 MPa	89.5 MPa	78.3 MPa
Flow Stress	100.8 MPa	85.5 MPa	83.5 MPa	73.6 MPa	64.1 MPa

The deformation of polycarbonate has been modeled under the Ree-Eyring model by Shen (Shen, 2007) and Reitsch (Rietsch & Bouette, 1990). Shen model is for flow stress shear deformation, so it cannot be used directly for compression. Reitsch & Bouette work was done with compression under a wide range of and gives yield stress for a given temperature and strain rate. The general form of the Ree-Eyring (Ree & Eyring, 1955) is as follows:

$$\sigma_{yield} = T\left[A_\alpha\left(\ln(2C_\alpha\varepsilon)\dot{+}\frac{Q_\alpha}{RT}\right) + A_\beta sin^{-1}\left(C_\beta\dot{\varepsilon}\exp\left(\frac{Q_\beta}{RT}\right)\right)\right] \qquad (5\text{-}35)$$

T is the absolute temperature in Kelvin. R is the universal gas constant $1.987\times10^{-3}\ \frac{kcal}{molK}$. A_α, C_α, Q_α, A_β, C_β, and Q_β were experimentally determined as by Reitsch as

$$A_\alpha = 6.0\ E-3\ \frac{MPa}{K}$$

$$C_\alpha = 4.1\ E-30\ sec$$

$$Q_\alpha = 68.0\ \frac{kcal}{mol}$$

$$A_\beta = 54.0\ E-3\ \frac{MPa}{K}$$

$$C_\beta = 2.9\,E-7\ sec$$

$$Q_\beta = 5.0\ \frac{kcal}{mol}$$ (Rietsch & Bouette, 1990)

The predicted yield stress vs. strain rate based on the model describe above is shown for

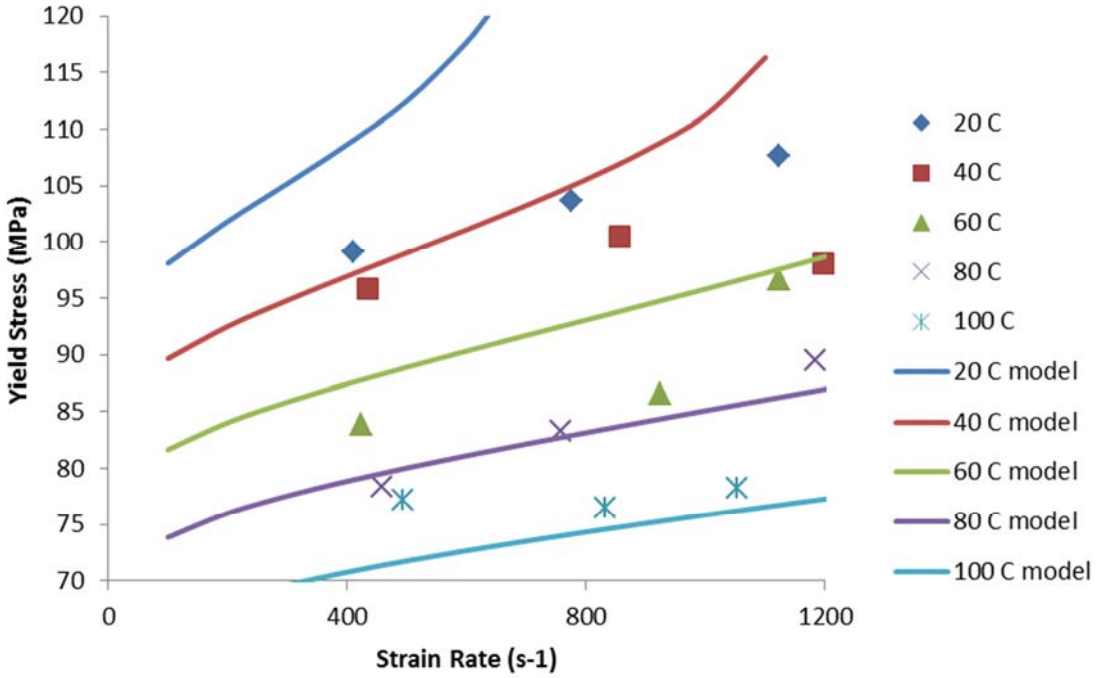

Figure 5-17: Experimental Results Plotted with Model (Rietsch & Bouette, 1990) Predictions

the five test temperatures in Figure 5-17. The experimental results are also plotted. There is good agreement between the model and the experimental results at high temperatures. Residual stress due to the machining of the sample may the reason there is agreement for higher temperatures but not lower temperatures. These stresses may make the sample weaker than an unstressed sample (Steer, Rietsch, Lataillade, Marchand, & El Bounia, 1985). Bringing the sample up to the elevated temperature likely anneals the sample.

5.4.3 Comparison with TKB Axial Response Tests

When the axial response of polycarbonate using the TKB method described in Chapter 3. it was found that the axial stress was on the order of a few megaPascals. When plastic flow occurs the sample is often in tension. In the compression test,s the pressure is one third the compressive stress of the sample and on the order of 30 MPa, which is significantly higher than the mean stresses achieved in the combined loading tests. When the stress of the TKB and CKB tests are converted to deviatoric invariant stress and the

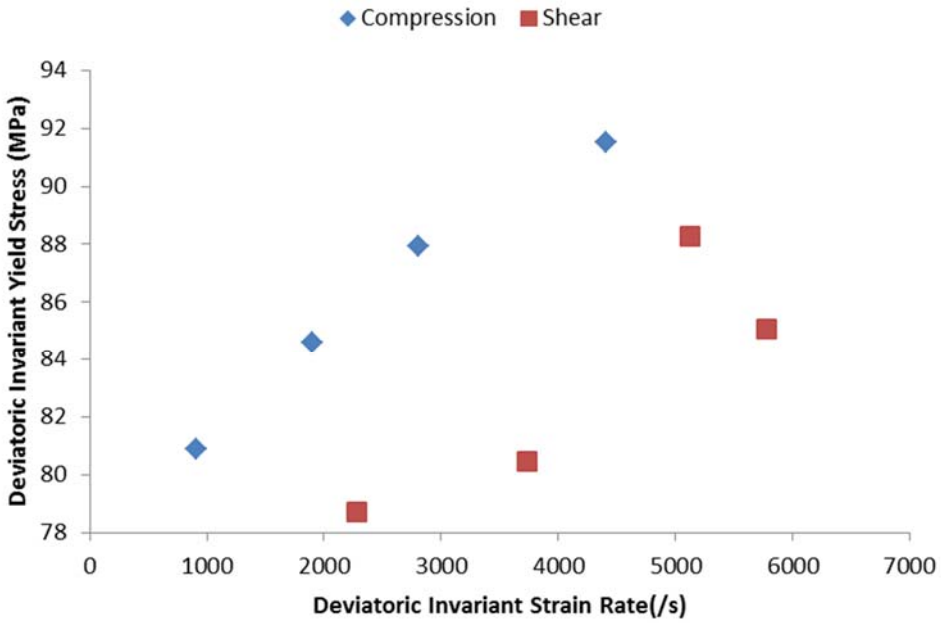

Figure 5-18: Comparison of Deviatoric Invariant Yield Stress for Compression and Shear Tests.

strain rates converted to deviatoric invariant strain rates, yield and flow stresses can be compared. Figure 5-18 shows the deviatoric invariant yield stress plotted versus the deviatoric invariant strain rate at the time yielding occurs. The trend is clear that the compression tests, with their higher pressure, yield at higher deviatoric invariant stresses for a given deviatoric invariant strain rate. Figure 5-19 shows deviatoric invariant flow

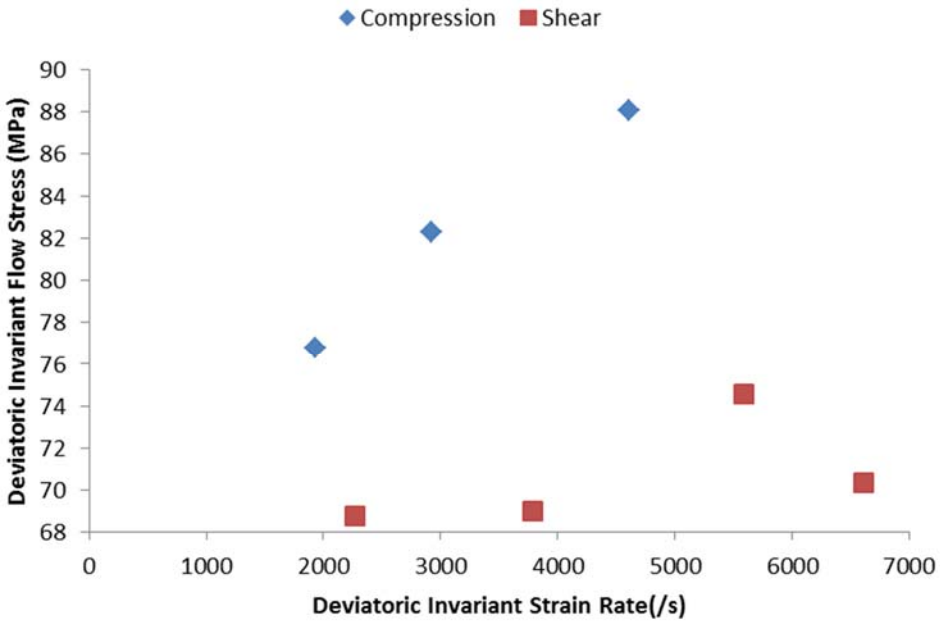

Figure 5-19: Comparison of Deviatoric Invariant Flow Stress for Compression and Shear Tests.

stress plotted vs. the deviatoric invariant strain rate at which flow occurs. The effect of the higher mean stress is even larger for flow stress than for yield stress. The addition of the mean stress due to compression appears to make flow stress 10 to 15 % higher for a given deviatoric invariant strain rate. The difference appears to increase with strain rate.

5.4.4 Regression Analysis

The values for deviatoric invariant yield and flow stress, deviatoric invariant strain rate at yielding and flow, and pressure at yielding and flow in Deviatoric invariant stress and pressure vs. deviatoric invariant strain and deviatoric invariant strain rate and engineering strain rate histories for tests 12-15 are shown in Appendix C.

Table 5-3 can be added to the values Table 4-2. Now the regression analysis can be reattempted with these extra data points. The extended set of data can be fit to the model

shown in equation 4-21. Deviatoric invariant stress and pressure vs. deviatoric invariant strain and deviatoric invariant strain rate and engineering strain rate histories for tests 12-15 are shown in Appendix C.

Table 5-3: Experimental Results from CKB Tests(* Flow did not develop)

	Deviatoric Invariant Yield Stress (Mpa)	Deviatoric Invariant Strain Rate at Yield (/s)	Pressure at Yield (Mpa)	Deviatoric Invariant Flow Stress (Mpa)	Deviatoric Invariant Strain Rate at Flow (/s)	Pressure at Flow (Mpa)
12	91.53314	4407.866	37.36825	88.03145	4610.942	35.93869
13	80.90442	914.4168	33.02909	*	*	*
14	87.91403	2805.061	35.89075	82.32412	2920.127	33.60868
15	84.61056	1899.884	34.54212	76.79175	1937.416	31.3501

Regression analysis is performed on all 15 tests using the model in equation $s_{yield/flow} = C_0 + C_1 \ln(\dot{\eta}) + C_2 P$(4-21 for both deviatoric invariant yield and flow stress. This regression analysis includes the compression test results. There is still a very wide band for intercepts. The coefficients for $\ln(\dot{\eta})$ and pressure are close to the values calculated in Table 4-3 and Table 4-4 and well within the 95% confidence bands. The low P-values show that the observed dependence of yield and flow stress on pressure and strain rate is very unlikely to be due to chance. The

Table 5-4: Regression Analysis for Deviatoric Invariant Yield Stress Including All Three Types of Tests

		Coefficients	*Standard Error*	*P-value*	*Lower 95%*	*Upper 95.0%*
C_0	Intercept	0.66901	16.721	0.96874	-35.765	37.102
C_1	$\ln(\dot{\eta})$	9.80148	2.0622	0.00047	5.3083	14.295
C_2	Pressure	0.28895	0.0674	0.00107	0.1419	0.4360

Table 5-5: Regression Analysis for Deviatoric Invariant Flow Stress Including All Three Types of Tests

		Coefficients	*Standard Error*	*P-value*	*Lower 95%*	*Upper 95%*
C_0	Intercept	-6.4213	24.496	0.7981	-60.336	47.493
C_1	$\ln(\dot{\eta})$	9.1671	3.0167	0.0113	2.5273	15.807
C_2	Pressure	0.4855	0.0873	1.7E-4	0.2933	0.6777

combined loading tests showed that pressure caused higher deviatoric invariant yield and flow stress in samples undergoing shear and could be modeled as a linear dependence. It was shown that the compression tests show higher deviatoric invariant yield and flow stresses for a given deviatoric invariant strain rate. The regression analysis shows that the higher deviatoric invariant yield and flow stresses observed in the compression tests can be explained and modeled using pressure. The intercept can be estimated by placing (Rietsch & Bouette, 1990)'s and (Bauwens-Crowet, Bauwens, & Homes, 1969)'s material constants into equation $C_0 = A\left[\ln(2C) + \frac{\Delta H}{kT}\right]$ (4-22). This yield order of magnitude. Therefore it is reasonable to assume the intercepts to be zero at room temperature. The regression analysis is performed with the intercept forced to be zero and Table 5-6 andTable 5-7.

Table 5-6: Regression Analysis for Deviatoric Invariant Yield Stress with Zero Intercept

		Coefficients	*Standard Error*	*P-value*	*Lower 95%*	*Upper 95.0%*
C_0	Intercept	0	N/A	N/A	N/A	N/A
C_1	$\ln(\dot{\eta})$	9.8837	0.1505	8.79E-18	9.5586	10.209
C_2	Pressure	0.2901	0.0589	2.76E-4	0.1629	0.4173

Table 5-7: Regression Analysis for Deviatoric Invariant Flow Stress with Zero Intercept

		Coefficients	*Standard Error*	*P-value*	*Lower 95%*	*Upper 95%*

C_0	Intercept	0	N/A	N/A	N/A	N/A
C_1	$\ln(\dot{\eta})$	8.3777	0.1729	3.92E-15	8.0009	8.7545
C_2	Pressure	0.4810	0.0823	7.88E-5	0.3018	0.6603

This tightens the 95% confidence band and brings the P-values well below 5%. The models deviatoric invariant yield and flow stress based on the regression analysis are:

$$s_{yield} = 9.88MPa\ln(\dot{\eta}) + 0.290P \tag{5-36}$$

$$s_{flow} = 8.38MPa\ln(\dot{\eta}) + 0.481P. \tag{5-37}$$

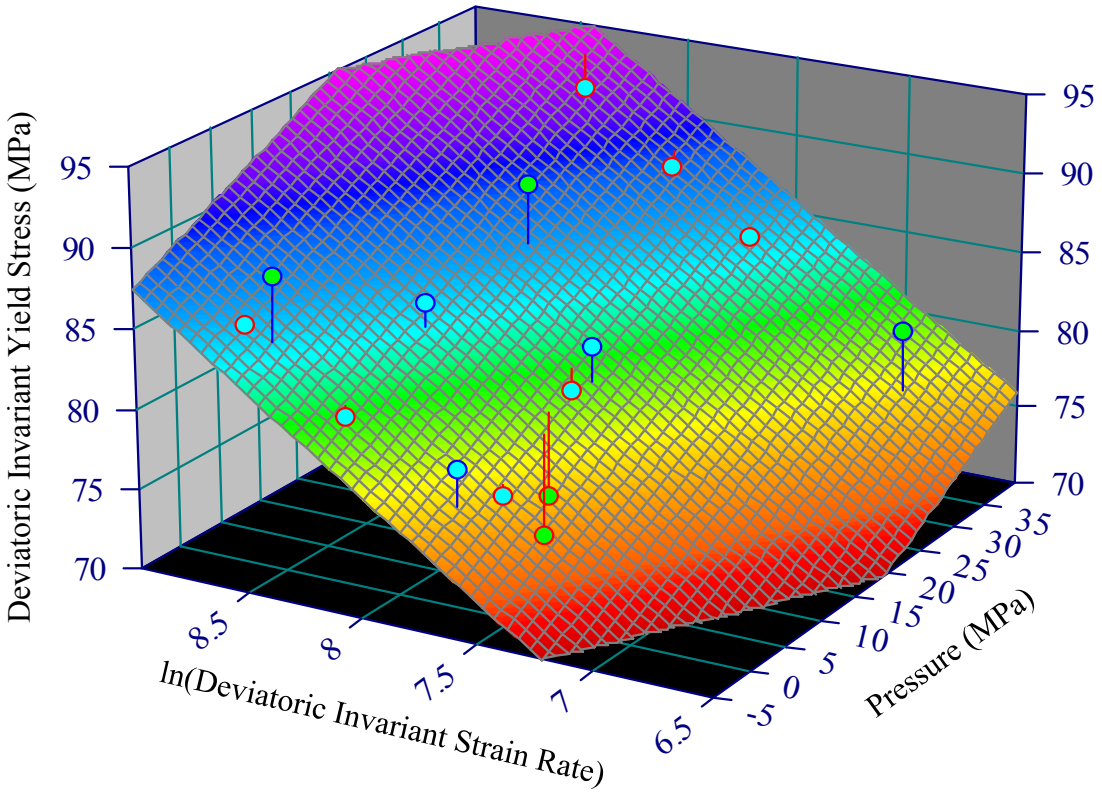

Figure 5-20: Model and Experimental Results for Deviatoric Invariant Yield Stress vs. ln(Deviatoric Invariant Strain Rate) and Pressure

Figure 5-20 shows deviatoric invariant yield stress models$s_{yield} = 9.88MPa\ln(\dot{\eta}) + 0.290P$

(5-36) fitted to the experimental data. Similarly, Figure 5-21 shows the model $s_{flow} = 8.38MPa\ln(\dot{\eta}) + 0.481P$.

(5-37) and experimental results for deviatoric invariant flow stress. The experimental data show increasing deviatoric invariant yield and flow stresses with increasing pressures and strain rates. The dependence on strain rate of yield and flow stress is well known and has been modeled (Bauwens-Crowet, Bauwens, & Homes, 1969) (Rietsch & Bouette, 1990) (Shen, 2007).

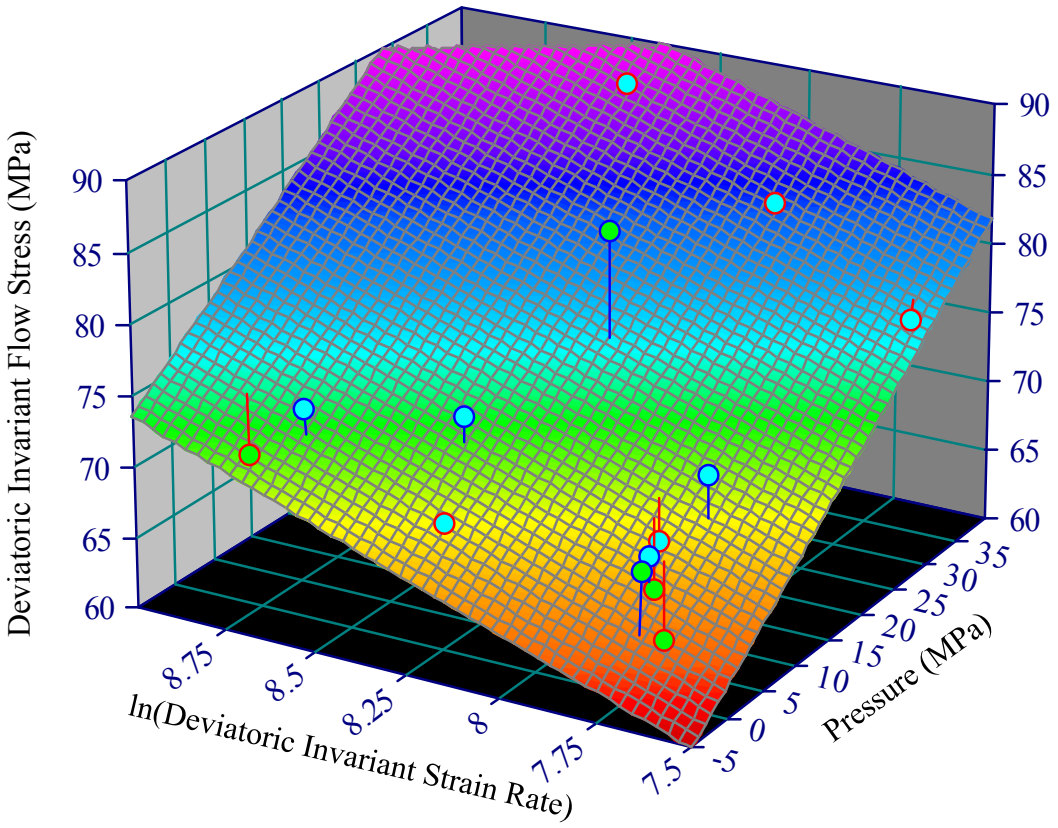

Figure 5-21: Model and Experimental Results for Deviatoric Invariant Flow Stress vs. ln(Deviatoric Invariant Strain Rate) and Pressure

However this shows that increasing pressure increase yield and flow stress and can be

used to explain the difference in deviatoric invariant yield and flow stress between observed in shear and compression tests.

CHAPTER 6. CONCLUSIONS

In this thesis three new experimental methods based on a striker-less Kolsky bar apparatus are developed for the study of the response of polycarbonate (PC) to various modes of large deformations at high strain rates and for various initial temperatures. These methods take advantage of the device's ability to achieve long pulse durations and incorporate techniques to enable specimen loading and response measurements in both axial compression/tension and shear modes. Hence, they provide the experimental techniques necessary for dynamic testing of a material whose response involves significant distortion-dilation coupling during large deformations. Although the methods developed have been applied only to the study of PC in this work, they are expected to be applicable for other polymeric solids displaying similar dynamic behaviors.

The first new technique is a variation on the standard torsional Kolsky bar (TKB) method with an extra axial strain gage sensor to measure the axial stress and strain in addition to the sample shear stress and strain measurements of the standard method. For a material having distortion-dilation coupling in its mechanical response, shear deformation induces dimensional or volumetric changes in the sample. If there are constraints such as the sample interfaces with the two stiffer metal bars in the TKB set-up, axial stress is induced. To make the output bar sensitive to the relatively small axial stress, the symmetric solid bar pairing used in the standard method is modified to an asymmetric pairing of a solid input bar and a hollow output bar. This magnifies the measured bar stress for a given sample stress by a factor of eight compared to the solid bar. Appropriate modifications are also made to the experimental analysis for the input and output bars with unbalanced impedances. The clamped distance is specially designed to prevent axial disturbances

associated with the release of the clamp from overlapping with the signal from the sample's shear-induced axial response. A series of tests with this new technique have been performed on PC. The experimental measurements show that PC expands when the shear deformation is elastic, and contracts when the shear deformation leads to yielding and plastic shear flow. The measured shear-induced axial response under elastic deformation agrees with the prediction of a nonlinear elastic model for PC (Goel, Strabala, Negahban, & Turner, 2009) for simple shear strains up to 3%.

The second new technique is a further variation on the first one. An axial piston and a steel stopper are incorporated into the TKB set-up so that a static axial compression can be applied to the entire apparatus including the sample before the sample it loaded with dynamic shear. The purpose is to measure the effect of confining stress on material yielding and flow stresses. It was speculated that high pressures would make it more difficult for polymer chains to move past each other. Tests with this method have been conducted on PC at a number of axial compressions and shear strain rates. Through linear regression analysis of the experimental measurements, it is found that both the deviatoric invariant yield and flow stresses increase with the compressive volumetric stress (equivalent to the pressure).

The last new experimental technique developed in this work is the striker-less compressional Kolsky bar method. Using the distantly separated friction clamp and axial piston to store and release compression pulses results in much longer pulse durations than what is achievable with the conventional split Hopkinson pressure bar (SHPB) method. These long compression pulses provide enough time for the material's plastic flow to develop fully in the compressive strain rate range of mid hundreds to lower thousands per

second, which is the gap between the high-rate hydraulic machine testing and the conventional SHPB experiment for the materials requiring 20% compressive strain or more for plastic flow to develop fully. A thermal chamber is also incorporated to heat the sample to a desired initial temperature. An extensive series of tests with this new method have been carried out on PC. Both the temperature and strain rate dependences of the material's yielding and flow behavior under dynamic compression are examined. The results of the high temperature tests correspond well with Ree-Eyring model (Rietsch & Bouette, 1990). Both the yield and flow stresses show significant strain rate hardening. For a given deviatoric strain rate, the compressive volumetric stresses are considerably higher for the compression tests than for the torsion tests and combined compression-torsion tests. The results from the three types of tests together indicate consistent pressure-dependent increases in the deviatoric yield and flow stresses of PC subjected to high-rate large deformations.

BIBLIOGRAPHY

Baker, W., & Yew, C. (1966). Strain rate effects in the propagation of torsional. *Journal of Applied Mechanics*, 33, 917-923.

Bauwens-Crowet, C., Bauwens, J., & Homes, G. (1969). Tensile Yield-Stress Behavior of Glassy Polymers. *Journal of Polymer Science*, 735-742.

Blumenthal, W., Cady, C., Lopez, G., Gray III, G., & Idar, D. (2001). Influence of Temperature and Strain Rate on the Compressive Behavior of PMMA and Polycarbonate Polymers. (M. Furnish, N. Thadhani, & Y. Horie, Eds.) *Shock Compression of Condensed Matter*, 665-668.

Eyring, H. (1936). Viscosity, Plasticity, and Diffusion as Examples of Absolute Reaction Rates. *The Journal of Chemical Physics*, 283-291.

Fleck, N. A., Stronge, W. J., & Liu, J. H. (1990). High strain-rate shear response of polycarbonate and polymethyl methacrylate. *Procedings of the Royal Society of London, Series A, Mathematical and Physical Sciences, 429*(1877), 459-479.

Goel, A., Strabala, K., Negahban, M., & Turner, J. A. (2009, October). Modeling the developement of elastic anisotropy as a result of plastic flow for glassy polycarbonate. *Polymer Engineering and Science, 49*(10), 1951-1959.

Hartley, K., Duffy, J., & Hawley, R. (1985). The torsional Kolsky (split-Hopkinson) bar. *ASM Metals Handbook*, 43, 873-896.

Hopkinson, B. (1914). A Method of Measuring the Preasure Produced in the Detonaltion of High Explosives or by the Impact of Bullets. *Philosophical Transactions of the Royal Society, 213*, 437- 456.

Kolsky, H. (1949). An investigation of the mechanical properties of materials at very high rates of loading. *Proceeding of the Physical Society*, B62, 676-700.

Lewis, J. a. (1972). The development and use of a torsiona lHopkinson bar apparatus. *Experimental Mechanics*, 12, 520-524.

Mehta, N., & Prakas, V. (2009). Uniaxial Compression and Combined Compression-and-Shear Response of Amorphous Polycarbonate at High Loading Rates. *Proceedings of the SEM Annual Conference.* Albuquerque New Mexico USA.

Moy, P., Weerasooriya, T., Hsieh, A., & Chen, W. (2009). Strain Rate Response of a Polycarbonate Under Uniaxial Compression. *SEM Proceeding*.

Ree, T., & Eyring, H. (1955). Theory of non-Newtonian flow: Part I- Solid plastic system. *Journal of Applied Physics, 26*, 793-800.

Rietsch, F., & Bouette, B. (1990). The Compression Yield Behaviour of Polycarbonate Over a Wide Range OF Strain Rates and Temperatures. *European Polymer Journal, 26*, 1071-1075.

Shen, X. (2007). *Thermomechanical Response of Polycarbonate at Various Strain Rates.* Masters Thesis, Univeristy of Nebraska-Lincoln, Department of Engineering Mechanics.

Steer, P., Rietsch, F., Lataillade, J., Marchand, A., & El Bounia, N. (1985). Viscoplasticité dynamique de polycarbonates aux grandes vitesses de deformation. *Journal of Physics, France, Colloq., C5*, 415-423.

Wright, S., Fleck, N., & Stronge, W. (1993). Ballistic Impact of Polycarbonate- An Experimental Investigation. *International Journal of Impact Engineering, 13*(1), 1-20.

APPENDIX A: INDIVIDUAL TESTS FOR SHEAR INDUCED AXIAL STRESS

Test 1

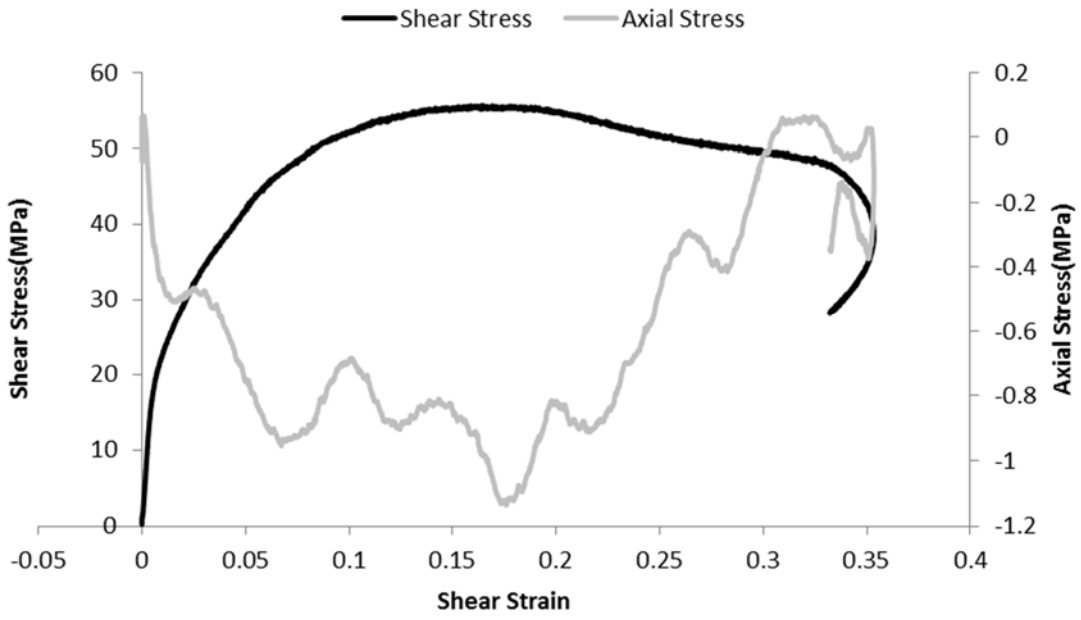

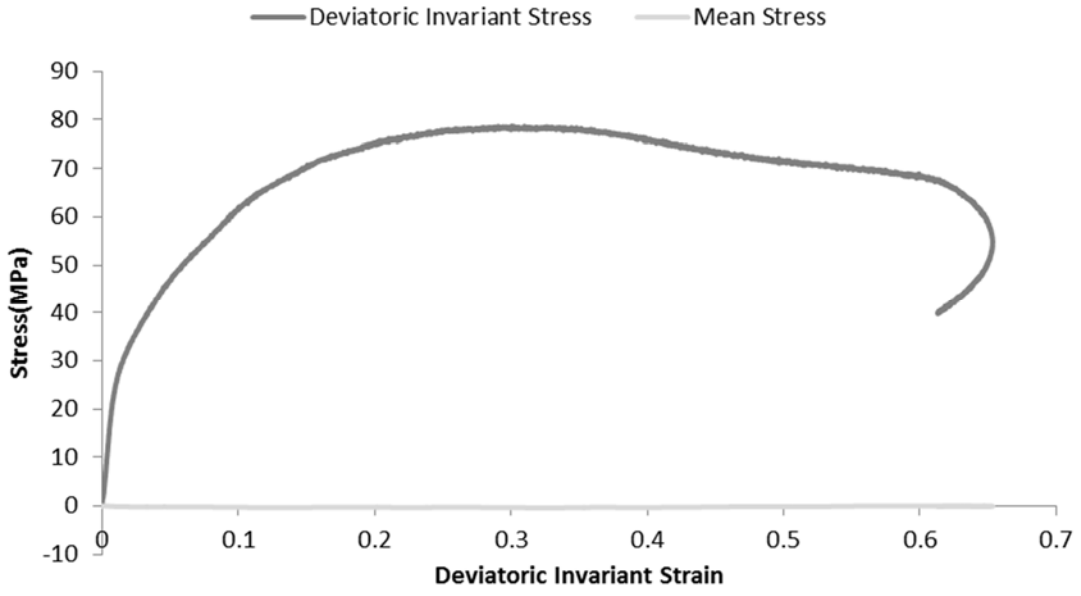

Test 2

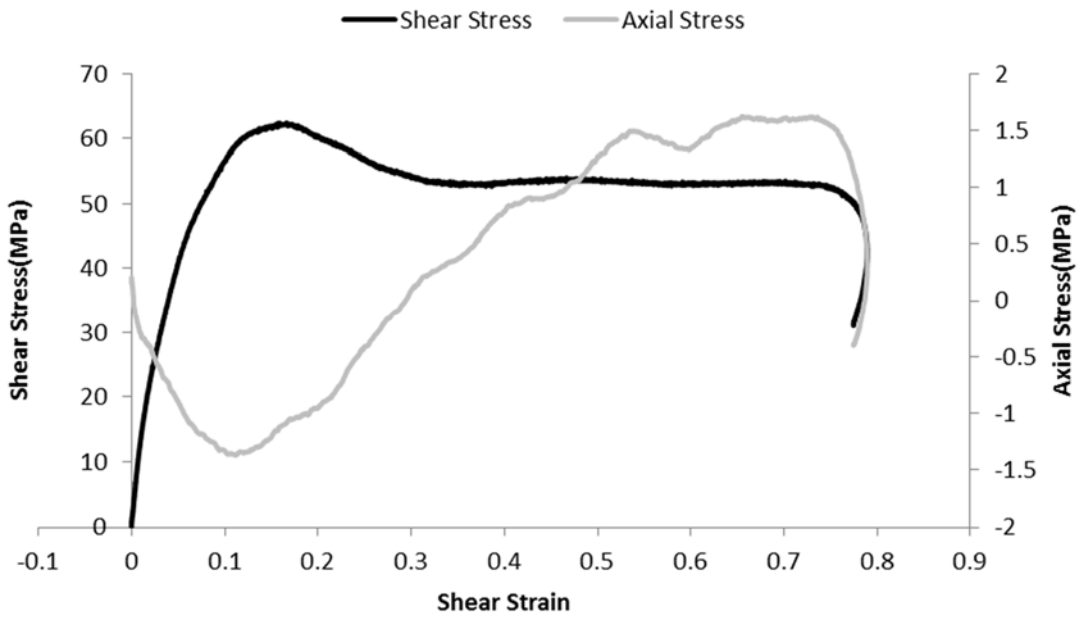
Shear Stress
Axial Stress
Shear Stress(MPa)
Axial Stress(MPa)
Shear Strain
70
60
50
40
30
20
10
0
2
1.5
1
0.5
0
-0.5
-1
-1.5
-2
-0.1
0
0.1
0.2
0.3
0.4
0.5
0.6
0.7
0.8
0.9

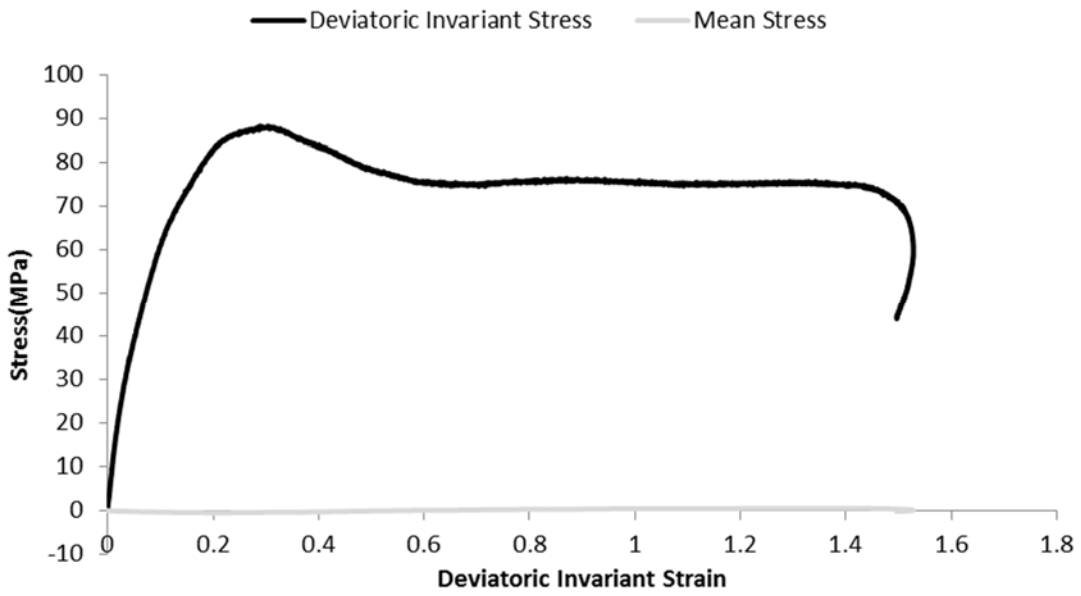
Deviatoric Invariant Stress
Mean Stress
Stress(MPa)
Deviatoric Invariant Strain
100
90
80
70
60
50
40
30
20
10
0
-10
0
0.2
0.4
0.6
0.8
1
1.2
1.4
1.6
1.8

Test 3

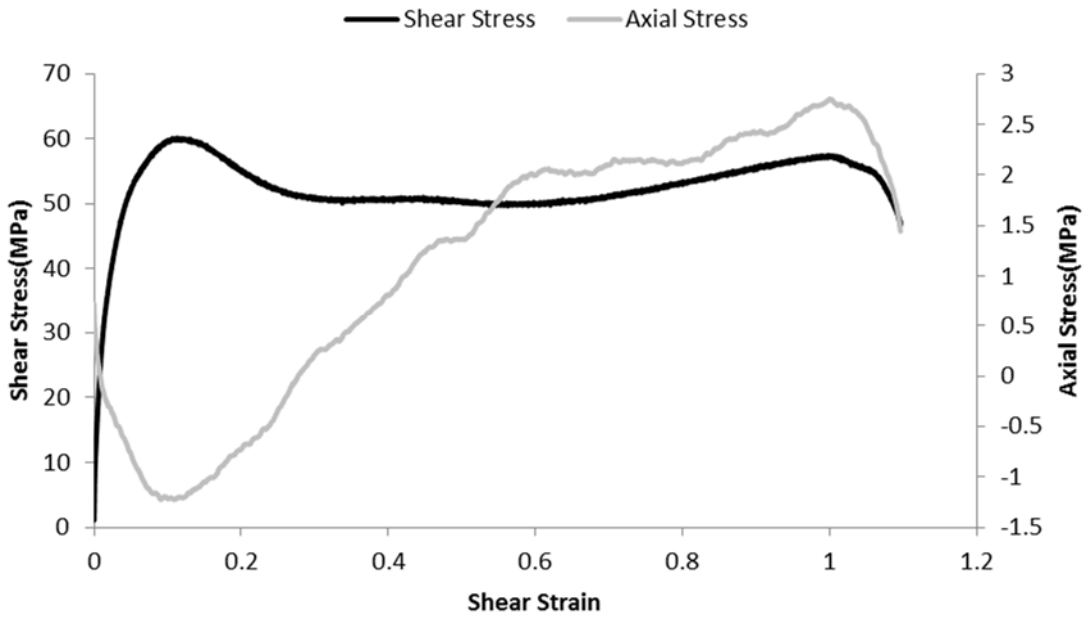
Shear Stress
Axial Stress
Shear Stress(MPa)
Axial Stress(MPa)
Shear Strain
0
10
20
30
40
50
60
70
-1.5
-1
-0.5
0
0.5
1
1.5
2
2.5
3
0
0.2
0.4
0.6
0.8
1
1.2

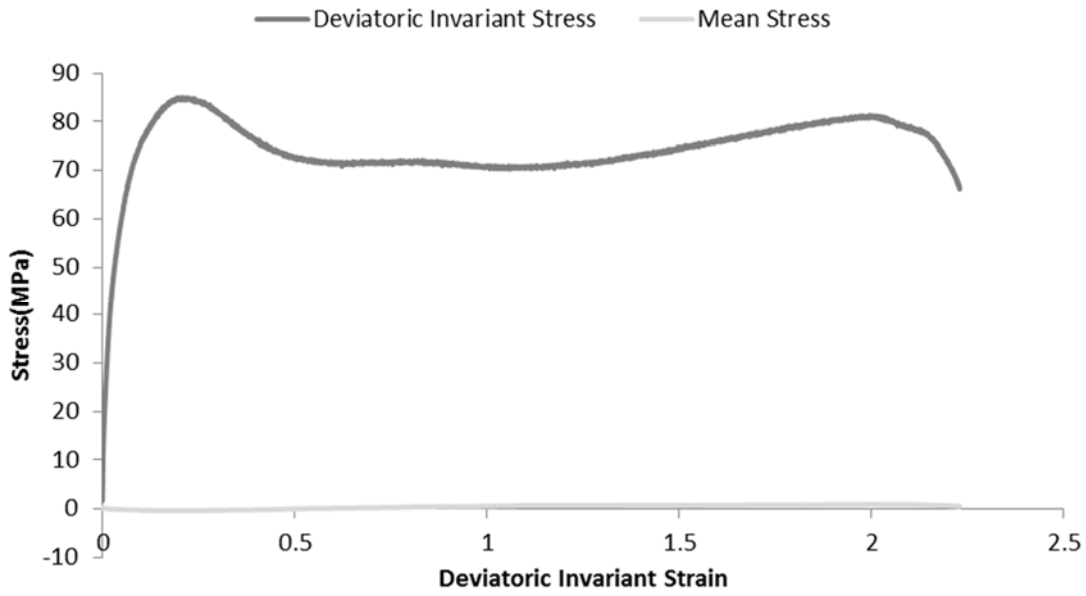
Deviatoric Invariant Stress
Mean Stress
Stress(MPa)
Deviatoric Invariant Strain
-10
0
10
20
30
40
50
60
70
80
90
0
0.5
1
1.5
2
2.5

Test 4

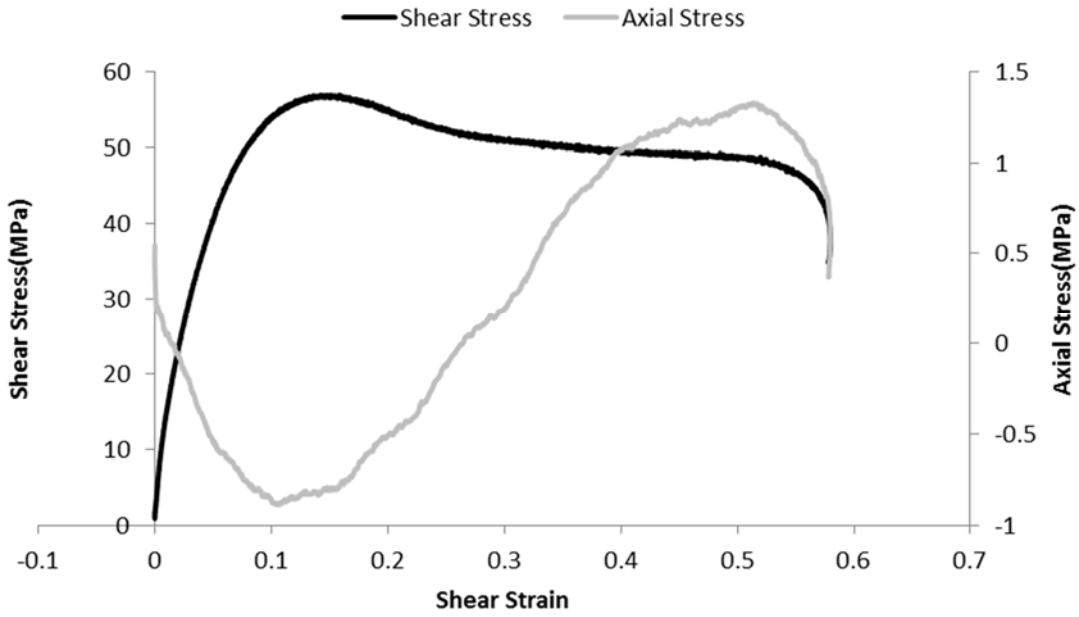
Shear Stress
Axial Stress
Shear Stress(MPa)
Axial Stress(MPa)
Shear Strain
60
50
40
30
20
10
0
1.5
1
0.5
0
-0.5
-1
-0.1
0
0.1
0.2
0.3
0.4
0.5
0.6
0.7

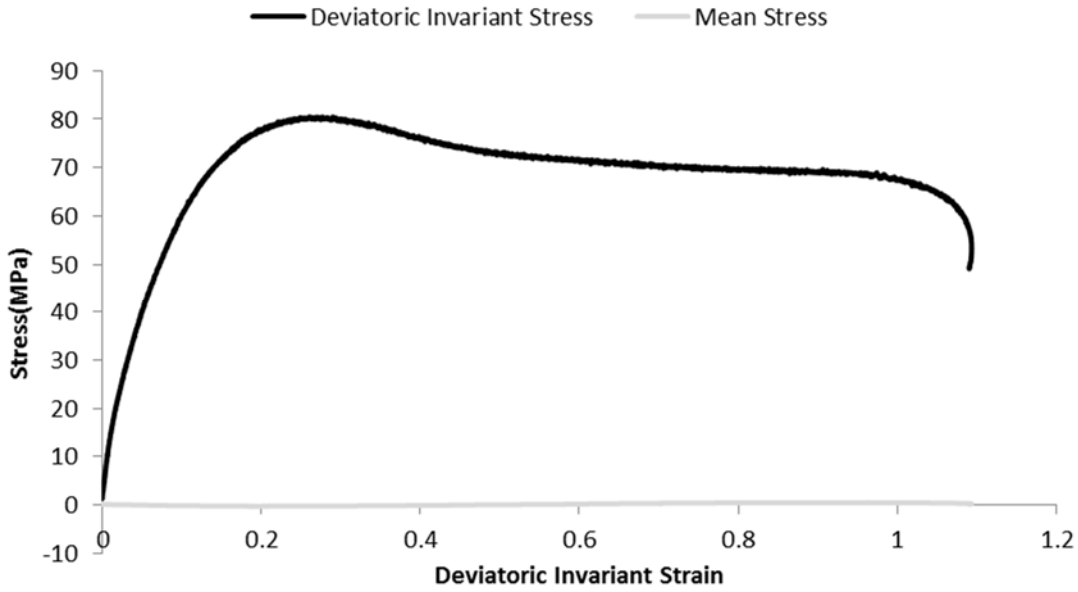
Deviatoric Invariant Stress
Mean Stress
Stress(MPa)
Deviatoric Invariant Strain
90
80
70
60
50
40
30
20
10
0
-10
0
0.2
0.4
0.6
0.8
1
1.2

APPENDIX B: COMBINED LOADING TESTS

Test 5

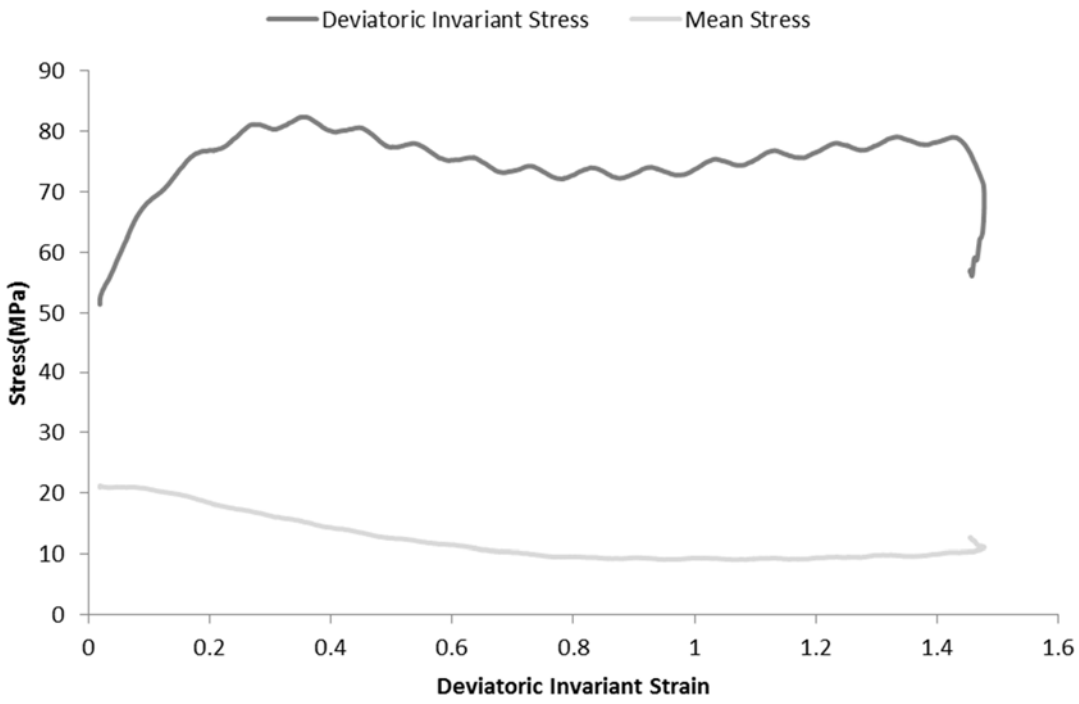

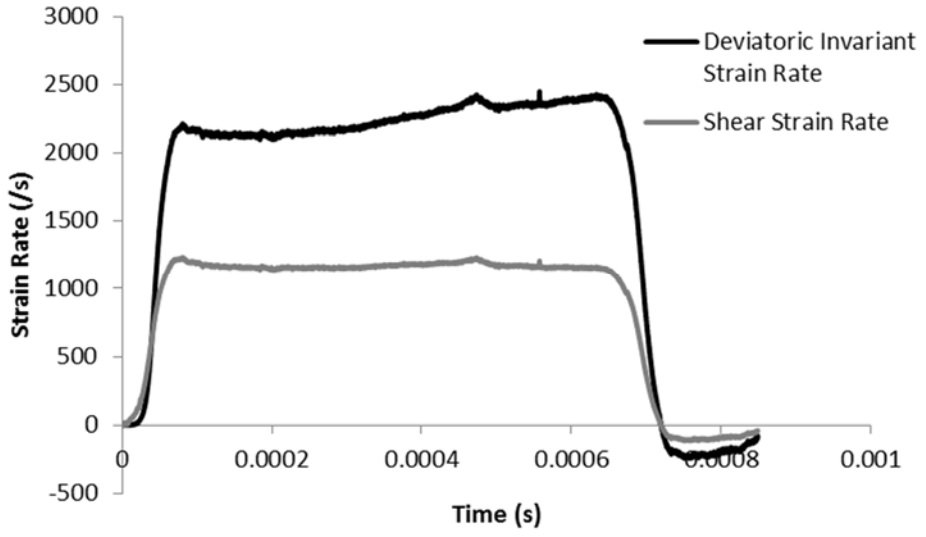

Test 6

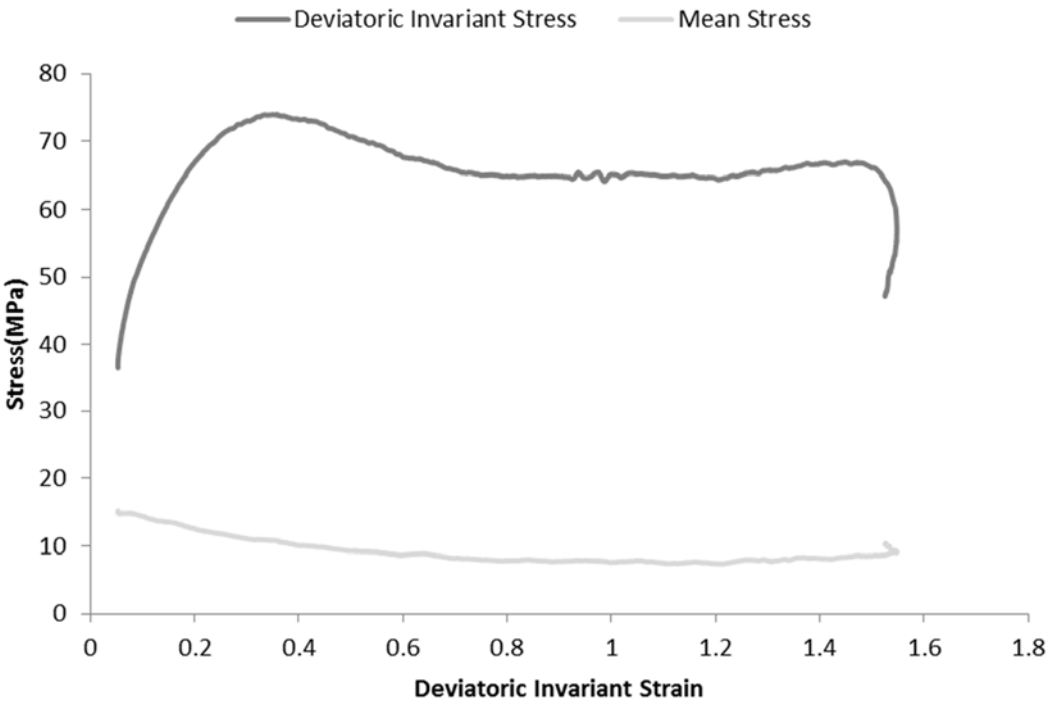
Deviatoric Invariant Stress
Mean Stress
Stress(MPa)
80
70
60
50
40
30
20
10
0
0
0.2
0.4
0.6
0.8
1
1.2
1.4
1.6
1.8
Deviatoric Invariant Strain

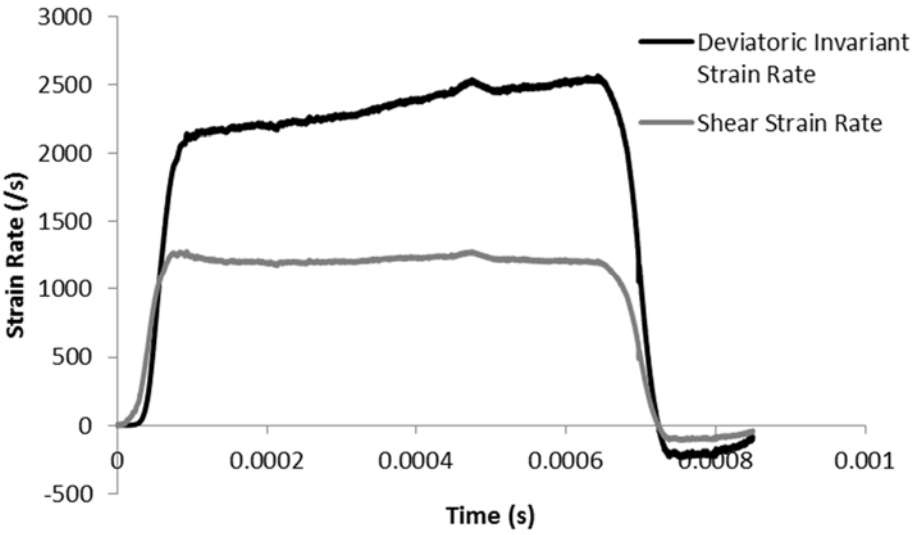
Deviatoric Invariant Strain Rate
Shear Strain Rate
Strain Rate (/s)
3000
2500
2000
1500
1000
500
0
-500
0
0.0002
0.0004
0.0006
0.0008
0.001
Time (s)

Test 7

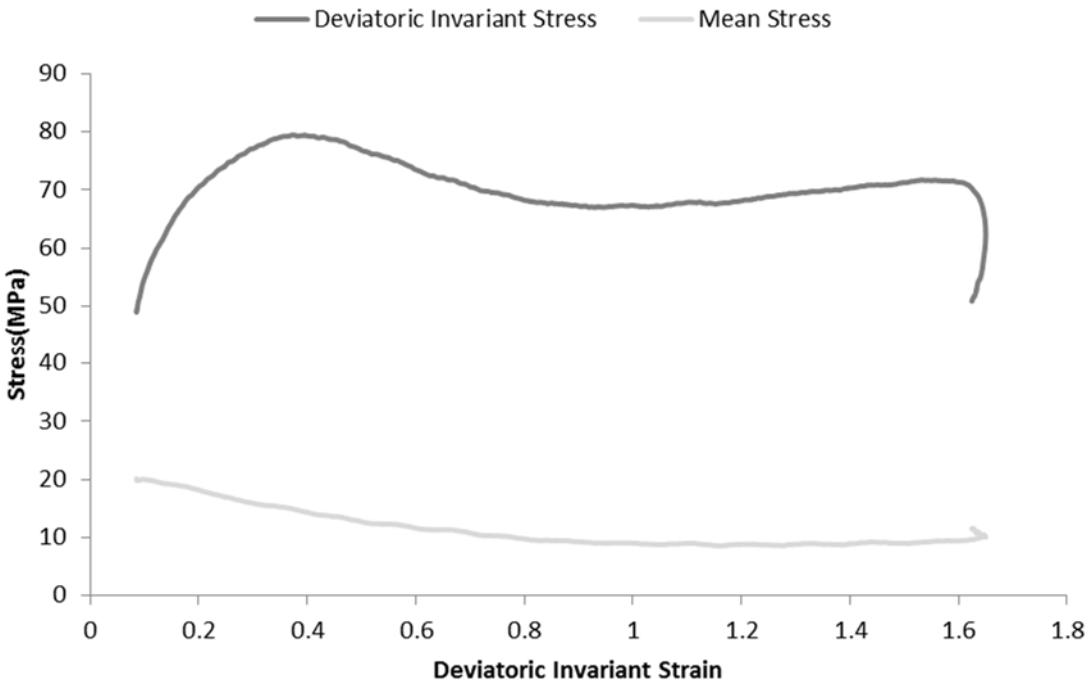
Deviatoric Invariant Stress
Mean Stress
Stress(MPa)
90
80
70
60
50
40
30
20
10
0
0
0.2
0.4
0.6
0.8
1
1.2
1.4
1.6
1.8
Deviatoric Invariant Strain

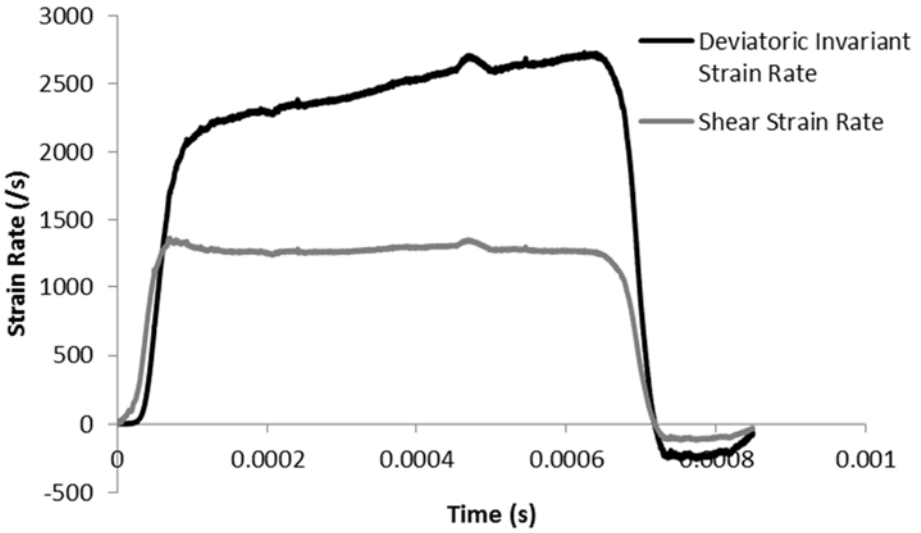
Deviatoric Invariant Strain Rate
Shear Strain Rate
Strain Rate (/s)
3000
2500
2000
1500
1000
500
0
-500
0
0.0002
0.0004
0.0006
0.0008
0.001
Time (s)

Test 8

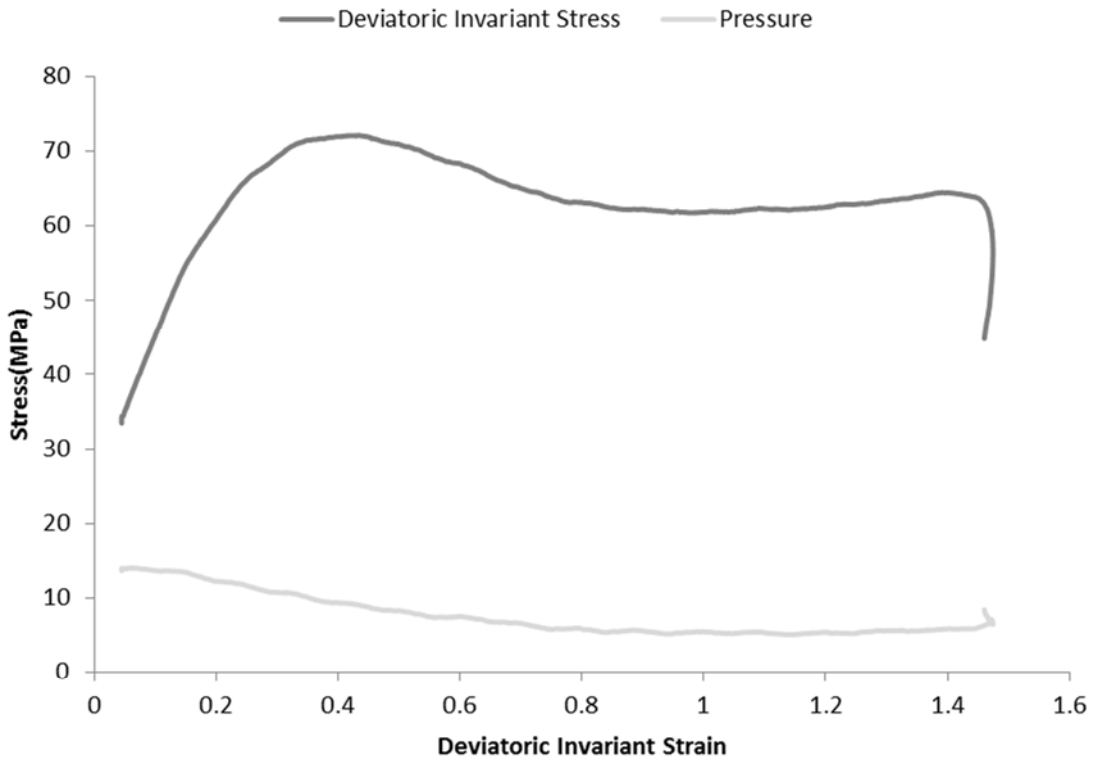
Deviatoric Invariant Stress
Pressure
Stress(MPa)
80
70
60
50
40
30
20
10
0
0
0.2
0.4
0.6
0.8
1
1.2
1.4
1.6
Deviatoric Invariant Strain

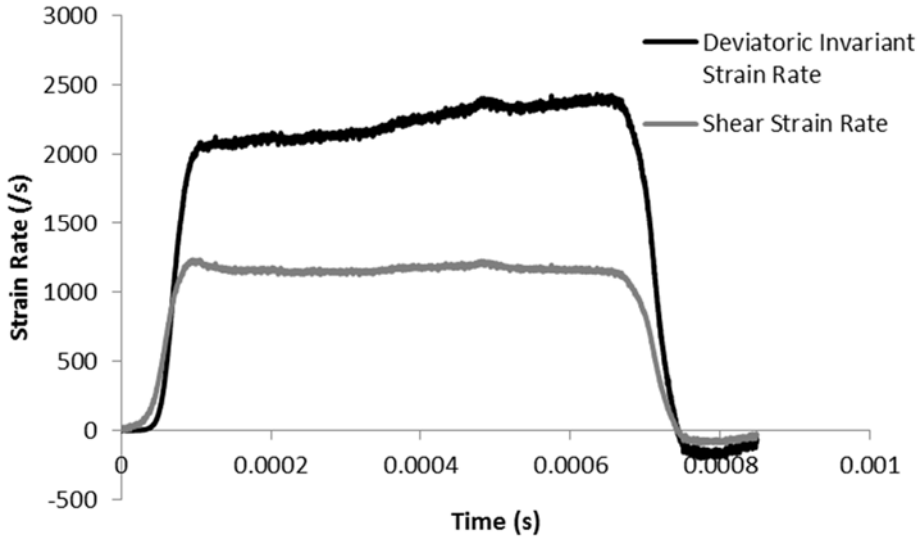
Deviatoric Invariant Strain Rate
Shear Strain Rate
Strain Rate (/s)
3000
2500
2000
1500
1000
500
0
-500
0
0.0002
0.0004
0.0006
0.0008
0.001
Time (s)

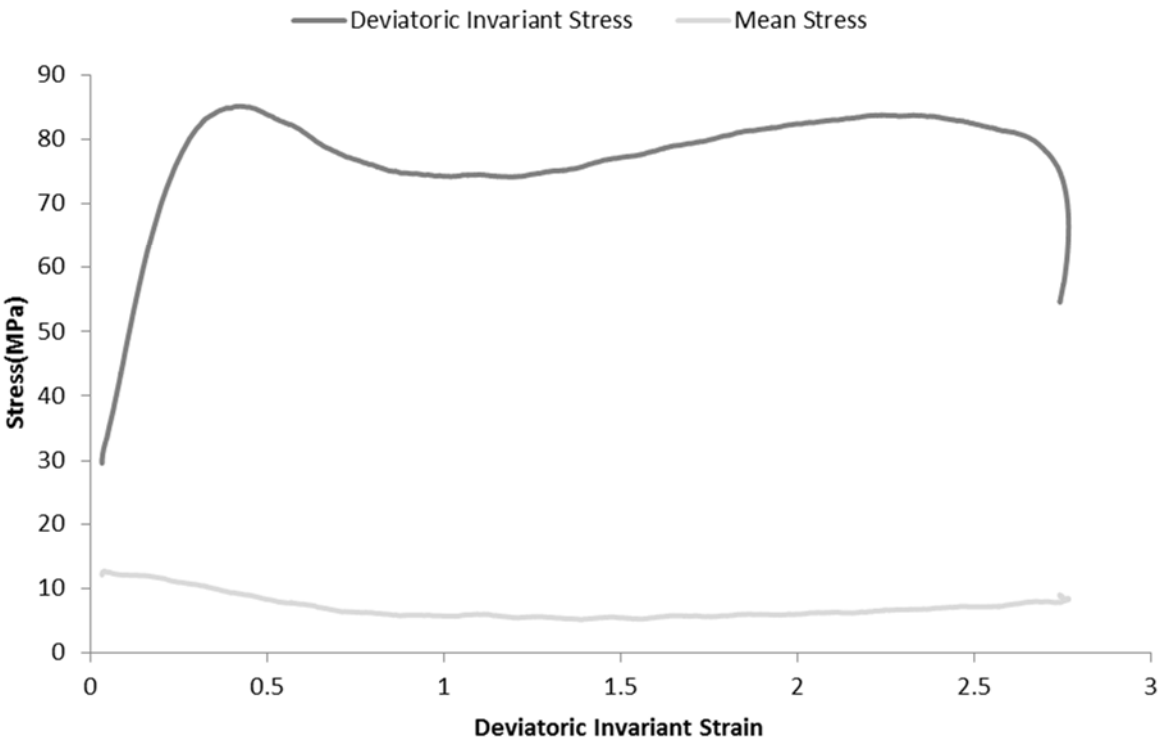
Deviatoric Invariant Stress
Mean Stress
Stress(MPa)
90
80
70
60
50
40
30
20
10
0
0
0.5
1
1.5
2
2.5
3
Deviatoric Invariant Strain

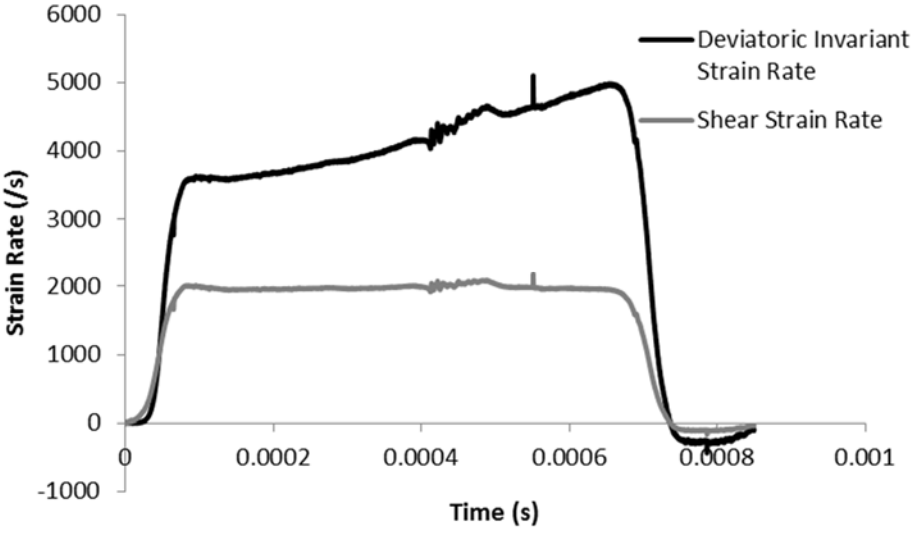
Deviatoric Invariant Strain Rate
Shear Strain Rate
Strain Rate (/s)
6000
5000
4000
3000
2000
1000
0
-1000
0
0.0002
0.0004
0.0006
0.0008
0.001
Time (s)

Test 9

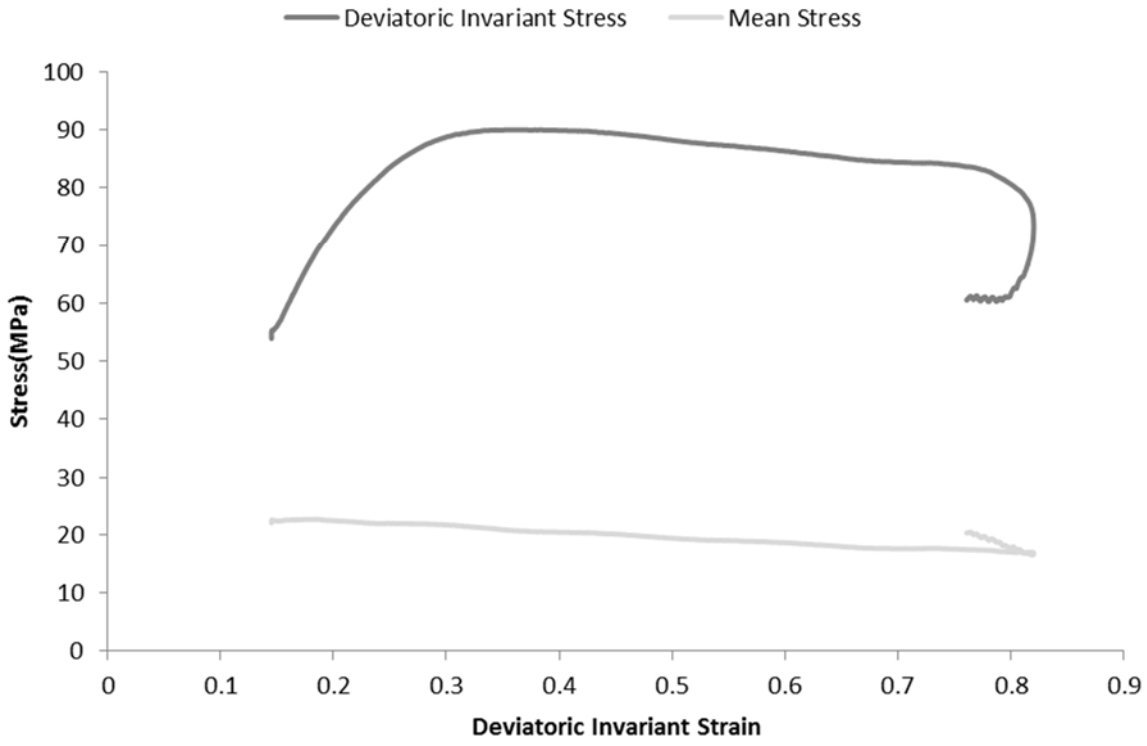
Deviatoric Invariant Stress
Mean Stress
Stress(MPa)
100
90
80
70
60
50
40
30
20
10
0
0
0.1
0.2
0.3
0.4
0.5
0.6
0.7
0.8
0.9
Deviatoric Invariant Strain

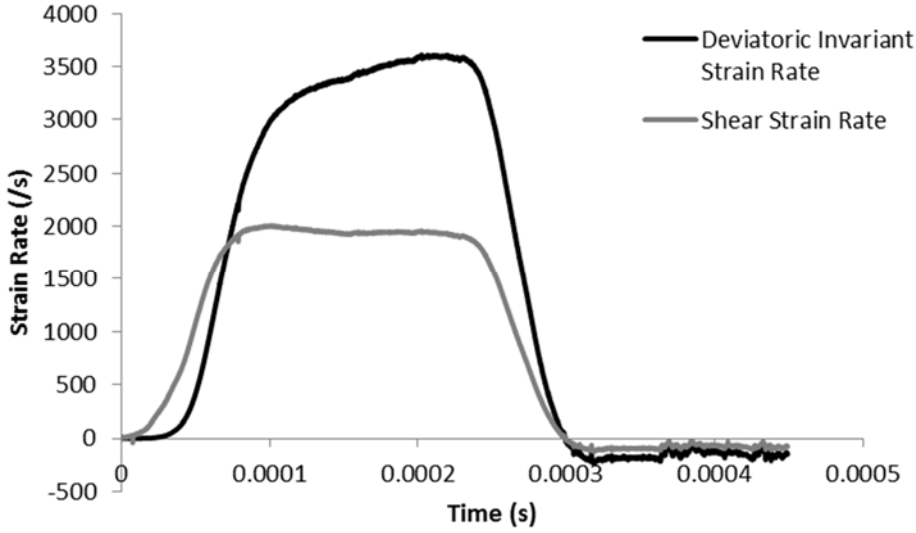
Deviatoric Invariant Strain Rate
Shear Strain Rate
Strain Rate (/s)
4000
3500
3000
2500
2000
1500
1000
500
0
-500
0
0.0001
0.0002
0.0003
0.0004
0.0005
Time (s)

Test 10

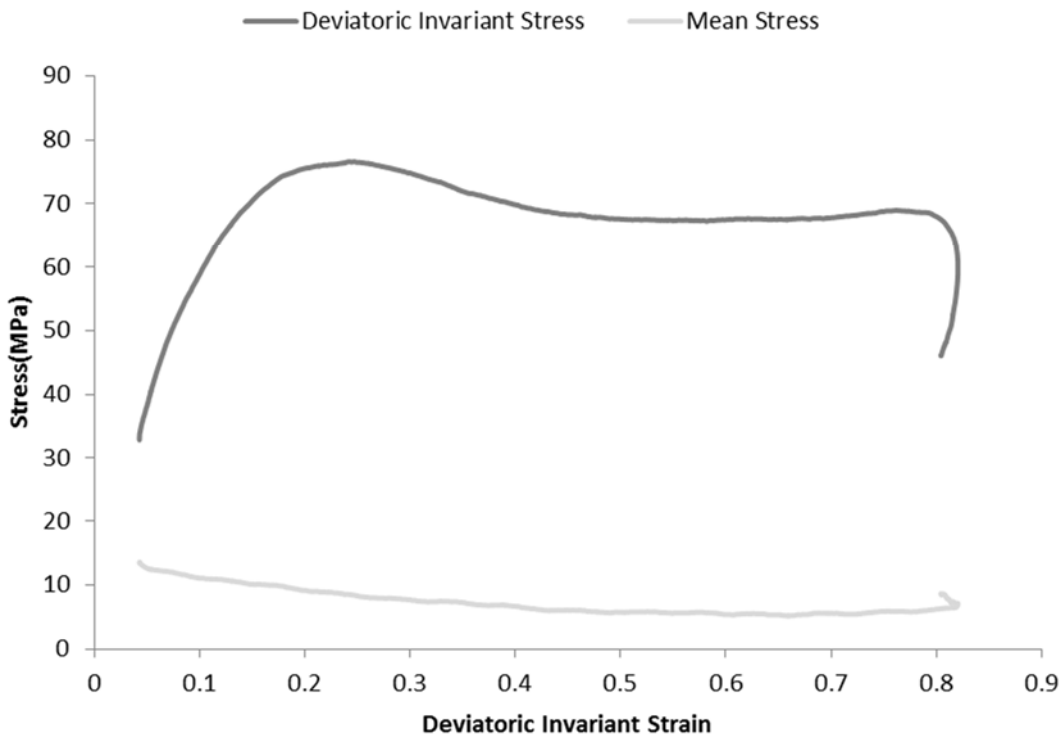
Deviatoric Invariant Stress
Mean Stress
Stress(MPa)
90
80
70
60
50
40
30
20
10
0
0
0.1
0.2
0.3
0.4
0.5
0.6
0.7
0.8
0.9
Deviatoric Invariant Strain

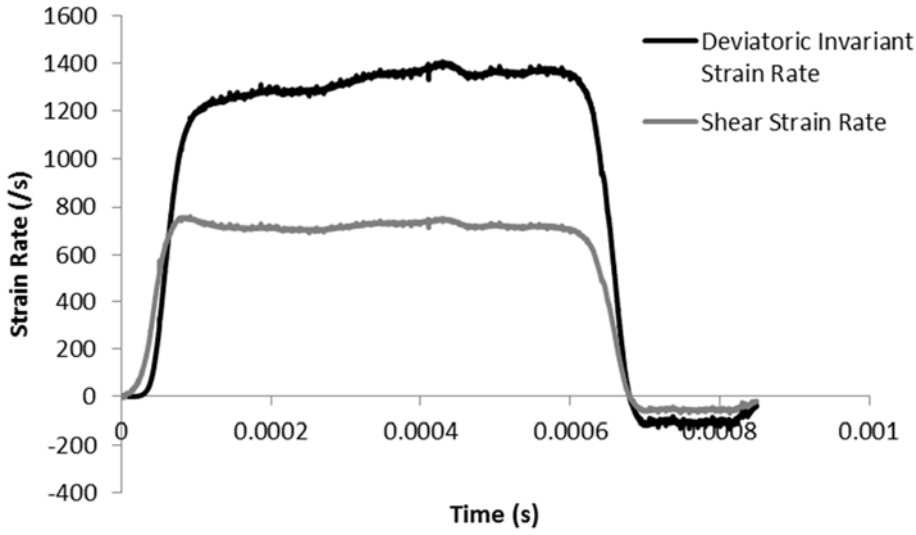
Deviatoric Invariant Strain Rate
Shear Strain Rate
Strain Rate (/s)
1600
1400
1200
1000
800
600
400
200
0
-200
-400
0
0.0002
0.0004
0.0006
0.0008
0.001
Time (s)

APPENDIX C: CKB TESTS

Test 11

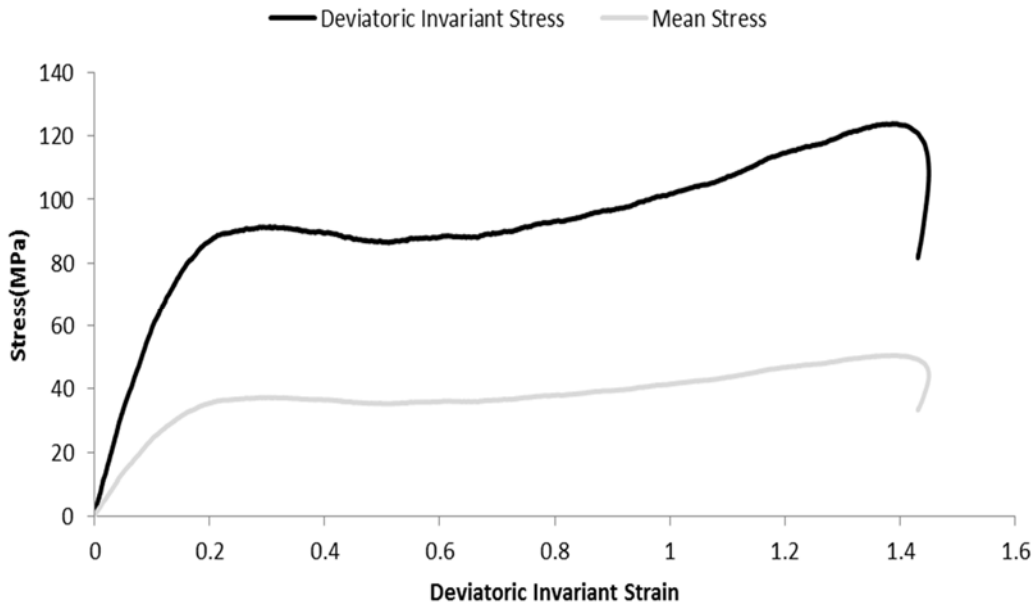

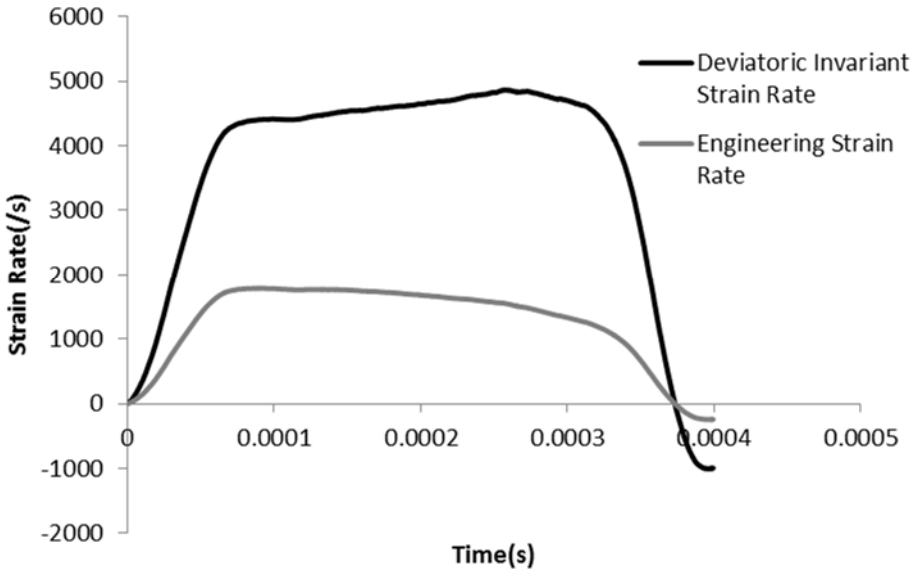

Test 12

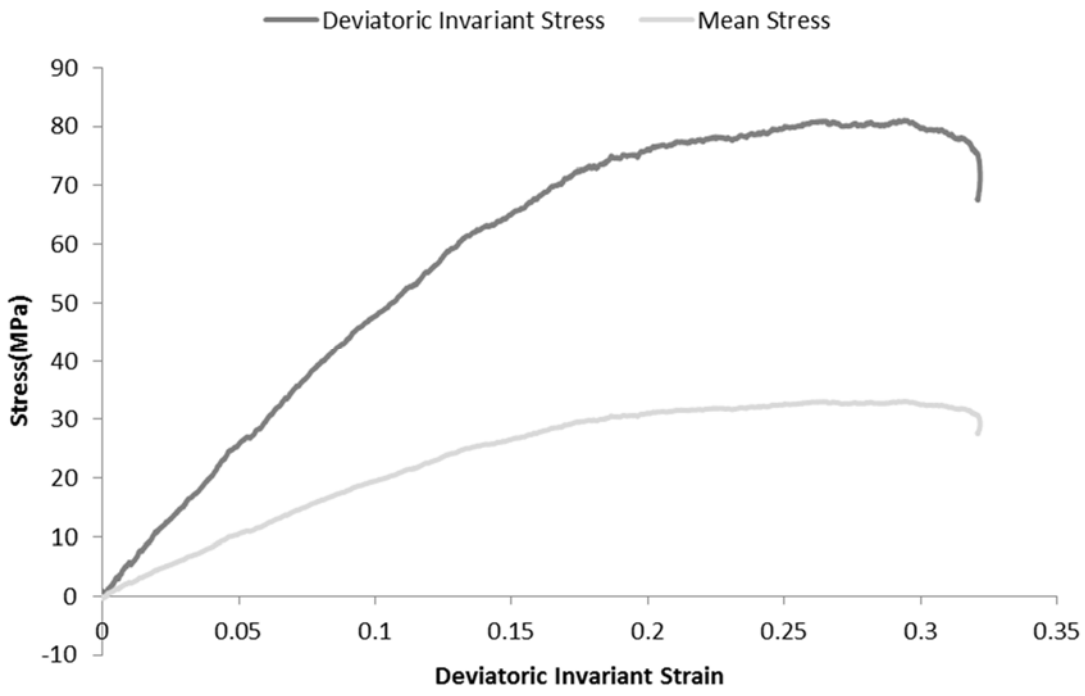
Deviatoric Invariant Stress
Mean Stress
90
80
70
60
50
40
30
20
10
0
-10
Stress(MPa)
0
0.05
0.1
0.15
0.2
0.25
0.3
0.35
Deviatoric Invariant Strain

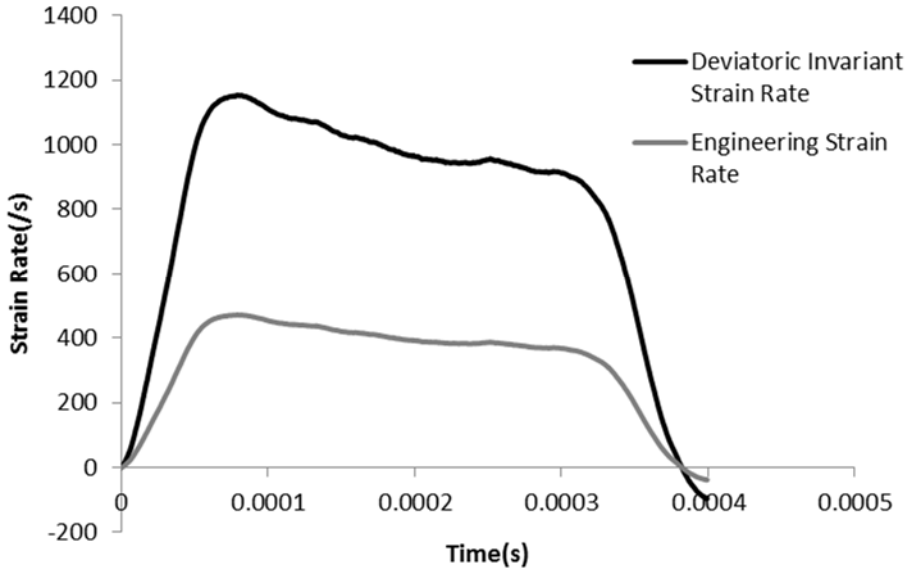
1400
1200
1000
800
600
400
200
0
-200
Strain Rate(/s)
Deviatoric Invariant Strain Rate
Engineering Strain Rate
0
0.0001
0.0002
0.0003
0.0004
0.0005
Time(s)

Test 13

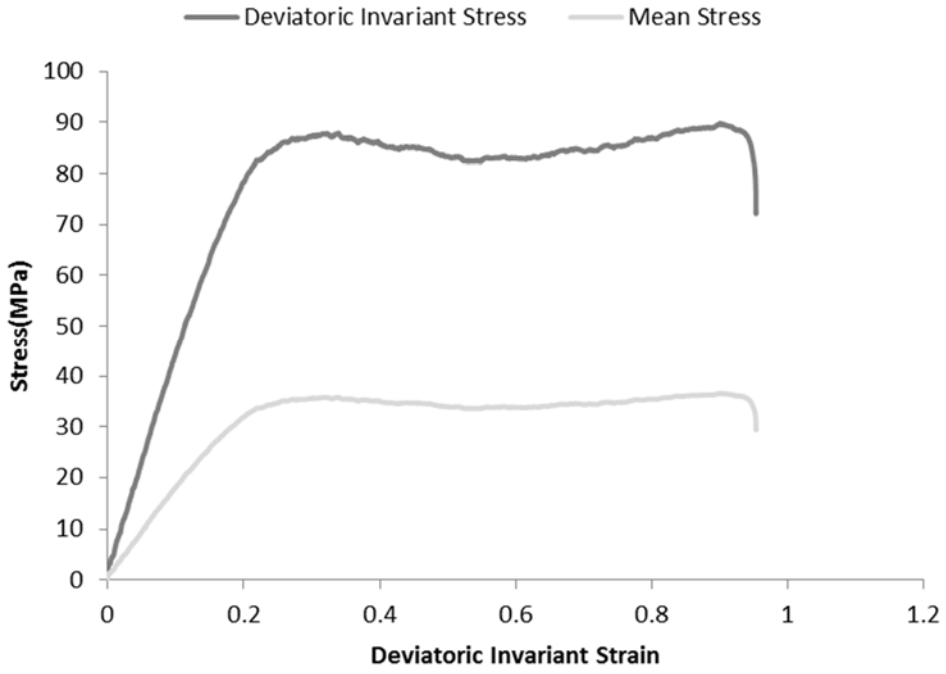
Deviatoric Invariant Stress
Mean Stress
100
90
80
70
60
50
40
30
20
10
0
Stress(MPa)
0
0.2
0.4
0.6
0.8
1
1.2
Deviatoric Invariant Strain

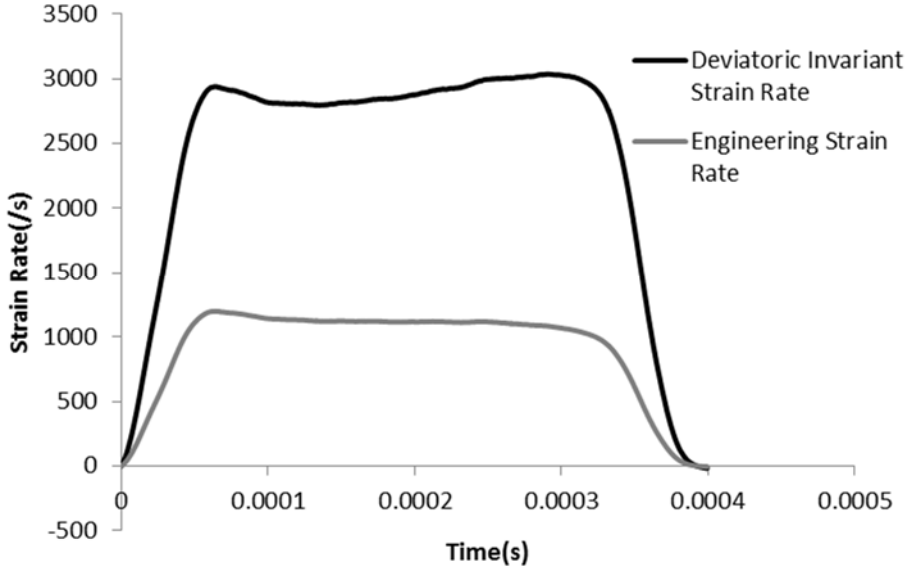
3500
3000
2500
2000
1500
1000
500
0
-500
Strain Rate(/s)
0
0.0001
0.0002
0.0003
0.0004
0.0005
Time(s)
Deviatoric Invariant Strain Rate
Engineering Strain Rate

Test 14

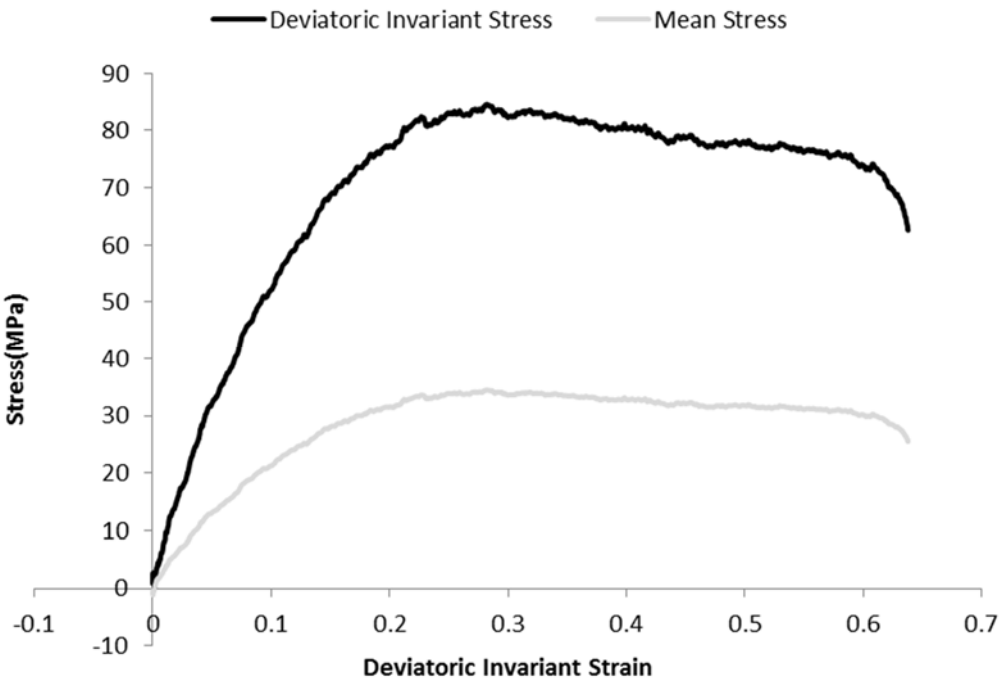
Deviatoric Invariant Stress
Mean Stress
Stress(MPa)
90
80
70
60
50
40
30
20
10
0
-10
-0.1
0
0.1
0.2
0.3
0.4
0.5
0.6
0.7
Deviatoric Invariant Strain

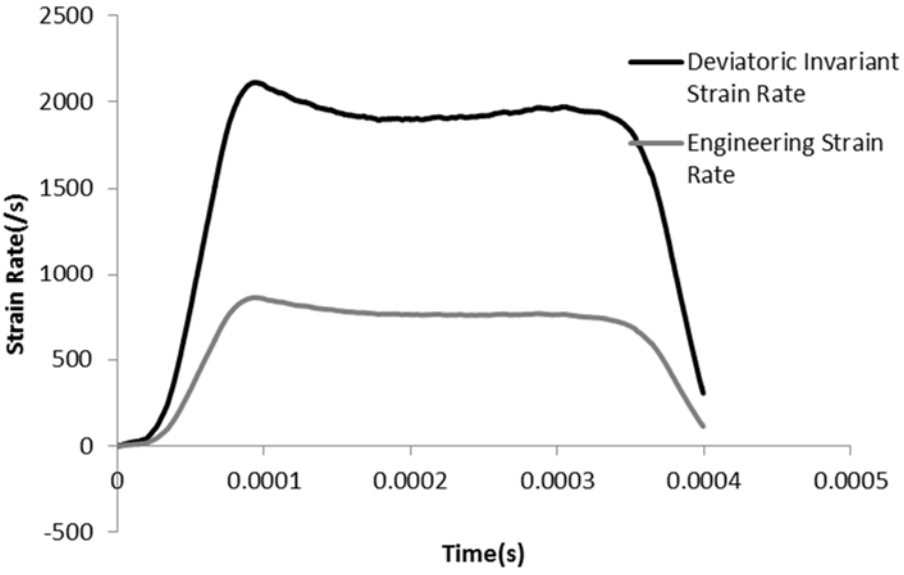
Deviatoric Invariant Strain Rate
Engineering Strain Rate
Strain Rate(/s)
2500
2000
1500
1000
500
0
-500
0
0.0001
0.0002
0.0003
0.0004
0.0005
Time(s)

s